الجمهوريـــــــة الجزائريـــــــــة الديمقراطيـــــــة الشعبيـــــــة

People's Democratic Republic of Algeria

وزارة التعليـــــم العالـــــــــي والبحـــــــــث العلمـــــــــي

Ministry of Higher Education and Scientific Research

FERHAT ABBAS UNIVERSITY-SETIF1

FACULTY OF TECHNOLOGY

DOCTORAL DISSERTATION

Submitted to the Department of Electronics

In fulfillment of the requirements for the

DOCTORAL DEGREE

Field: Science and Technology

Sector: Telecommunications **Option: Telecommunications Systems**

Presented By

MEKKI Samira

THEME

Modeling of Planar Microwave Sensor and Optimized Dielectric Resonator Antenna

Defended on 19 /06 /2024 before the Jury:

MAYOUF Abdelhalim	**Pr.**	**Ferhat Abbas University Setif-1-.**	**President**
ZEBIRI Chemeseddine	**Pr.**	**Ferhat Abbas University Setif-1-.**	**Supervisor**
FERHAT Hamida Abdelhak	**Pr.**	**Ferhat Abbas University Setif-1-.**	**Examiner**
OUABDIA Nabila	**MCA.**	**Constantine 1 University**	**Examiner**
KHELIL Abdelatif	**Pr.**	**El-oued University**	**Examiner**
SAYAD Djamel	**MCA.**	**Skikda University**	**Guest**

2023/2024

Dedication

I dedicated this modest work

To my dear father

The man who merits all my great respect; and my sincere feelings; Today I would like to dedicate to him my success, and my happiness; the man who helped me a whole lot to finish my studies, who sacrificed himself. May he find here the expression of my affection and a reward for the sacrifices made for me. May Allah protect you and give you good health and a long life, best father.

To my dear and tender mother

To the one who suffered everything, without making me suffer, may she find in this thesis the expression of my gratitude and appreciation for all the sacrifices, the deep love, and the kindness she offered me to see me succeed. May Allah preserve you for us mom; good health and long life all my feelings of gratitude for you my dear mom.

To my dear sisters and my brother

To my friends especially Amina; Samia, Nor, Chahra, and Meryem; all the best to all my friends, to all the people I love, to all the people who love me.

Samira

Acknowledgment

*All praise and glory to **ALLAH,** the all-powerful, who opened the way to success for me, and gave me the patience, courage, and perseverance during all those long years of study, so that I could achieve this stage and complete this thesis project.*

I confess that as I write these lines, strong emotions are welling up in me, and my mind is full of memories. For me, this moment marks the end of an exceptional experience marked by many difficulties, which I have been able to overcome thanks to the peoples who have supported me over all these years, and to whom I have the pleasure of expressing my sincere thanks.

*I would like to express my sincere gratitude and thanks to my estimable and honorable supervisor, Professor **Zebiri Chemseddine**, from the Department of Electronic Engineering. Beyond being an exceptional professor with a profound perspective, he also exemplifies kindness. I extend my sincere thanks to him for his guidance and exemplary encouragement, in particular for allowing me to benefit from his considerable scientific experience, his confidence and support provided me with the inspiration to make the right decisions at the most important times, and I am happy to be working under his direction. **I hope your life is full of happiness and success.***

*I would like also to express my sincere gratitude to Dr. **Kamil Karaçuha** from Istanbul Technical University turkiy, for his assistance and availability.*

I would also like to extend my gratitude to the members of jury:

*Professor. **MAYOUF Abdelhalim**, from the Department of Electronics at Ferhat Abbas University Setif 1, who presided over the jury for this thesis.*

*Professor. **Ferhat Abdelhak Hamida**, from the Department of Electronics at Ferhat Abbas University Setif 1, serving as an Examiner.*

*Docteur **OUABDIA Nabila**, from the Department of Electronics at Constantine University, serving as an Examiner.*

*Professor **KHELIL Abdelatif**, from the Department of Electrical Engineering at El-Oued University, as an Examiner.*

*Docteur. **Djamel Sayad**, in the Department of Electrical Engineering at Skikda University, kindly participated as a guest.*

*I would like to express **my sincere thanks** to my colleagues and friends at the University of Setif, and especially to **Dr. Rami Zegadi** for his daily support in helping me to complete this work, notably during this period.*

*I would like to thanks also my good friend and sister **Hanane** for having supported me every day in the construction of this work, for her precious and permanent help as well as morale, especially during this period.*

*I can't end these thanks without expressing my deep appreciation to my dear sisters whom I love dearly: they have encouraged and supported me throughout this thesis. **Special thanks to you Amel** for your financial and moral support. Special thanks to my **only brother Fateh.***

*I am also thinking of my dear friend and sister **Seloua,** for all her support, help, and sincere love for me. You will always be part of my memory.*

*The best for last: **thank you** to **my dear parents** for their support during good times and bad. Thank you for your care and attention. **Thank you** for having encouraged me and enabled me to undergo the difficulties of this thesis. **Thank you** for your great financial support. Thank you for teaching me that I should keep going even when I think it is impossible, that I can face life's obstacles, that I am strong, and that my dreams will one day come true.*

I would like to honor you in this manuscript because, without you, I would never have made it this far!

Contents

Chapter II: Dual port MIMO Cylindrical Dielectric Resonator Antenna (CDRA) at 5.8 GHz for WLAN Application

Chapter III: Equivalent Circuit of a Planar Microwave Liquid Sensor

Chapter IV: Equivalent Circuit Modeling of a Cylindrical Dielectric Resonator MIMO Antenna For WLAN Application

List of Figures

List of Tables

Abbreviations used

ADS	Advanced Design System
CCL	Channel Capacity Loss
CDRA	Cylindrical dielectric resonator antenna
CPW	Coplanar Waveguide
CSRR	Complementary Split Ring Resonator
DG	Diversity Gain
DRA	Dielectric Resonator Antenna
DR	Dielectric Resonator
ECC	Envelope Correlation Coefficient
EM	Electro-Magnetic
FBR	Front-to-Back Ratio
HEM	Hybrid Modes
HFSS	High-Frequency Structure Simulator
LTCC	Low-Temperature Co-fired Ceramic
LTE	Long-Term Evolution
MEG	Mean Effective Gain
MIMO	Multiple Input Multiple Output
MPA	Micro-strip Patch Antenna
RLC	Resistor-Inductance-Capacitor
SRR	Split Ring Resonator
TE	Transverse Electric
TM	Transverse Magnetic
VSWR	Voltage Standing Wave Ratio
WLAN	Wireless Local Area Network
TARC	Total Active Reflection Coefficient

General Introduction

General Introduction

We are currently facing profound developments in the field of telecommunications, such as mobile phones, wireless networks, satellite television, radar applications...etc. This rapid progress in wireless communication has generated enormous needs and rapid growth development of the electronic systems associated with these applications. In addition to all the necessary functions for digital transmission and modulation, these systems also include the antennas needed to transmit and receive these signals.

Antennas are critical components used for radiating and receiving electromagnetic fields. They come in various types, including wire, horn, microstrip, dielectric resonator, and printed antennas, among others. A comprehensive understanding of their operation is crucial for selecting the appropriate antenna design to achieve optimal performance. Given their essential role in communication systems, antennas must be studied in detail. Improving an antenna's performance involves adapting it to the latest applications and meeting the challenges of frequency band multiplication, increased bandwidth, and integration. Moreover, it is vital that the antenna's characteristics remain minimally influenced by environmental factors. A deep understanding of antenna functionality is necessary for designing and implementing effective antennas that meet these demands and ensure reliable communication.

To make wireless communication systems more efficient, MIMO (multiple-input multiple-output) technology has emerged as a solution to the need for high data rates, wide coverage, and reliability in new wireless communication systems.

Over the last two decades, two classes of new antennas have been studied and presented in the literature. These are the microstrip patch antenna and the dielectric resonator antenna. Before the emergence of dielectric resonator antennas (DRA), microstrip patch antennas were widely preferred for a range of wireless communication applications. Either type of antenna is ideally suited to the development of modern wireless communications.

Dielectric resonator antennas (DRAs) have appeared as interesting MIMO antenna system candidates due to their greater efficiency, higher gain, and better radiation patterns [1]. In this thesis, we mainly focused on the study and design of antennas based on dielectric resonators (DRA).

Initially, dielectric resonators were used in designing filters, oscillators, and microwave circuits. As technological demands increased, they were subsequently proposed for use as radiating elements. Since then, extensive research [2-8] has been conducted to understand

dielectric resonators and leverage their advantages, especially regarding miniaturization and operational stability.

This thesis aims to build on this foundation by studying, designing, and creating new MIMO antennas using dielectric resonator technology for wireless communication systems. The focus is on using the benefits of dielectric resonators to make antennas smaller, more stable, and better suited to meet the demands of modern wireless communications.

In the other hand An antenna is a device that converts electromagnetic waves into electrical signals, which can then be processed and analyzed. This conversion process is a fundamental aspect of sensing, as it allows the antenna to detect and measure the properties of the electromagnetic waves it is exposed to. For example, an antenna can be used to measure the frequency, amplitude, and polarization of incoming electromagnetic waves, which can be used to determine the location, speed, and direction of the source of the waves. This information can be used to track objects, detect changes in the environment, and even monitor the health of electronic systems. In this sense, antennas are sensors that provide valuable information about the world around us, and they play a critical role in many modern technologies, including wireless communication systems, radar systems, and navigation systems [9].

In the past, traditional devices for analyzing different materials were often complex, expensive, large, and difficult to use. They also required a lot of time for sample preparation and result analysis. Recently, researchers have been developing microwave sensors. These sensors are simpler, smaller, and cheaper to make. They are also very sensitive and durable. Because of these benefits, microwave sensors are becoming popular in fields like biomedicine, food safety, and industry.

The microwave sensor changes the incoming electromagnetic signal into an electrical or magnetic wave at the output, making it user-friendly. Its main role is to provide an easy and efficient way to analyze and identify the components of various materials, such as liquids, solids, and molecular substance [10].

Generally, it consists of a selective sensitive component (resonator) for processing and a data transmission system (transmission line) for exciting the device. When the sensor is excited by an electromagnetic field at the transmission line, an interaction occurs which can take the form of refraction, diffusion, emission, or absorption between the sensor and the medium to be detected, depending on the situation [11]. Here, the Simulation process was done by using high frequency Simulation Software (HFSS) 2021.

The most important part of this work concerns Equivalent circuit models, which have recently emerged as a crucial tool in the field of research in antenna design. They play a vital role in modeling planar structures and antennas. These models allow for the simplification of complex systems by representing them with fundamental elements such as resistors, capacitors, and inductors. The use of equivalent circuit models provides researchers with more understanding of the behavior of planar structures and antennas more effectively.In particular, it enables the analysis and optimization of key parameters, such as impedance. In our study, we place a strong emphasis on the utilization of equivalent circuit modeling to simplify the modeling process, analyze the performance of antennas, and facilitate their integration into more intricate systems. This approach enhances our understanding of antenna behavior and aids in the development of efficient solutions tailored to specific applications in the field. In this thesis, an electrical model was firstly studied for a filter with two ports, which has never been studied in advance in the literature, and in second part, an electrical model for a dielectric resonator antenna has been presented. Two equivalent circuits are effectively modeled, for a filter and a CDRA MIMO antenna, in order to better understand the behavior of this type of resonator.

This manuscript is structured into four distinct chapters as follows:

- **The first chapter** introduces dielectric resonator antennas in terms of the literature and other antenna families. This is followed by a detailed description of their theory and operating principles, with a brief review of the most commonly used shapes and the different techniques to excite them. Special attention will then be given to antennas with cylindrical dielectric resonators.
- **The second chapter** presents a single-element cylindrical-shaped dielectric resonator antenna CDRA-based MIMO antenna excited by a dual-port probe presented to operate at 5.8 GHz for WLAN applications. A brief parametric study is carried out to study the influence of the most important parameters of the structure on the radiation performance. Then, the manufacturing and measurement methodologies will be treated.
- **The third chapter** is focused first of all on the simulation of planar structures based on a micro-strip transmission line and square CSRR meta-material resonators with three rings led by a test capillary tube with different diameters and different positions. All these structures are simulated using the HFSS microwave structure simulator which allows us to extract the transmission parameter S_{21}, as well as the sensitivity S

and the quality factor Q for different structures. A model of the CSRR resonator was established using the ADS interface by schematizing a sequence of parallel RLC blocks.

- **The last chapter** is focused on the equivalent circuit CDRA-based MIMO antenna for WLAN. The equivalent circuit was modeled as a parallel RLC using ADS. Software The new approach is based on the derivation of the circuit impedance parameters Z_{ij} instead of the S_{ij} parameters amplitudes used by the more common approaches.

A general conclusion will end this manuscript, presenting an overview of what has been developed in this thesis project and highlighting the results obtained. In addition, a few lines of research will be proposed for future work.

References

[1] Mujawar, M. and Pramono, S., 2024. Dielectric Resonator Antenna for Multiple Input Multiple Output Applications. *Digital Convergence in Antenna Designs: Applications for Real-Time Solutions*, pp.171-189.

[2]Yaduvanshi, R.S. and Parthasarathy, H., 2016. Rectangular dielectric resonator antennas. *doi*, *10*, pp.978-81.

[3] Soltan, A., Asfour, R. and Khamas, S.K., 2024. Frequency-Reconfigurable Millimeter-Wave Rectangular Dielectric Resonator Antenna. *Sensors*, *24*(12), p.3906.

[4] Gaya, A., Jamaluddin, M.H., Ali, I. and Althuwayb, A.A., 2021. Circular patch fed rectangular dielectric resonator antenna with high gain and high efficiency for millimeter wave 5G small cell applications. *Sensors*, *21*(8), p.2694.

[5] Kuznetcov, M.V., Podilchak, S.K., Clénet, M. and Antar, Y.M., 2021. Hybrid dielectric resonator antenna for diversity applications with linear or circular polarization. *IEEE Transactions on Antennas and Propagation*, *69*(8), pp.4457-4465.

[6] Altaf, A., Jung, J.W., Yang, Y., Lee, K.Y. and Hwang, K.C., 2020. Reconfigurable dual-/triple-band circularly polarized dielectric resonator antenna. *IEEE Antennas and Wireless Propagation Letters*, *19*(3), pp.443-447.

[7] Alanazi, M.D., 2023. A review of dielectric resonator antenna at mm-wave band. *Eng*, *4*(1), pp.843-856.

[8] Gupta, V.K., Alam, M., Yadav, A. and Sharma, A., 2024. Two-port dielectric resonator antenna loaded with meta-surface for improving isolation and circular polarization generator. *International Journal of Communication Systems*, p.e5676.

[9] Balanis, C.A. ed., 2011. *Modern antenna handbook*. John Wiley & Sons.

[10] Polivka, J., 2007. An overview of microwave sensor technology. *High Frequency Electronics*, *6*(4), pp.32-42.

[11] Abdolrazzaghi, M., Zarifi, M.H., Pedrycz, W. and Daneshmand, M., 2016. Robust ultra-high resolution microwave planar sensor using fuzzy neural network approach. *IEEE Sensors Journal*,*17*(2),pp.323-3.

Chapter I:

Theoretical Study

I .1. Introduction

Today's wireless communication sector is booming, and the antenna is an essential element in the transmission system. Dielectric resonator antennas (DRAs) are one of the many types of antennas available, which have become very important in recent years due to the evolution of telecommunication systems, intending to reduce the size, and weight of systems, increasing frequency and bandwidth [1].

The term dielectric resonator (DR) was first used in 1939 by Ritchmyer [2] when he demonstrated that dielectric objects could resonate in different excited modes. He appropriately named these structures dielectric resonators (DR). Ritchmyer also proved that a dielectric resonator (DR) placed in free space must emit due to boundary conditions at the interface between the dielectric and the air. The theory of DRA was done by Okaya and Barash who analyzed their modes and reported the first ever DR in the form of a single crystal TiO2 [3] in the 1960s. More experimental work on DRAs, done by Long in 1980, proved that DRAs can become efficient radiators and can be used as antennas. This property provided the fundamental theory for the dielectric resonator antenna (DRA) later invented in 1983[4] and since then, have been known as dielectric resonator antennas (DRA).

This chapter describes the basic theory of DRAs, including the characteristics of the DRA and the advantages, compared to microstrip antennas, different feeding methods (coaxial feed, slot aperture, microstrip feed line, co-planar feed, dielectric image guide), and the basic DRA shapes with different parameters and after that, we pass into planar resonator structures and explore their applications.

I .2. Dielectric resonator antenna

I .2.1. Definition

Dielectric resonators are made of low-loss dielectric material, in the form of ceramic, poly-crystalline, bare, or metalized (disk, cylinder). They were initially introduced as filter devices in microwave circuits and oscillators in the microwave domain, because of their high permittivity between (10 and 100) [5]. The high permittivity of the DR and free-space interfaces produces a stationary electromagnetic wave inside the resonator.

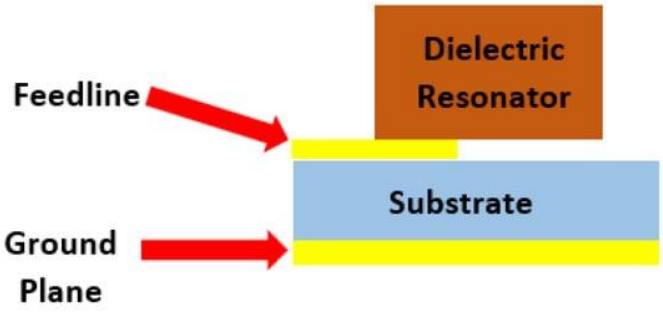

Figure I-1. DRA standard layout [6].

I.2.2. Investigations on Dielectric Resonator Antenna

For numerous years, dielectric resonators (DRs) have predominantly found application in microwave circuits, such as oscillators and filters. Typically composed of high permittivity material with a dielectric constant (ε_r) exceeding 20, DRs exhibit unloaded Q-factors ranging between 50 and 500, occasionally reaching values as high as 10,000. Traditionally regarded as energy storage devices rather than radiators due to these applications, the concept of utilizing DRs as antennas was not widely embraced until the publication of the seminal paper on cylindrical dielectric resonator antennas (DRAs) in 1983 [7]. It was during this period that the frequency range of interest for many systems gradually shifted towards the millimeter and near-millimeter range (100-300 GHz). At these frequencies, the conductor loss of metallic antennas becomes pronounced, leading to a significant reduction in antenna efficiency.

I.2.3. Dielectric resonator antenna shape

A distinctive quality of a Dielectric Resonator Antenna (DRA) lies in its flexibility to adopt diverse shapes. Furthermore, the operational mode and performance of a Dielectric Resonator Antenna (DRA) can be adjusted by choosing a dielectric resonator with the desired structure [8].fabrication the selection of the shape, dimensions, and permittivity of the resonator can produce a well-defined radiation pattern [5].

Therefore, various Dielectric Resonator Antenna (DRA) geometries have been explored through experimental in the literature. The initial systematic investigation, both theoretically and experimentally, focused on the cylindrical disk DRA geometry [9] Subsequently, McAllister and colleagues studied rectangular [10] and hemispherical [11] shapes. In 1997, Mongia et al. carried out in-depth studies on the theory of rectangular resonators [12]. Varieties of shapes have also been studied, such as the cylindrical ring [13], triangular [14], spherical [15], and conical [16]. Many other shapes have been analyzed through research carried out in this field to improve the characteristics of DRAs.

Figure I-2 illustrates the diverse geometries of Dielectric Resonators (DR). While several shapes have been introduced, the cylindrical and rectangular DRAs remain the most extensively researched and commonly employed structures. Their popularity can be attributed to the ease of design, fabrication, and analysis associated with these configurations.

Figure I-2. Different shapes of dielectric resonator antennas [17].

I .2.4. Basic Characteristics of DRA

Dielectric resonator antennas (DRAs) offer many specific characteristics that make them highly suitable for millimeter-wave applications in particular, high radiation efficiency, bandwidth, and polarization flexibility make them far more efficient than conventional antennas (MPA) [5]. The DRA exhibits some interesting features, which make it very promising for wireless applications.

DRAs have several attractive properties, notably [7]:

- The size of the DRA is proportional to $\lambda_0/\sqrt{\varepsilon_r}$, where λ_0 is the free-space wavelength at the resonant frequency, and ε_r the dielectric constant of the material.
- High radiation efficiency due to the absence of surface waves.
- Various feeding methods can be applied to excite the DRA [17].
- The dielectric resonator antenna offers a considerable impedance bandwidth compared to the microstrip antenna. This disparity arises from the fact that the dielectric resonator antenna radiates across its entire surface, excluding the ground plane, whereas the microstrip antenna radiates solely through narrow slots [18].
- The DRA element can excite different modes depending on the shape of the resonator. These modes yield diverse radiation patterns tailored to specific coverage needs. Moreover, the Q-factor of certain modes is contingent upon the aspect ratio of the DRA, thereby offering an additional dimension of flexibility in the design process.

- A large range of permittivity constants can be used (ε_r= 10 - 100), which allows the designer to monitor the physical size of the DRA and its bandwidth [19].

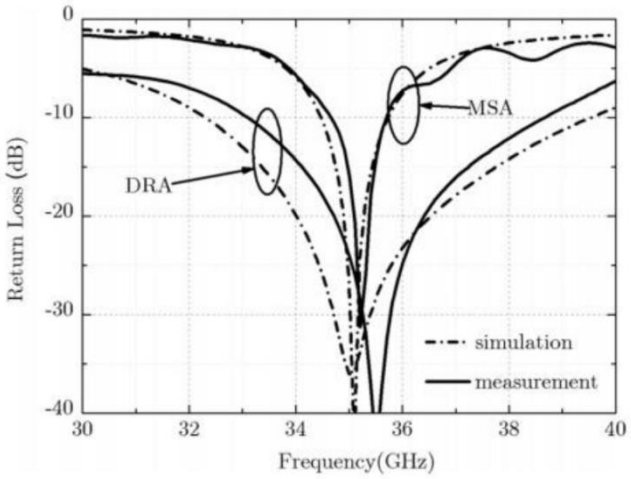

Figure I-3. Comparison between the reflection coefficients of a microstrip and a dielectric resonator antenna resonator antenna [19].

I .2.5. Materials used in DRA

One of the most important electrical properties of dielectric materials is the dielectric permittivity (ε_r), which represents the response of the media to electrical excitation. According to the value used, frequency bands are associated with the dielectric resonator, so the choice of the material's dielectric constant is very important in the design of dielectric resonator antennas.

- Low permittivity materials (between 6 and 10) are characterized by very low

losses (between 3 and 10.10-5) and are used for frequencies between 50 and 100 GHz [20].

- Medium permittivity materials (between 15 and 25) are much more suitable for the [20]
- The frequency range between 20 and 30 GHz [20].

Medium permittivity materials (between 30 and 40) can be used in the frequency range frequencies between 7 and 12 GHz [20].

- Materials with permittivity greater than 50 are associated with relatively high loss ($tan\delta$= 10-3) and are designed for frequencies between 0.8 and 3 GHz [20].

In 1971, Mass and his co-authors developed the first ceramics to be used as dielectric resonators by proposing a new dielectric material. It has been developed with a dielectric constant value of ε_r = 38, stable with temperature and with low loss at microwave frequencies and good mechanical properties [21]. Later, in 2004, Zhen proposed in [22] the use of bismuth ceramics {Bi3xZn2-x-yAy (ZnxNb2-x-zBz O7} with high dielectric constants of ε_r =

97.71 *et* 37, for both rectangular and cylindrical dielectric resonator antennas. Parida studied in [23] the dielectric properties of the material {S_r (ZrxTi1-x) O3} for the design of dielectric resonator antennas. This study has shown that the resonance frequency and bandwidth depend on material permittivity. Measurements carried out on the DRA have confirmed the feasibility of using these materials for compact antennas. The material {Ba (1-x) La (2x/3) ZrO3} was studied in [24] and demonstrated the possibility of using it for dielectric resonator antennas. In 2015, Ubaid Ullah studied [25] numerically and experimentally a cylindrical dielectric resonator antenna using two different materials: MgTiO3 (MTO) and CoTiO3 (CTO), for broadband applications.

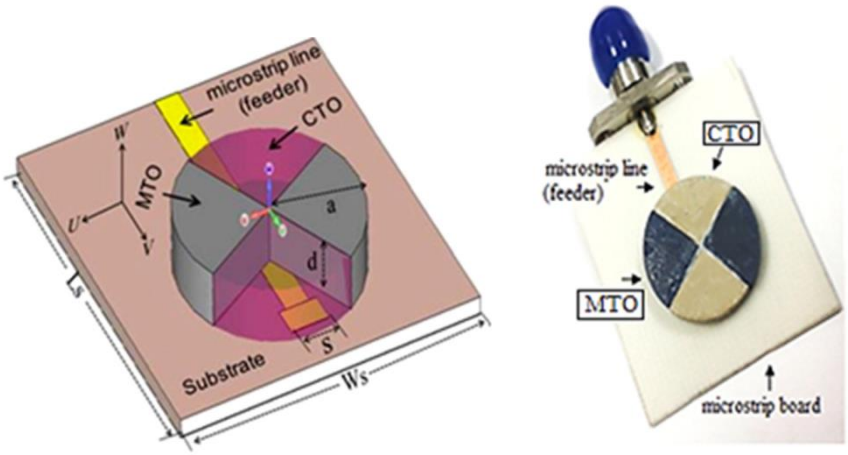

Figure I-4. Multi-permittivity dielectric resonator antenna: (a) simulation model and (b) experimental prototype [25].

Table I.1. Various materials used in DRA design.

Materials	Dielectric constant (ε_r)	Operating frequency (GHz)	Applications	Reference
FR4 RogersT/Duroid 6010 RogersT/Duroid 6006	4.4 10.2 6.15	3.66 4.94	Multibands Systems	[26]
MgTiO3 (MTO) CoTiO3 (CTO)	15 10	12.2-21.65	Wideband Applications	[25]
Bismuth Bi3xZn2-3x-Ay	33.3 71	2.8	-	[22]

(ZnxNb2-x-zBz) O7	96.7			
Rogers RT6010 Zinc Tantalum (BZT)	10.2 27.5	5.3-6.1 7.2-7.8	Multibands applications	[27]
Arlon 600 substrate	6.15	5.8		[28]
BaTiO3	1000	2.8	Mobile applications	[29]
Rogers RO3010	10.2	1.67-6.7	GSM-1800, WiMax…	[30]
Rogers TMM10	9.2	5.3-6.05	Wireless Applications	[31]
Teflon Alumina	2.2 9.8	3.85-6.2	Wideband applications	[32]

I .2.6. Improved DRA gain

In typical cases, the gain of a dielectric resonator antenna is limited. Several techniques have been developed to overcome this limitation, such as the use of cavities [33]. Sequential-rotation networks have also been implemented with dielectric resonators to increase gain [34] Figure I.5. Another technique has been proposed by Rana et al [35], to improve gain by using a bandpass frequency selective surface (FSS) as a superstrate. Later, another study was carried out to examine the influence of a narrow air gap between a dielectric resonator and the ground plane on the radiation parameters of the antenna, operating in higher-order Modes. This study has shown an improvement in gain for an optimum air-gap size air [28] (Figure I.6.)

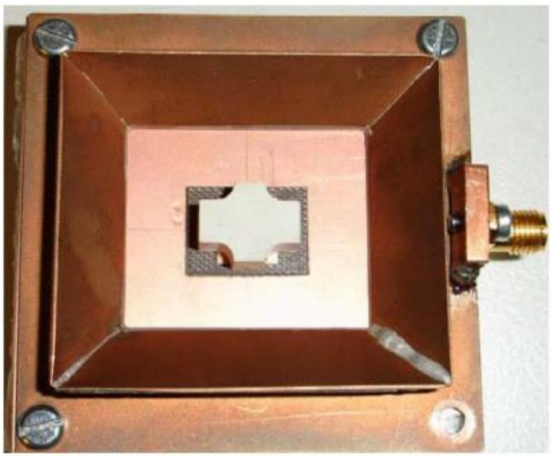

Figure I-5. A prototype of the compact DRA antenna was proposed in [34].

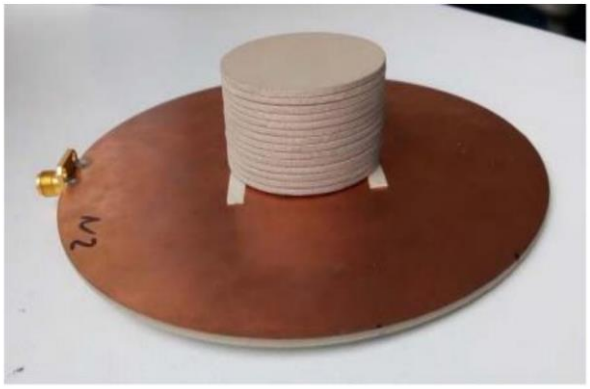

Figure I-6. Cylindrical DRA design was proposed in [28].

I .2.7. Different excitation techniques applied to the DRA

Electromagnetic energy can be coupled to the DR by various mechanisms, each one of them able to exert a significant influence on the resonant frequency and Q-factor. Several feeding techniques have been extensively documented in the literature. Among the most commonly used techniques to excite the desired mode in a dielectric resonator antenna (DRA) are:

- **Coaxial probe excitation**

The coaxial probe can be positioned either adjacent to the Dielectric Resonator Antenna (DRA) or embedded within it. The degree of coupling can be optimized by adjusting the probe height and the DRA location. Additionally, depending on the probe's location, different modes can be excited. When the probe is located adjacent to the rectangular DRA, it excites the magnetic fields of the $TE_{11\delta}$ mode (which radiate like a horizontal magnetic dipole). For a probe located at the center of a cylindrical DRA, the TE_{011} mode is excited (radiating like a vertical dipole) [36]. Using probe coupling offers the advantage of direct integration into a 50Ω system without the necessity for a matching network. Probes prove beneficial at lower frequencies; especially in cases where aperture coupling may be impractical due to the substantial slot size required [37-39].

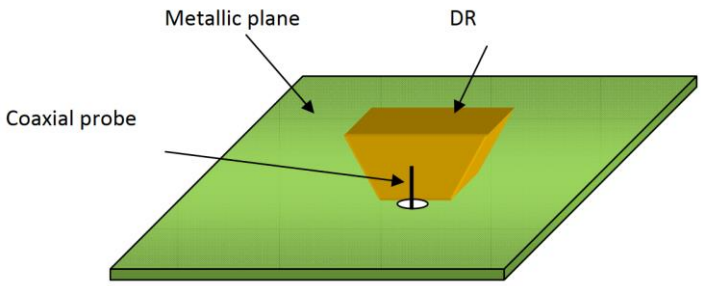

Figure I-7. Dielectric Resonator Antenna (DRA) fed by a coaxial probe.

- **Aperture Coupled feed**

The excitation of a real mode in the DRA can be enhanced by using a slot or aperture-coupled power supply. Any improper EM waves from the feed line or from probes that come into contact with the DRA are blocked by the aperture-coupled feed. The slot length is typically λ/2. DRA has also been used to produce orthogonal modes and circular polarization using an asymmetrical transverse slit design. On the same substrate, aperture power supplies can be easily integrated with the DRA [41, 43].

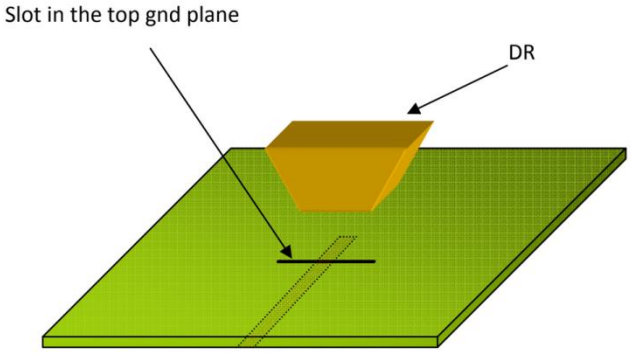

Figure I-8. Aperture coupled feed.

- **Microstrip transmission line**

Proximity coupling to microstrip lines is another prevalent method for connecting with dielectric resonators in microwave circuits. This approach is equally applicable.

In the case of Dielectric Resonator Antennas (DRAs) illustrated in Figure I-9, microstrip coupling is employed. Microstrip coupling induces the excitation of magnetic fields within the DRA, resulting in the generation of the short horizontal magnetic dipole mode. This configuration involves etching a metallic strip of a specific width on one side of a low-loss dielectric substrate with known permittivity and thickness. The opposite side is metalized and grounded. One advantage of the microstrip feed is its ease of fabrication, matching, and modeling.

The coupling of electromagnetic (EM) energy and the input impedance is established by adjusting the lateral position of the Dielectric Resonator (DR) relative to the strip line [44, 45]. This adjustment proves to be more convenient for arrays of DRAs as well. However, one drawback of this feeding method is that at higher frequencies, surface wave modes are also induced in the substrate, affecting the radiation pattern and efficiency of the DRA [46]. For DRAs requiring wide bandwidth and lower permittivity values, the level of coupling is typically minimal.

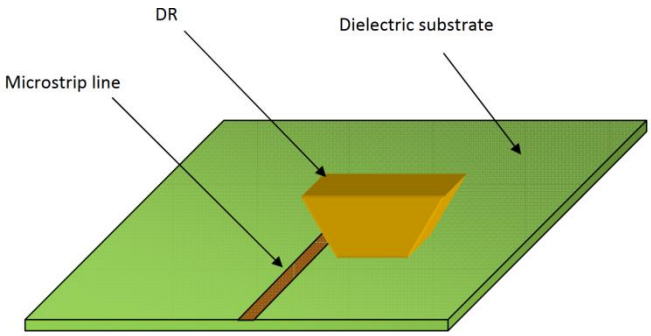

Figure I-9. Microstrip line feeding technique to excite DRA.

- **Coplanar feeding technique**

Placing the Dielectric Resonator Antenna (DRA) over the loop is a configuration where the coupling behavior resembles that of a coaxial probe. However, the loop provides the advantage of being non-obtrusive. By adjusting the position of the loop from the edge to the center of the DRA, it becomes possible to couple with either the $HE_{11\delta}$ mode or the TE_{011} mode of the cylindrical DRA [47, 48]. Another method involves using a coplanar slot to feed the DRA, as illustrated in the figure.

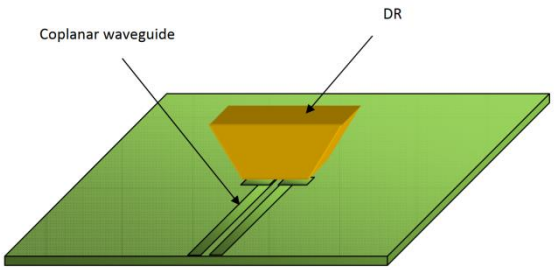

Figure I-10. Coplanar feeding technique to excite DRA.

- **Waveguide feeding technique**

The primary advantage of using a waveguide lies in its exceptional low-loss characteristics, especially in the millimeter-wave band. Given that the wave is fully guided within the metallic structure, the risk of radiation loss is effectively eliminated when the waveguide serves as a feed line. The combination of both the low-loss waveguide and the Dielectric Resonator (DR) creates an outstanding synergy for developing communication systems in the millimeter-wave range with minimal losses [49, 50]. Coupling to the DR can be accomplished through either a probe [51] or a slot [52]. Figure I-11 depicts a configuration with a waveguide probe feeding the DRA.

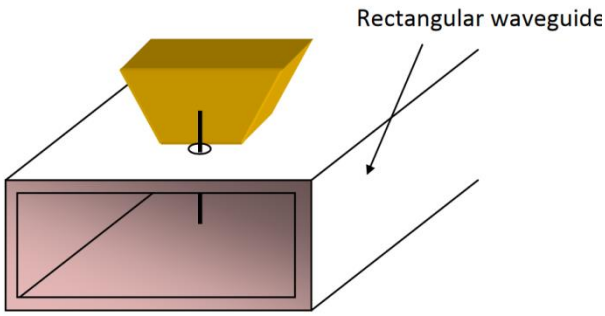

Figure I-11. Waveguide probe fed DRA.

I .3. Cylindrical dielectric resonator antenna (CDRA)

Regardless of its specific geometric form whether cylindrical, rectangular, or hemispherical a dielectric resonator antenna (DRA) is subjected to analysis involving resonant modes, near-field distribution within the resonator, far-field radiation, resonant frequency, and impedance bandwidth. Resonant modes are typically classified into Transverse Electric (TE) and Transverse Magnetic (TM), both referencing a particular coordinate axis. For instance, in the context of TE, it denotes the disappearance of the electric field component in the direction of propagation, transitioning to a transverse (perpendicular) orientation [53].

In the examination of cylindrical DRAs, employing a mode analysis based on a cavity resonant model is recommended. This model approximates the outer surfaces of the cavity with perfect magnetic walls, facilitating the utilization of Eigen function expansion for the fields. Following a consistent analytical approach, this methodology can be extended to the mode analysis of DRAs with rectangular or hemispherical shapes. To make use of the Cylindrical Dielectric Resonator (CDR) in antenna design, it is necessary to know how it works. The cylindrical dielectric resonator antenna (CDRA) is the first to be used for this generation of antennas. Where a cylindrical dielectric resonator antenna is characterized by the following parameters: height h, radius a, and dielectric permittivity ε_r is deposited on a finite ground plane [54]. Figure I-12 shows the basic configuration for a cylindrical dielectric resonator antenna.

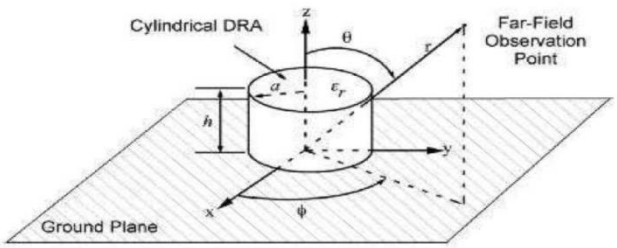

Figure I-12. Cylindrical dielectric resonator antenna configuration [5].

I .3.1. Resonance mode

Like all cavities, a large number of modes can be excited. They are classified into three categories, which allow us to obtain different radiation characteristics depending on the required application [55-57].

The modes of an isolated cylindrical dielectric resonator can be divided as follows:

- Transverse electrical modes (TE).
- Transverse magnetic modes (TM).
- Hybrid modes (HEM) are Also known as the HE and HM sub-families.

In the case of TE and TM modes, the fields are rotationally symmetrical, they have no azimuthal dependence. On the other hand, hybrid modes are φ-dependent.

The spatial configuration of the electromagnetic field of the modes is indicated by the three numerical integers m, n, and p representing the number of variations of the field along the three directions of the cylindrical reference plane:

- m (m = 0,1, 2...) represents the number of azimuthal variations of the field (in φ)
- n (n = 1, 2, 3...) represents the number of radial variations of the field (in r).
- p (p = 0, 1, 2…) représente le nombre de variations longitudinales du champ (en z).

The number of longitudinal variations being rarely definable by an integer, a real δ intervenes such that $0 < \delta < 1$. The third index will therefore be expressed by the term p + δ. The modes are therefore named $TE_{mnp+\delta}$, $TM_{mnp+\delta}$, and $HEM_{mnp+\delta}$

I .3.2. Electrical transverse modes or $TE_{m,n,p}$ modes

Pure electric transverse modes do not have azimuthal variations (m=0). The radial and axial components of the electric field E_r, and E_z are zero. The azimuthal component of the magnetic field is also zero. The electric and magnetic fields can be decomposed by the following equation:

$$\vec{E} = E_\varphi \vec{e}_\varphi \quad \text{And} \quad \vec{H} = H_r \vec{e}_r + H_z \vec{e}_r$$

I .3.3. Magnetic transverse modes or TM m, n, p modes

This type of electromagnetic mode is the reciprocal of the previous one, the axial component of the magnetic field Hz is zero. Electric and magnetic fields are presented by the following relationships:

$$\vec{H} = H_\varphi \vec{e}_\varphi \text{ And } \vec{E} = E_r \vec{e}_r + E_z \vec{e}_r$$

I .3.4. Hybrid modes or HEM modes

The HEM hybrid modes have six non-zero components of the electromagnetic field. These modes can be excited either by electrical or magnetic coupling. The equation represents its simplified design formula.

I .3.5. Standard mode excitation

Based on the desired resonant frequency and the required radiation pattern type, such as broadside or end-fire, a specific mode is selectively activated. Achieving this effectively involves the careful selection of appropriate excitation methods, primarily guided by:

- The nature of the excitation feed.
- The placement of the excitation feed.

Consider the case of a coaxial probe that excites the TM_{110} (HEM_{11}) mode. To achieve a corresponding broadside radiation pattern, the probe should be positioned near the peripheral boundary of the cylindrical Dielectric Resonator Antenna (DRA), whether embedded inside or equidistantly poled outside it. However, by gradually shifting the same probe toward the center of the DRA, the dominance of the TM_{110} mode diminishes, giving way to the emergence of the $TM_{01\delta}$ mode. Consequently, instead of exhibiting a broadside pattern, the antenna now presents an end-fire radiation pattern.

In contrast, if an aperture slot is used, it should be placed at the center to generate a broadside radiation pattern. Shifting the aperture slot towards the boundary of the DRA is necessary to attain an end-fire pattern.

It is crucial to highlight the significance of the aspect ratio (a/h). This parameter indicates that a taller Dielectric Resonator Antenna (DRA) with a smaller diameter can result in the same resonance frequency as a structure that is very short but large in diameter. However, it is essential to note that these structures possess different Q values. The aspect ratio (a/h) becomes particularly relevant when considering different permittivity values, as there exists a limit beyond which further control of the shape may not be feasible. Moreover, the aspect ratio (a/h) plays a pivotal role in determining whether two closely resonating modes should be merged to generate a broader -10dB bandwidth or not

To enhance clarity on the concept, we delve into the near-field distributions within cylindrical Dielectric Resonator Antennas (DRAs) and explore their corresponding far-field radiation patterns concerning the TE_{01}, TM_{01}, and TM_{110} (HEM_{11}) resonant modes [58-60].

- **Mode TE_{01}:**

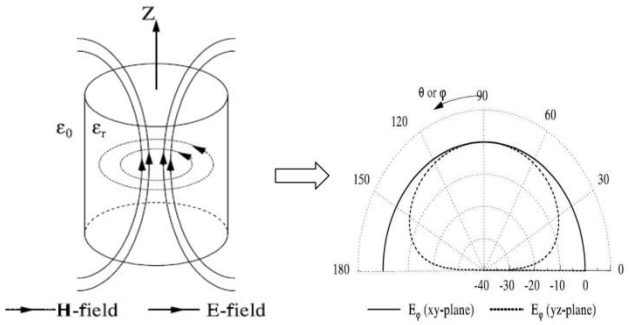

Figure I-13. The TE_{01} mode exhibits a broadside far-field radiation pattern [61].

- **Mode TM_{01}:**

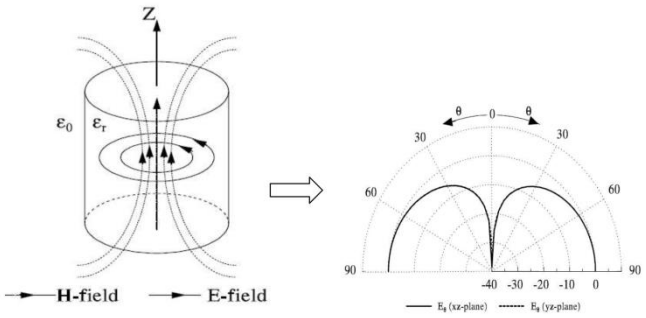

Figure I-14.TM_{01} Mode and its monopole-like far-field radiation pattern [61].

- **Mode TM_{110} (HEM_{11})**

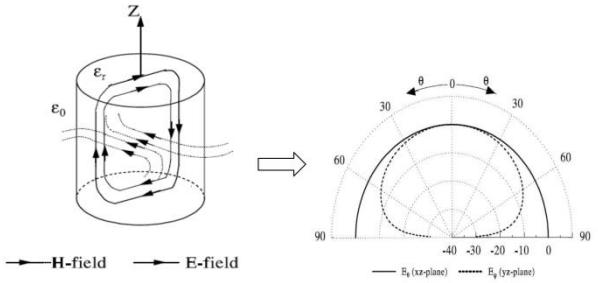

Figure I-15. Mode TM_{110} (HEM_{11}) and its broadside far-field radiation pattern [61].

In practical scenarios, the excitation source may concurrently resonate with multiple modes [62]. The strength of the field for a specific mode is contingent on the precision of the feed location and its operational frequency.

These far-field radiation patterns exhibit a distinct resemblance to other well-known antenna types. The TE_{01} pattern, for instance, resembles the radiation pattern of a half-wavelength narrow slot on the ground plane, directed toward the axis of the resonator. Similarly, the radiation pattern from TM_{01} appears analogous to a quarter- wavelength situated above the ground plane [62]. Meanwhile, the HEM_{11} pattern bears a resemblance to that of a half-wavelength narrow slot on the ground plane. Figure I-16 provides a graphical

representation, illustrating how the pattern shape undergoes a gradual transformation corresponding to changing locations by an aperture slot beneath the Dielectric Resonator Antenna (DRA).

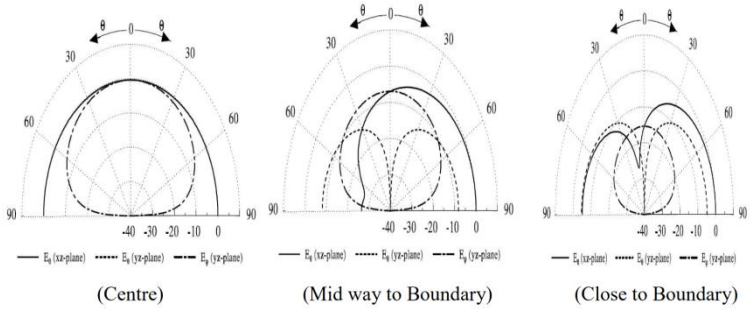

Figure I-16. Modifying radiation patterns aligning with diverse slot positions beneath the Dielectric Resonator Antenna (DRA) [61].

It is noteworthy to observe that when the slot is precisely positioned at the center, the generated pattern is perfectly symmetrical with no cross-polarization. However, as the slot shifts from the center towards the boundary, cross-polarization increases and eventually transforms into a completely different pattern.

I.4.Techniques to Improve Bandwidth

The utilization of broadband devices in modern communication systems is increasing. Therefore, for practical purposes, an antenna is expected to possess a wider bandwidth [63-65]. The bandwidth limitation of an antenna is often attributed to its input impedance, which tends to vary with frequency. Therefore, improving the impedance response can play a crucial role in expanding the antenna's bandwidth.

This approach can be categorized into four main groups:

- Simple structures.
- Q-factor reduction; introducing air gaps.
- Utilization of matching networks.
- Deployment of multiple resonators.

I.4 .1. Simple Structures

Among numerous options, it is the simplest and most outcome-oriented approach. Once the resonant mode is chosen, the dielectric constant value of the resonator and its aspect ratio (a/h) define the achievable bandwidth. In straightforward geometric shapes like cylindrical DRAs, the use of the smallest possible εr value lowers the Q-factor, consequently leading to a broader bandwidth [66].

$$BW = \frac{S-1}{Q\sqrt{S}}.100\%$$

Where S represents the desired Voltage Standing Wave Ratio (VSWR) at the input of the Dielectric Resonator Antenna (DRA) port.

However, every design type comes with its set of limitations, and in this case, although the Q-factor can be reduced by lowering the dielectric constant, an excessively low value may result in the inability to capture an adequate amount of electromagnetic energy, rendering it inefficient as a resonator. Alternatively, selecting an appropriate aspect ratio value (for cylindrical DRAs, a/h=0.329) that induces two closely merged resonances can yield a broader (-10dB) impedance bandwidth. Due to its simplicity in fabrication, this approach is favored over other techniques. An illustration of such a device is provided below.

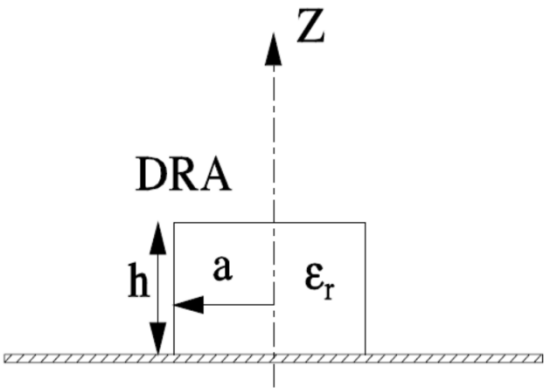

Figure I-17. A singular DRA structure with a radius a and height h [61].

I.4.2. Reduction in Q-factors

The introduction of an air gap surrounding the monopole and enclosed by the Dielectric Resonator Antenna (DRA) contributes to reducing the effective dielectric constant of the DRA [67]. This, in turn, decreases the Q-factor, resulting in increased bandwidth while pushing the resonant frequency upward. Although wider bandwidths can be achieved, this comes at the expense of a more intricate fabrication process. Figure I-18. illustrates one such model. It is crucial to note that a slight displacement of the DRA concerning the centrally located monopole can shift the resonance frequency from the desired position. A meticulous and highly precise cutting and grinding process for the DRA piece is necessary to avoid undesirable variations in the air gap size that could significantly impact the results.

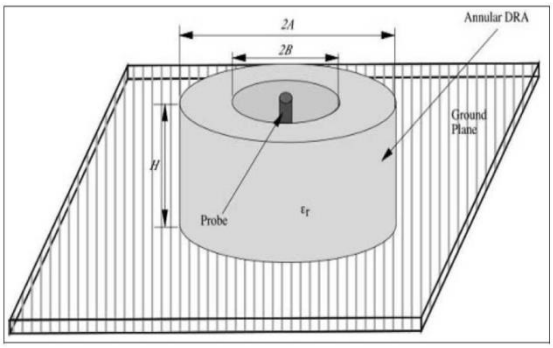

Figure I-18. Structure with an enclosed air gap for bandwidth enhancement [5].

I.4.3. Impedance matching

Bandwidth enhancement can also be achieved by optimizing impedance matching through the use of various materials preceding the matching with the desired Dielectric Resonator Antenna (DRA). Common techniques include flat matching inserts, loaded notches, and multi-segment DRAs. The integration of a high permittivity insert between the feed and the resonating body element efficiently couples the energy. Figure I-19 illustrates a rectangular-shaped DRA with an underlaid high permittivity insert. Back radiation is a common issue with aperture slot feeds; however, the careful selection of an insert not only improves coupling but also controls back radiation.

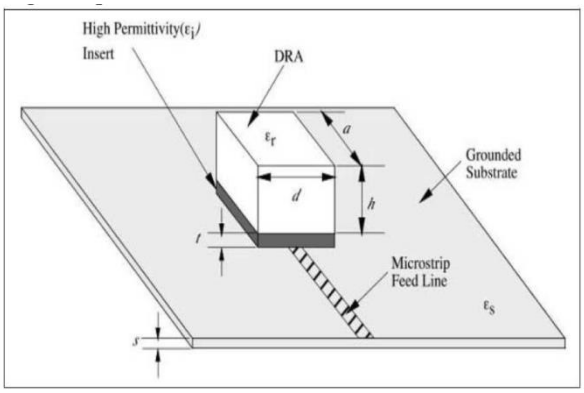

Figure I-19. DRA with high permittivity is inserted in its structure to enhance bandwidth. [61].

I.4.4. Multi resonator

Taking into account distinct design dimensions, multiple elements are configured to resonate at slightly different frequencies. These elements are carefully tuned to either converge, providing a broader bandwidth, or diverge, resulting in the creation of multiple frequency bands [68, 69]. Stacked DRAs excited by a probe, as illustrated in Figure I-20, face a major drawback in the difficulty of accurately positioning and affixing the upper element. A

more effective solution to this challenge lies in employing an appropriate aspect ratio factor, eliminating the need to cut the pieces into different dimensions.

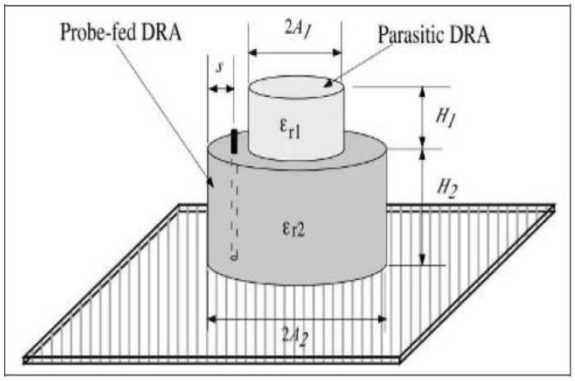

Figure I-20. Utilizing stacked Dielectric Resonator Antennas (DRAs) to combine two closely resonant frequencies for bandwidth enhancement [5].

I.5.Questions relating to the manufacture of DRA

An inherent advantage of Dielectric Resonator Antennas (DRAs) lies in their applicability at millimeter-wave frequencies. However, their fabrication involves a challenging process, and until a highly sophisticated method aided by micromachining becomes widely available, the current fabrication process remains suboptimal. While newer methodologies like Low-Temperature Co-fired Ceramic (LTCC) technology have matured to handle such intricacies, their widespread availability or cost-effectiveness for manufacturing may still be limited. Consequently, alternative methods are often relied upon, albeit with slight variations in the expected results.

When assessing performance, the Dielectric Resonator Antenna (DRA) may encounter the following factors:

- Fabrication tolerance of DRA structure and feed network.
- Precision in DRA cutting and mounting.
- Potential variations in permittivity values.
- Characteristics of adhesive materials used to affix DRA bodies to the ground planes.
- Ted air gaps.

The impact of these factors on fabricated designs can be assessed by consistently comparing theoretical results with measured outcomes.

I.6. Planar resonator structure

I.6.1. Definition

A planar resonator is an electronics device used to accumulate and manipulate electromagnetic signals, typically in the microwave and radio frequency domains. These resonators are usually manufactured using printed circuit board techniques [70].

I.6.2. Different applications of planar resonator

Microstrip planar resonators can be used as antennas [71] or other components such as oscillators, and filters, which are used in microwave integrated circuits (MIC), since the bandwidth of such resonators around their resonant frequencies is very, narrow [72].

I.6.2.1. Planar microstrip filters

The production of microwave filters uses various types of technologies, including planar structure technology. Microwave filters are commonly used in radar systems, satellites, and mobile communications systems. These are generally band pass, or selective bandwidth, devices with stringent insertion loss characteristics. Which refers to the amount of signal power lost when passing through the filter. The construction of these filters involves arranging coupled resonant circuits, also known as resonators, in a manner that achieves a desired frequency-selective transfer function [73].

I.6.2.2. Planar antennas

Since 1970, there has been a significant expansion in the field of micro-antennas or patch antennas, driven by advancements in microelectronics technology and the demand for miniaturization and electronic integration. Microstrip patches are generally configured to radiate in a wide direction, with the main beam perpendicular to the patch element. Figure I-21 gives a visual representation of a rectangular patch antenna. They also perform very well in terms of resonance, polarization, input impedance, and radiation pattern [74].

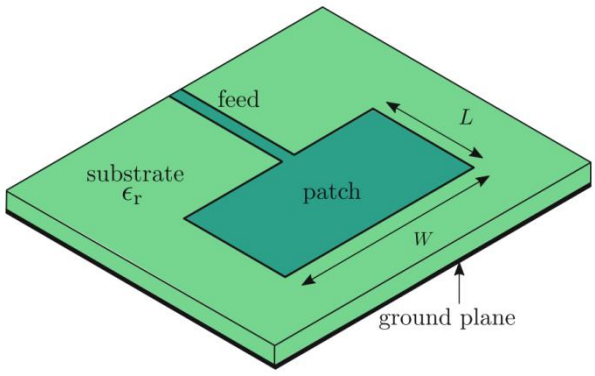

Figure I-21. The rectangular microstrip antenna is composed of a grounded dielectric substrate with a radiating patch mounted on it [74].

I.7.Conclusion

In this chapter, we have set the context for the present study, given that there is currently strong interest from industrial users in dielectric resonator antennas. Firstly, we presented a general study of dielectric resonator antennas, the fundamental characteristics and performance aspects, the different materials used for Dielectric Resonator Antennas (DRAs) and the different excitation techniques most used to excite this type of antennas. We carried out also a detailed study on cylindrical dielectric resonators, which presents the origin of all forms in the literature where a rigorous classification of modes and expressions for the calculation of their frequencies of resonance and their quality factors were developed, and their near-field distributions were demonstrated We also gave a brief presentation on the structure of planar resonators and their applications.

References

[1] Singhwal, S.S., Matekovits, L. and Kanaujia, B.K., 2023. Glueless multiple input multiple output dielectric resonator antenna with improved isolation. *Electronics*, *12*(5), p.1125.

[2] Richtmyer, R.D., 1939. Dielectric resonators. *Journal of applied physics*, *10*(6), pp.391-398.

[3] Shehbaz, M., Du, C., Zhou, D., Xia, S. and Xu, Z., 2023. Recent progress in dielectric resonator antenna: Materials, designs, fabrications, and their performance. *Applied Physics Reviews*, *10*(2).

[4] G. Dubost, S. Zisler, "Les Antennes indépendantes de la fréquence", French, Book, Illustrated edition, Paris, New York: Masson, 1976.

[5] A. Petosa, ―Dielectric Resonator Antenna Handbook‖, Artech House Publishers, 2007.

[6] Abd Rahman, N.A., Mohd Yasin, M.N., Ibrahim, I.M., Jusoh, M., Noor, S.K., Ekscalin Emalda Mary, M.R., Zamin, N. and Nurhayati, N., 2022. A Review of Circularly Polarized Dielectric Resonator Antennas: Recent Developments and Applications. *Micromachines*, *13*(12), p.2178.

[7] Long, S., McAllister, M. and Shen, L., 1983. The resonant cylindrical dielectric cavity antenna. *IEEE Transactions on Antennas and Propagation*, *31*(3), pp.406-412.

[8] Soren, D., Ghatak, R., Mishra, R.K. and Poddar, D., 2014. Dielectric resonator antennas: Designs and advances. *Progress In Electromagnetics Research B*, *60*, pp.195-213.

[9] Long, S., McAllister, M. and Shen, L., 1983. The resonant cylindrical dielectric cavity antenna. *IEEE Transactions on Antennas and Propagation*, *31*(3), pp.406-412.

[10] McAllister, M.W., Long, S.A. and Conway, G.L., 1983. Rectangular dielectric resonator antenna. *Electronics letters*, *19*, p.218.

[11] McAllister, M.W. and Long, S.A., 1984. Resonant hemispherical dielectric antenna. *Electronics Letters*, *20*, pp.657-659.

[12] Mongia, R.K. and Ittipiboon, A., 1997. Theoretical and experimental investigations on rectangular dielectric resonator antennas. *IEEE Transactions on antennas and propagation*, *45*(9), pp.1348-1356.

[13] Tam, M.T. and Murch, R.D., 2000. Circularly polarized circular sector dielectric resonator antenna. *IEEE Transactions on Antennas and Propagation*, *48*(1), pp.126-128.

[14] Ittipiboon, A., Mongia, R.K., Antar, Y.M.M., Bhartia, P. and Cuhaci, M., 1993. Aperture fed rectangular and triangular dielectric resonators for use as magnetic dipole antennas. *Electronics Letters*, *23*(29), pp.2001-2002.

[15] Hong-Twu, C., Yuan-Tung, C. and Shyh-Yeoung, K., 1999. Probe-fed section spherical dielectric resonator antennas. In *Asia Pacific Microwave Conference* (Vol. 2, pp. 2001-2002).

[16] Kishk, A.A., Yin, Y. and Glisson, A.W., 2002. Conical dielectric resonator antennas for wide-band applications. *IEEE Transactions on Antennas and Propagation*, *50*(4), pp.469-474.

[17] Luk, K.M. and Leung, K.W., 2003. Dielectric resonator antennas research studies press Ltd. *Baldock, Hertfordshire, England*.

[18] A. A. Kishk and Y. M. M. Antar: Dielectric Resonator Antennas, from J. L. Volakis: Antenna Engineering Handbook, Chapter 17, 4th ed., McGraw-Hill, USA; 2007.

[19] Lai, Q., Almpanis, G., Fumeaux, C., Benedickter, H. and Vahldieck, R., 2008. Comparison of the radiation efficiency for the dielectric resonator antenna and the microstrip antenna at Ka band. *IEEE Transactions on Antennas and Propagation*, *56*(11), pp.3589-3592.

[20] A. Benomar, «Etude des Antennes à Résonateurs Diélectriques : Application aux Réseaux de Télécommunications,» Thése de doctorat de l'université Tlemcen et Limoges, 2015.

[21] Masse, D.J., Pucel, R.A., Readey, D.W., Maguire, E.A. and Hartwig, C.P., 1971. A new low-loss high-k temperature-compensated dielectric for microwave applications. *Proceedings of the IEEE*, *59*(11), pp.1628-1629.

[22] Peng, Z., Wang, H. and Yao, X., 2004. Dielectric resonator antennas using high permittivity ceramics. *Ceramics International*, *30*(7), pp.1211-1214.

[23] Parida, S., Rout, S.K., Subramanian, V., Barhai, P.K., Gupta, N. and Gupta, V.R., 2012. Structural, microwave dielectric properties and dielectric resonator antenna studies of Sr (ZrxTi1− x) O3 ceramics. *Journal of Alloys and Compounds*, *528*, pp.126-134.

[24] Parida, S., Rout, S.K., Subramanian, V., Barhai, P.K., Gupta, N. and Gupta, V.R., 2012. Structural, microwave dielectric properties and dielectric resonator antenna studies of Sr (ZrxTi1− x) O3 ceramics. *Journal of Alloys and Compounds*, *528*, pp.126-134.

[25] Ullah, U., Ali, W.F.F.W., Ain, M.F., Mahyuddin, N.M. and Ahmad, Z.A., 2015. Design of a novel dielectric resonator antenna using MgTiO3–CoTiO3 for wideband applications. *Materials & Design*, *85*, pp.396-403.

[26] Chaudhary, R.K., Srivastava, K.V. and Biswas, A., 2015. Multi-band cylindrical dielectric resonator antenna using permittivity variation in azimuth direction. *Progress In Electromagnetics Research C*, *59*, pp.11-20.

[27] Ain, M.F., Ullah, U., Othman, M.A., Ahmad, Z.A., Zubir, I.A., Mahyuddin, N.M., Abdullah, M.Z. and Marzuki, A.B., 2014, September. A novel multi-band dual-segment

rectangular Dielectric Resonator Antenna. In *2014 International Symposium on Wireless Personal Multimedia Communications (WPMC)* (pp. 34-37). IEEE.

[28] Mrnka, M. and Raida, Z., 2016, September. Gain improvement of higher order mode dielectric resonator antenna by thin air gap. In *2016 International Conference on Broadband Communications for Next Generation Networks and Multimedia Applications (CoBCom)* (pp. 1-3). IEEE.

[29] Ain, M.F., Hassan, S.I.S., Singh, M., Othman, M.A., Nawang, B., Sreekantan, S., Hutagalung, S.D. and Ahmad, Z.A., 2007. 2.5 GHz BaTiO3 dielectric resonator antenna. *Progress in Electromagnetics Research*, *76*, pp.201-210.

[30] Agrawal, S., Gupta, R.D., Parihar, M.S. and Kondekar, P.N., 2017. A wideband high gain dielectric resonator antenna for RF energy harvesting application. *AEU-International Journal of Electronics and Communications*, *78*, pp.24-31.

[31] Mukherjee, B., 2015. A novel half Hemispherical Dielectric Resonator Antenna with array of slots loaded with a circular metallic patch for wireless applications. *AEU-International Journal of Electronics and Communications*, *69*(12), pp.1755-1759.

[32] Das, G., Sharma, A. and Gangwar, R.K., 2016, March. Two elements dual segment cylindrical dielectric resonator antenna array with annular shaped microstrip feed. In *2016 Twenty Second National Conference on Communication (NCC)* (pp. 1-6). IEEE.

[33] Nasimuddin, K.P., 2007. Antennas with dielectric resonators and surface mounted short horns for high gain and large bandwidth. *IET Microwaves, Antennas & Propagation*, *1*(3), p.723.

[34] Esselle, K.P., 2007. A low-profile compact microwave antenna with high gain and wide bandwidth. *IEEE transactions on antennas and propagation*, *55*(6), pp.1880-1883.

[35] Rana, B., Chatterjee, A. and Parui, S.K., 2015, December. Gain enhancement of a direct microstrip line fed dielectric resonator antenna using FSS. In *2015, IEEE Applied Electromagnetics Conference (AEMC)* (pp. 1-2). IEEE.

[36] A. Petosa, A. Ittipiboon, and Y. M. M. Antar, Rectangular dielectric Resonator
Antennas, chapter 2 - Dielectric Resonator Antennas, Edited by K.M. Luk, K. W.

[37] Zhou, G., Kishk, A.A. and Glisson, A.W., 1993, June. Input impedance of a hemispherical dielectric resonator antenna excited by a coaxial probe. In *Proceedings of IEEE Antennas and Propagation Society International Symposium* (pp. 1038-1041). IEEE.

[38] Junker, G.P., Kishk, A.A., Glisson, A.W. and Kajfez, D., 1994. Effect of an air gap around the coaxial probe exciting a cylindrical dielectric resonator antenna. *Electronics Letters*, *30*(3), pp.177-178.

[39] Junker, G.P., Kishk, A.A. and Glisson, A.W., 1994. Input impedance of dielectric resonator antennas excited by a coaxial probe. *IEEE Transactions on Antennas and Propagation*, *42*(7), pp.960-966.

[40] Cooper, M., Petosa, A., Ittipiboon, A. and Wight, J.S., 1996, August. Investigation of dielectric resonator antennas for L-band communications. In *1996 Symposium on Antenna Technology and Applied Electromagnetics* (pp. 167-170). IEEE.

[41] Pozar, D.M., 2011. *Microwave engineering*. John Wiley & sons.

[42] Petosa, A., Ittipiboon, A. and Thirakoune, S., 2002. Perforated dielectric resonator antennas. *Electronics Letters*, *38*(24), p.1.

[43] Ashraf, K., 2023. A Review Paper on Design and Development of Dielectric Resonator Antenna. *Available at SSRN 4470350*.

[44] Kranenburg, R.A. and Long, S.A., 1988. Microstrip transmission line excitation of dielectric resonator antennas. *Electronics Letters*, *24*, p.1156.

[45] Leung, K.W., Chow, K.Y., Luk, K.M. and Yung, E.K., 1997. Low-profile circular disk DR antenna of very high permittivity excited by a microstrip line. *Electronics Letters*, *33*(12), pp.1004-1005.

[46] Mongia, R.K. and Bhartia, P., 1994. Dielectric resonator antennas—A review and general design relations for resonant frequency and bandwidth. *International Journal of Microwave and Millimeter-Wave Computer-Aided Engineering*, *4*(3), pp.230-247.

[47] Zhou, G., Kishk, A.A. and Glisson, A.W., 1993, June. Input impedance of a hemispherical dielectric resonator antenna excited by a coaxial probe. In *Proceedings of IEEE Antennas and Propagation Society International Symposium* (pp. 1038-1041). IEEE.

[48] Cooper, M., Petosa, A., Ittipiboon, A. and Wight, J.S., 1996, August. Investigation of dielectric resonator antennas for L-band communications. In *1996 Symposium on Antenna Technology and Applied Electromagnetics* (pp. 167-170). IEEE.

[49] Leung, K.W., Lo, H.Y., So, K.K. and Luk, K.M., 2002. High-permittivity dielectric resonator antenna excited by a rectangular waveguide. *Microwave and Optical technology letters*, *34*(3), pp.157-158.

[50] Leung, K.W. and So, K.K., 2003. Rectangular waveguide excitation of dielectric resonator antenna. *IEEE Transactions on Antennas and Propagation*, *51*(9), pp.2477-2481.

[51] Eshrah, I.A., Kishk, A.A., Yakovlev, A.B. and Glisson, A.W., 2005. Excitation of dielectric resonator antennas by a waveguide probe: Modeling technique and wide-band design. *IEEE Transactions on Antennas and Propagation*, *53*(3), pp.1028-1037.

[52] Eshrah, I.A., Kishk, A.A., Yakovlev, A.B. and Glisson, A.W., 2005. Theory and implementation of dielectric resonator antenna excited by a waveguide slot. *IEEE Transactions on Antennas and Propagation*, *53*(1), pp.483-494.

[53] Kajfez, D. and Kishk, A.A., 2002, May. Dielectric resonator antenna-possible candidate for adaptive antenna arrays. In *Proceedings VITEL 2002, International Symposium on Telecommunications, Next Generation Networks and Beyond* (pp. 13-14).

[54] Kajfez, D. and Kishk, A.A., 2002, May. Dielectric resonator antenna-possible candidate for adaptive antenna arrays. In *Proceedings VITEL 2002, International Symposium on Telecommunications, Next Generation Networks and Beyond* (pp. 13-14).

[55] Kajfez, D. and Kishk, A.A., 2002, May. Dielectric resonator antenna-possible candidate for adaptive antenna arrays. In *Proceedings VITEL 2002, International Symposium on Telecommunications, Next Generation Networks and Beyond* (pp. 13-14).

[56] Luk, K.M. and Leung, K.W., 2003. Dielectric Resonator Antennas, Research Studies.

[57] Kajfez, D. and Guillon, P., 1986. Dielectric resonators. *Norwood*.

[58] Kobayashi, Y. and Tanaka, S., 1980. Resonant modes of a dielectric rod resonator short-circuited at both ends by parallel conducting plates. *IEEE Transactions on Microwave Theory and Techniques*, *28*(10), pp.1077-1085.

[59] Kajfez, D. and Guillon, P., 1986. Dielectric resonators. *Norwood*.

[60] Lee, K.F., Luk, K.M. and Tam, P.Y., 1995. Crosspolarisation characteristics of circular patch antennas. *Microstrip Antennas: The Analysis and Design of Microstrip Antennas and Arrays*, *10*, p.87.

[61] Kwai- Man Luk and Kwok-Wa Leung; Dielectric Resonator Antennas Research Studies Press LTD, England.

[62] Leung, K.W., Luk, K.M., Lai, K.Y.A. and Lin, D., 1993. Theory and experiment of a coaxial probe fed hemispherical dielectric resonator antenna. *IEEE Transactions on Antennas and Propagation*, *41*(10), pp.1390-1398.

[63] Kouyoumjian, R.G. and Pathak, P.H., 1974. A uniform geometrical theory of diffraction for an edge in a perfectly conducting surface. *Proceedings of the IEEE*, *62*(11), pp.1448-1461.

[64] Balanis, C.A., 1982. Antenna Theory: Analysis and Design,‖ Harper & Row. *Publishers, New York*.

[65] Best, S.R., 1999. Antenna polarization considerations in wireless communications systems. *Cushcraft Corporation*, *2002*.

[66] Drossos, G., Wu, Z. and Davis, L.E., 1996. Circular polarised cylindrical dielectric resonator antenna. *Electronics Letters*, *32*(4), pp.281-283.

[67] Shum, S.M. and Luk, K.M., 1995. Stacked annular ring dielectric resonator antenna excited by axi-symmetric coaxial probe. *IEEE Transactions on Antennas and Propagation*, *43*(8), pp.889-892.

[68] Kishk, A.A., Glisson, A.W. and Junker, J.P., Study of broadband dielectric resonators. In *Proceedings of the 1999 Antenna Applications Symposium* (pp. 45-68).

[69] Kishk, A.A., Ahn, B. and Kajfez, A.D., 1989. Broadband stacked dielectric resonator antennas. *Electronics Letters*, *18*(25), pp.1232-1233.

[70] Balanis, C.A., 2016. *Antenna theory: analysis and design*. John Wiley & sons.

[71] James, J.R. and Hall, P.S. eds., 1989. *Handbook of microstrip antennas* (Vol. 1). IET.

[72] Michalski, K.A. and Zheng, D., 1992. Analysis of microstrip resonators of arbitrary shape. *IEEE transactions on microwave theory and techniques*, *40*(1), pp.112-119.

[73] Wyndrum, R.W., 1965. Microwave filters, impedance-matching networks, and coupling structures. *Proceedings of the IEEE*, *53*(7), pp.766-766.

[74] Du Preez, J. and Sinha, S., 2016. *Millimeter-wave antennas: configurations and applications*. Springer.

Chapter II:

Dual port MIMO Cylindrical Dielectric Resonator Antenna (CDRA) at 5.8 GHz for WLAN Applications

II.1. Introduction

As part of the search for higher speeds in wireless communication networks, MIMO technology has appeared as a solution to satisfy the increasing requirements for high-speed data transmission, wide-area coverage, and reliability [1-2-3].

Recently in wireless communication, dielectric resonator antennas (DRA) have been chosen as the best candidate for MIMO antennas due to the absence of surface waves, high radiation efficiency, high gain, low cost, various shapes, and feed mechanisms [4-6]. Several research papers into DRA concepts for WLAN and ISM applications at 5.8GHz have been published in the literature, with different methods of excitation [7-10]. Since DRAs offer lower levels of mutual coupling in MIMO systems, [11, 12], they have been widely proposed for wireless communication applications [11-14]. DRA has three basic shapes, which are rectangular, cylindrical, and hemispherical geometries [15].

The single-element MIMO antenna design is an interesting concept that consists of a single antenna element with multiple ports to realize MIMO capabilities [16]. Single-element MIMO is a promising application for small portable devices in which the size and price are significant considerations, as it may reduce the size and cost of the design. Numerous MIMO antenna systems based on a single patch element have been proposed in the literature. These devices have proven their capability to achieve particularly high gain, wide bandwidth, high port-to-port isolation, and omnidirectional radiation patterns [17, 18].

DRAs have also been used in single-element MIMO antennas. Roslan et al. [19] have developed a single DRA MIMO for 2.60 GHz Long Term Evolution (LTE) applications. Two orthogonal modes were excited using coplanar waveguide (CPW) and coaxial probe feed. Good performance was achieved in terms of antenna gain (4.97dB), isolation (-20dB), and bandwidth (2.40–3.09 GHz). However, the use of shorting pins and metallic strips results in a complex configuration. Varshney et al. [20] have proposed a DRA MIMO antenna with pattern diversity in which the radiating mechanism is based on the excitation of the $HE_{11\delta}$ and $TM_{01\delta}$ orthogonal modes. The antenna provides a maximum gain of 6.5 dBi. Abdalrazik et al. [21] have presented a high-gain DRA MIMO design for X-band applications. A hybrid combination of a probe and two microstrip lines was used as a feeding mechanism. The radiation concept is based on the excitation of three modes.

This work studies the optimization steps for designing a cylindrical DR antenna-based MIMO antenna with dual ports to operate at 5.8GHz for WLAN applications. The suggested antenna contains only a single radiator with two coaxial cables feed, compared to Traditional

MIMO systems typically include multiple radiators. Therefore, with this new design the size of the antenna is significantly reduced. The proposed antenna is designed and simulated using HFSS software. The following sections are devoted to parametric studies, simulated and measured results, as well as the performance evaluation of the proposed antenna.

II.2. Geometric design of the proposed antenna

Figure II-1 shows the geometry of our proposed antenna which consists of cylindrical DRA. The dimensions of the proposed cylindrical DRA have height H=7.3mm and radius R1=5mm. The dielectric constant of the material used for the proposed antenna structure is ε_r=15. The CDRA was placed on a metal ground plane of dimensions 50mm × 50mm × 3mm and has been excited by two coaxial probes a 50 Ω which touches the end of the CDRA as shown in Figure II-1 Port 1, with an internal conductor of radius (r_f), is situated along the x-axis at the edge of the DR at a height (h_{f1}). Port 2, at a height (h_{f2}), is localized on the y-axis near the edge of the dielectric resonator at an eccentric distance (R2) and angular offset (θ), resulting in the excitation of the HE_{x11} and HE_{y11} radiation modes, respectively. The geometric dimensions of the designed MIMO antenna are shown in Table II.1.

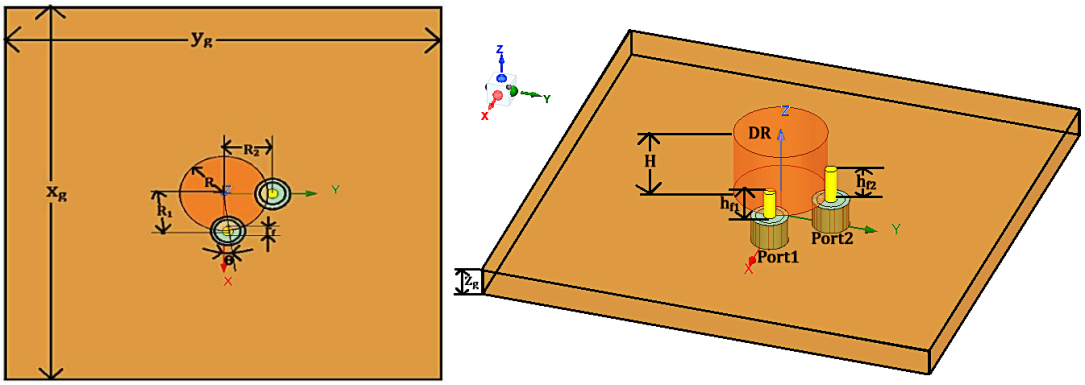

(a) (b)

Figure II-1. Dimensional of the proposed antenna (a): top view, (b): 3D view.

Table II.1. Geometric parameters of the antenna structure.

Parameter	***Value***	***Parameter***	***Value***
X_g	*50mm*	h_{f2}	*3mm*
Y_g	*50mm*	R_1	*5.6mm*
Z_g	*3mm*	R_2	*5.1mm*
R	*5mm*	θ	*5°*
H	*7.3mm*	r_f	*0.6mm*
h_{f1}	*3.8mm*		

II.3. Simulation and discussion of the results.

II.3.1. Antenna optimization

To design an optimized antenna, a change of position was first carried out by varying the position for each port, and in the second step, a parametric study was conducted by varying the h_f height for the two ports.

- **Impact of changes in probe height variation**

In cylindrical dielectric resonator antennas (CDRAs), adjusting the height of the probe feed line enables the optimization of radiation characteristics, ultimately leading to enhanced antenna performance. Initially, the antenna is developed with a single coaxial probe feed port at the top of the cylindrical DR Figure II-2a.

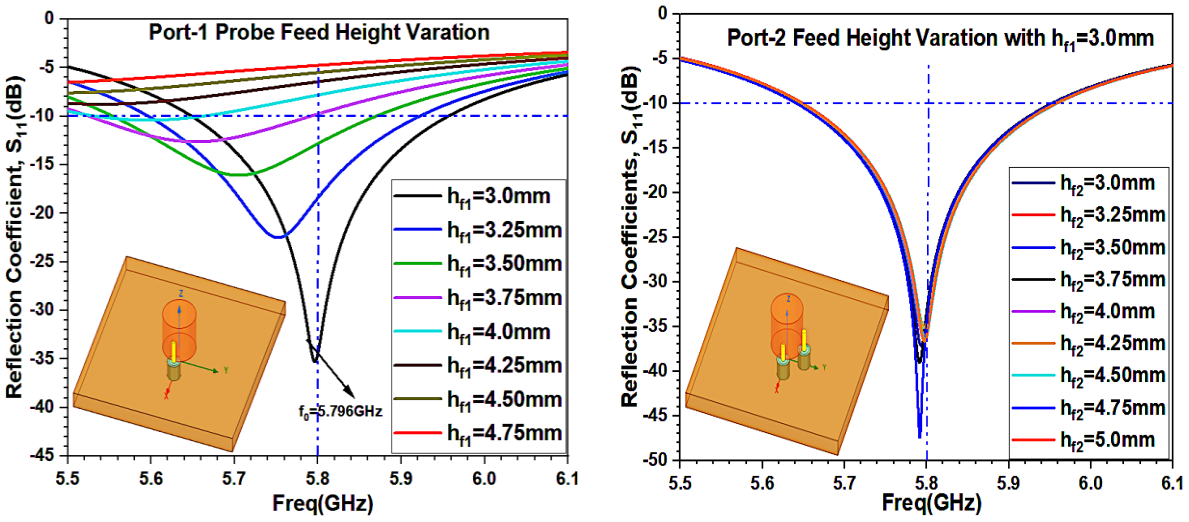

(a) (b)

Figure II-2. Simulated reflection coefficient for different Port 2 and 1 heights for (a) Single port CDRA; and (b) Two-port CDRA.

Figure II-2a. Depicts an assessment of the reflection coefficient as a function of the varying feed height (h_{f1}) for Port 1, ranging from 3.0 mm to 4.75 mm. At the desired resonance frequency of 5.8 GHz, Port 1 exhibits optimal performance with a reflection coefficient of -35.39 dB, achieved at a frequency of 5.796 GHz when the feed line height is set to h_{f1}=3.0mm, with an offset angle θ =0°.

To achieve a linear polarization and the MIMO functionality and also to get high isolation between the ports, the DR is excited with the help of two orthogonal coaxial cable feed lines with a 90◦ phase difference and are printed close to the perimeter of the resonator as shown in Figure II-2b.

Figure 3b presents the reflection coefficient for different Port 2 heights (h_{f2}) with h_{f1} fixed at3.0mm**.**It can be noticed that Port 2 height improves the reflection and helps to fine-

tune the resonant frequency to 5.8GHz with improved impedance matching. For a probe height h_{f2}=4.75 mm, a reflection coefficient of S_{11}= –47.40 dB at 5.792 GHz is obtained, while for h_{f2}=4.75 mm the reflection coefficient, S_{11}= –47.40 dB at 5.791 GHz. Further, it is noticed that the probe height h_{f2}=3.75 mm of Port 2 achieves approximately the same reflection coefficient, S_{11}= -39.05 dB at 5.796 GHz which is approximately the same as that with probe height of Port 1(h_{f1}=3.0 mm). Therefore, probe heights of 3.0 mm and 3.75 mm, for Port 1 and Port 2, respectively, are the best choice for better reflection coefficients.

- **Isolation and Impedance Matching Improvement using Port1 Angular Shift (θ)**

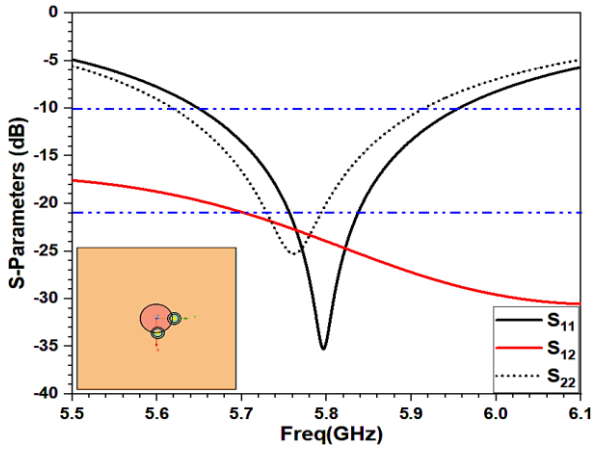

Figure II-3. S-parameters of two orthogonal ports with offset angle θ =0°.

Figure II-3 shows the simulated S-parameters of the dual probe-fed CDRA for θ =0°.To preserve the orthogonally between the two ports, the angular position shift of Port 1 is varied within a sweep range of ±10°. Better isolation coefficient (S_{12}/S_{21}) and improved impedance matching results are achieved for a small change in the value of angular position (θ=5°) which still preserves the dual orthogonally mode characteristics.

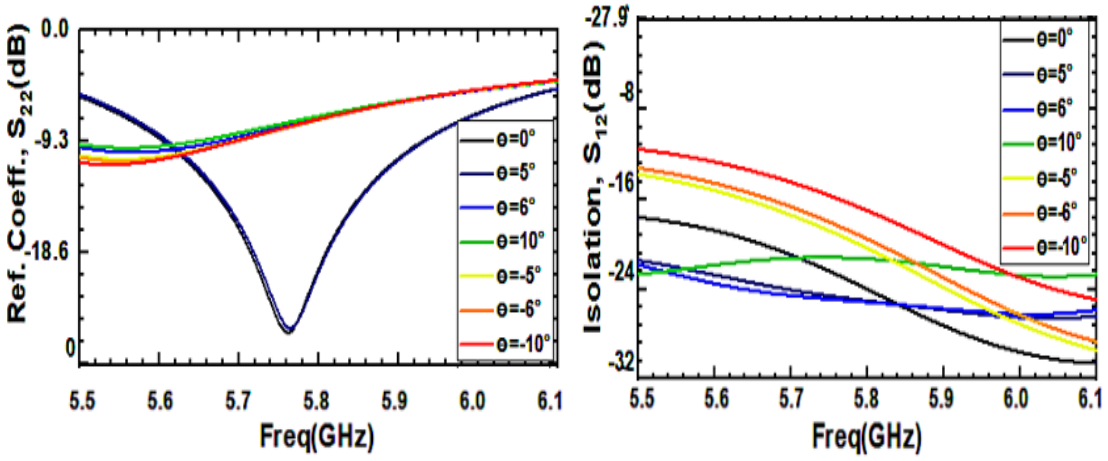

(a) (b)

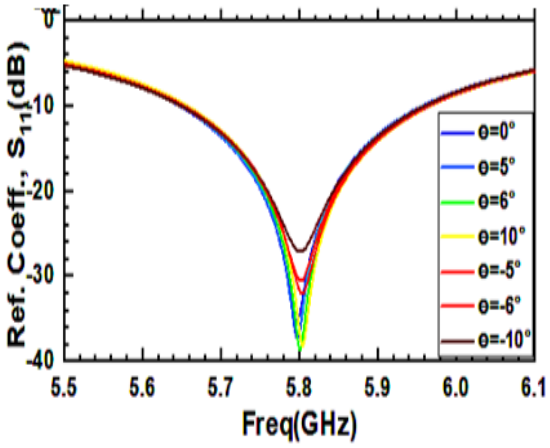

(c)

Figure II-4. Comparison of the simulated reflection coefficient by changing the feed position of port 1 for different rotation angles θ.

Figure II-4 illustrates the comparison of the reflection coefficient for different angles of rotation of port 1 along the periphery of the CDR base and keeping the position of port 2 constant. The optimum value chosen for the angle of the port 1 position is θ= 5°.

- **Effect of Port 1 Probe Height (h_{f1}) Variation**

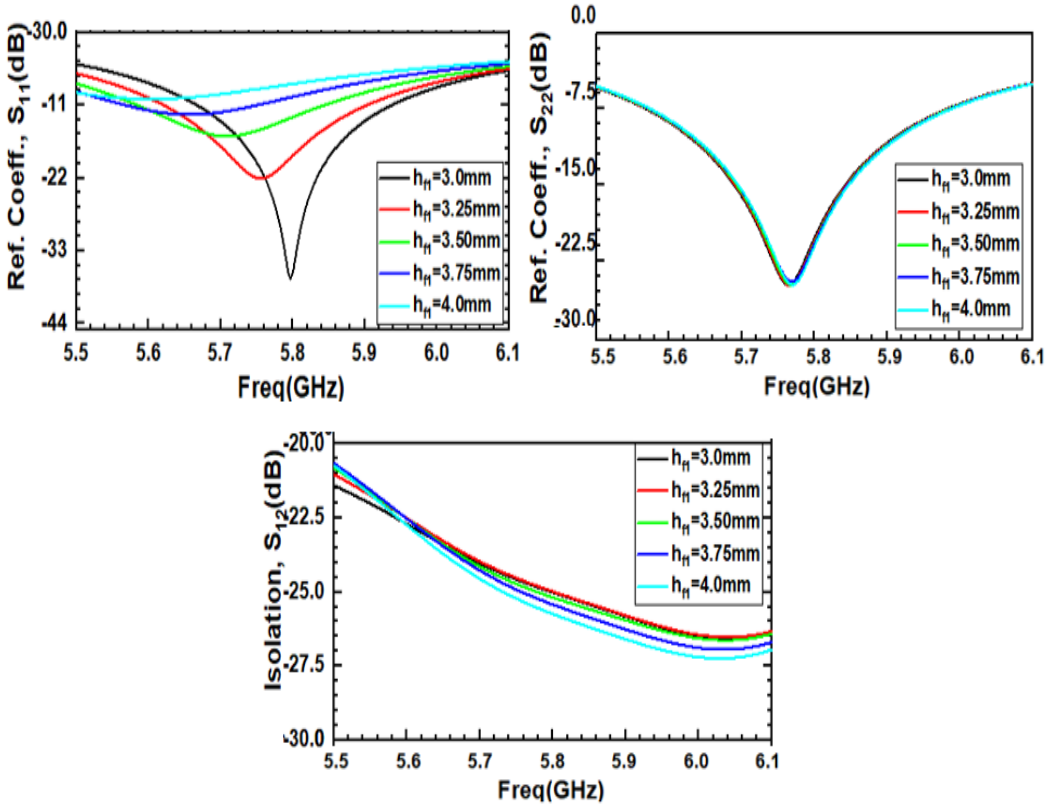

Figure II-5. Comparison of simulated reflection coefficient for different feed heights of Port1.

Figure II-5 depicts the effect of varying feed length (h_{f1}) on the reflection coefficient. From this figure, it can be observed that adjustments to the feed length result in corresponding

changes in the reflection coefficient and operating frequency band. The desired results in terms of resonance frequency (5.8 GHz) and best impedance matching are obtained for h_{f1}=3 mm.

- **Effect of Port 2 Off-Center (Radial) Distance (R_1) Variation**

The effect of Port 1 position off-centre distance (R_1) on the mutual coupling (isolation) coefficient (S_{12}) is examined by increasing R_1 from 4.2 to 5.6 mm.

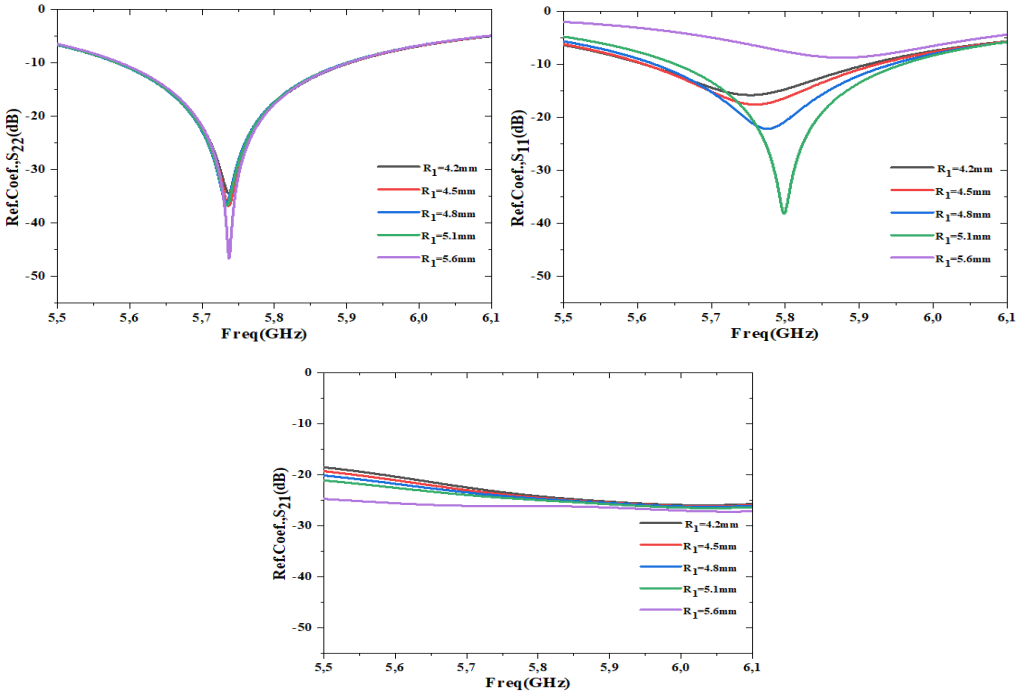

Figure II-6. The simulated reflection coefficients for different distances R2 from the center of the resonator.

The two-port configuration S-parameters for different Port 1 off-centre distances are illustrated in Figure II-6.The optimal performances (S_{11}= –40 dB, S_{12}= –25 dB) are achieved for R_1=5.1 mm at the resonant frequency of 5.8GHz.

II.4. Validation Results of the Proposed MIMO Antenna and Discussion

A simulation and analysis of the proposed dual-port single-element CDRA MIMO antenna design is carried out using Ansoft HFSS software. For improved antenna performances, the positioning and heights of the two probe feeds have been carefully optimized. This serves to improve the antenna radiation efficiency and gain in addition to enhancing port-to-port isolation. The radiating mechanism within the proposed design is attributed to the excitation of the orthogonal modes HE_{x11} and HE_{y11} in the CDRA due to the feeding technique. In this setup two probe feed lines can excite different modes, such as TE and TM modes, which then interact and combine to form a hybrid mode. The 90° space

between the feed lines helps to create a phase difference between the fields, which enhances the hybrid mode excitation. The fields from each feed line interact and combine to form a hybrid mode. The 90° space between the feed lines helps to create a phase difference between the fields, which enhances the hybrid mode excitation. So as conclusion using two probe feed lines in the periphery of the CDRA with a 90° space between them can indeed excite hybrid modes. This configuration is known as a dual-feed, which can create a hybrid mode by combining the fields from each feed. The radiating mechanism within the proposed design is attributed to the excitation of the orthogonal dual hybrid modes in the CDRA. The hybrid mode analysis of the CDR MIMO antenna is conducted by analyzing the electric field distribution, megnatectic field distribution, and surface current density field distributions. The antenna is first excited by port 1 and then excited by port 2. These excitations will generate the TE and TM modes. When the proposed antenna is excited by two ports simultaneously, then two TE and TM modes combine to generate hybrid modes (HE) at the resonating frequency of 5.8 GHz. The two orthogonal polarization planes of the E-field, H-field, and surface current density vector field distributions due to Port 1 and Port 2 at a frequency of 5.8 GHz are represented in Figure II-7.

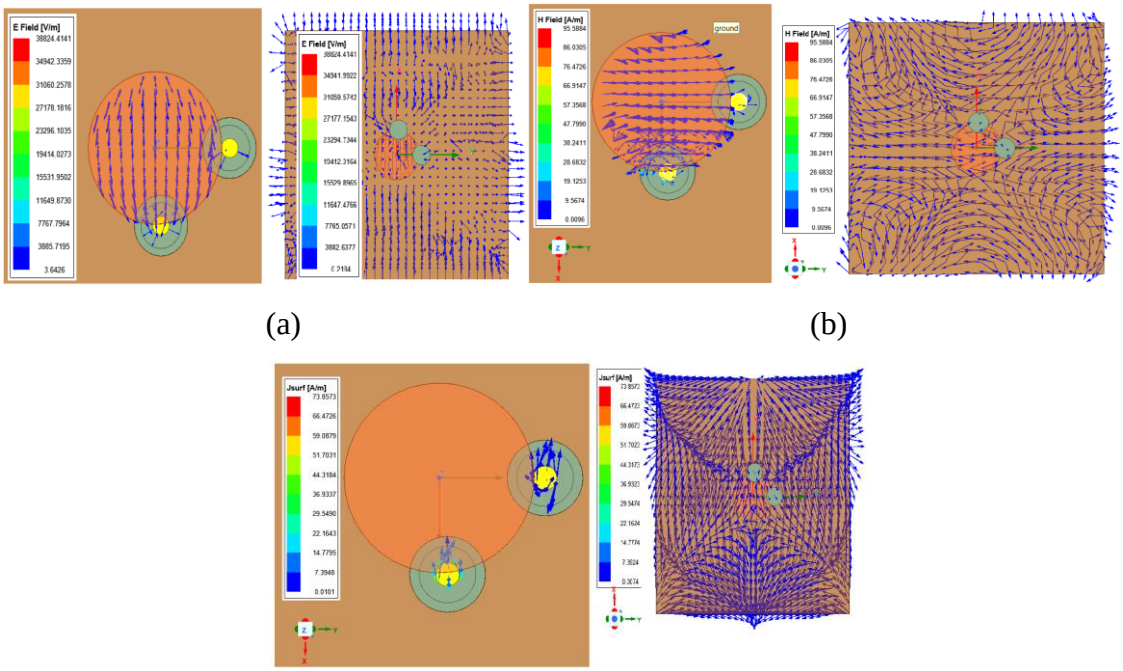

(a) (b)

(c)

Figure II-7. Simulated field distribution at 5.8 GHz (a) E-field distribution top and side view due to Port 1 and port 2 hybrid mode excitation, (b) H-field distribution top view and side view due to both ports, and (c) Surface current density distribution top and side view due to both ports.

It has been observed that the port 1 and port 2 excitations separately set the upper bound and the lower bound of the E-field, H-field, and surface current distribution magnitudes at the resonance frequency of 5.8 GHz. For hybrid modes, the fields never cross these upper and lower field magnitude boundaries, as shown in the Figure II-7 data boxes. The E-field and H-fields exist at an angle of 90°. It is noticed that no current exists on the CDR, and the minimum current amount exists at the bottom.

A prototype of the antenna design is fabricated and measured to validate the simulation results. Figure II-8 presents a photograph of the realized antenna prototype. Simulated and measured S-parameters for the realized CDRA MIMO antenna are shown in Figure II-9.

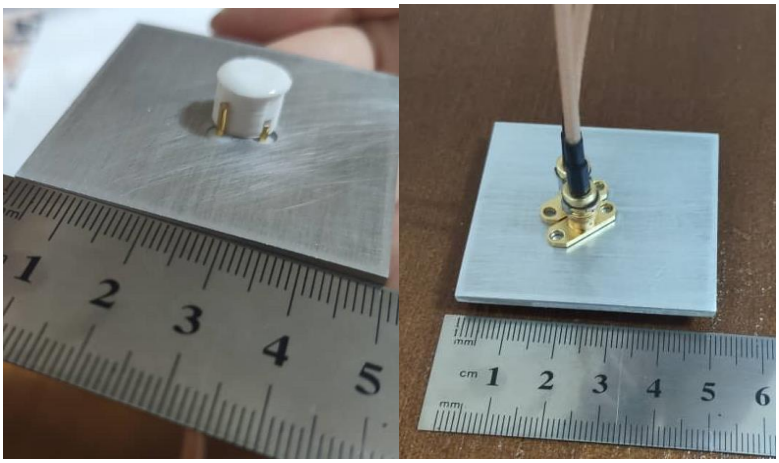

(a) (b)

Figure II-8. Prototype of the realized antenna: (a) 3D view and (b) bottom view.

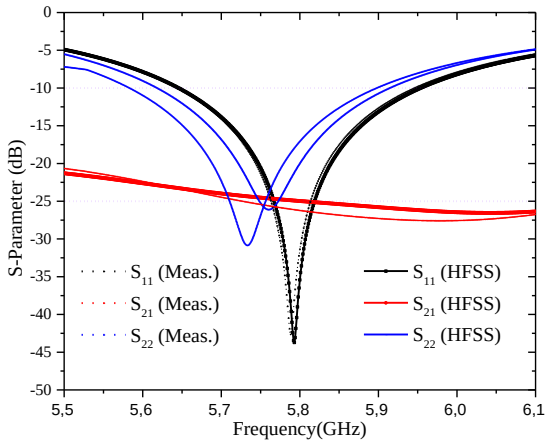

Figure II-9. Simulated and measured S parameters of the realized MIMO antenna.

The simulated and measured results are found to agree within the operating band. Good impedance matching is achieved and the measured reflection coefficients S_{11} and S_{22} parameters are around -45 and -22 dB at 5.8 GHz, respectively. The proposed design exhibits good isolation between the two ports (S_{21}) at the desired band that exceeds 25 dB.

The gain plot of the proposed CDRA MIMO antenna is shown in Figure II-10 compared with measurements. Good agreement is observed at the operating frequency. The measured gain value is about 8.91 and 8.97 dB_i for Port 1 and Port 2, respectively, at 5.8GHz.

The radiation efficiency plot of the proposed MIMO antenna is shown in Figure II-11. It can be observed that for both ports the proposed MIMO antenna achieves a measured radiation efficiency greater than 90% at the resonant frequency, for both results (simulated and measured).

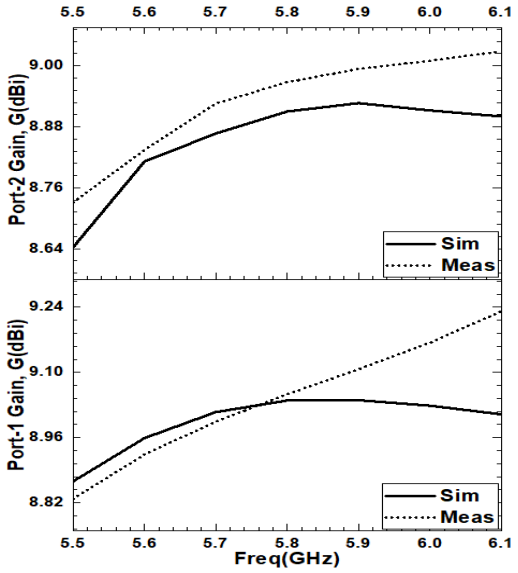

Figure II-10. Simulated and measured antenna gain of the realized MIMO antenna.

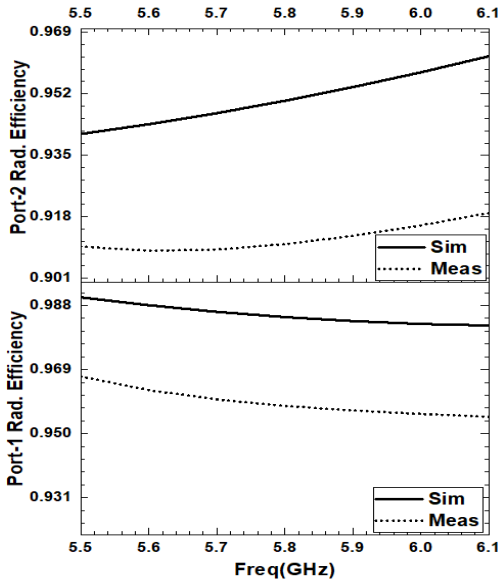

Figure II-11. Radiation efficiency plot of the proposed CDR MIMO antenna.

Figure II-12 illustrates the measured and simulated normalized radiation pattern of the proposed dual port MIMO antenna for both ports in different planes at 5.8 GHz. The antenna exhibits typical broadside radiation patterns. Port 1 and Port 2 possess orthogonal polarization planes, ensuring high port-to-port isolation. In the XY-plane, a bidirectional pattern is observed, while in the XZ and YZ planes, the radiation pattern is omnidirectional for both ports. It is noteworthy that the proposed antenna design maintains a cross-polarization value less than -10 dB below the co-polarization value for each port. This is achieved by excitation the orthogonal hybrid modes HE_{11}^{x} and HE_{11}^{y} in the CDRA with the two probe feed lines spaced 90° apart. The 90° port spacing is the key factor that allows to achieve cross-polarization levels lower than the co-polarization levels. These orthogonal hybrid modes have their electric and magnetic field components oriented in a mannar that minimizes the cross-polarization, resulting in the cross-polarization levels being lower than the co-polarization levels.

This low cross-polarization indicates that the antenna effectively suppresses radiation in unwanted polarization planes, enhancing its overall performance. Both simulated and measured results demonstrate a similar radiation pattern, indicating good agreement between theoretical predictions and practical measurements. Any minor discrepancies between the two might be attributed to factors such as manufacturing tolerances or measurement errors.

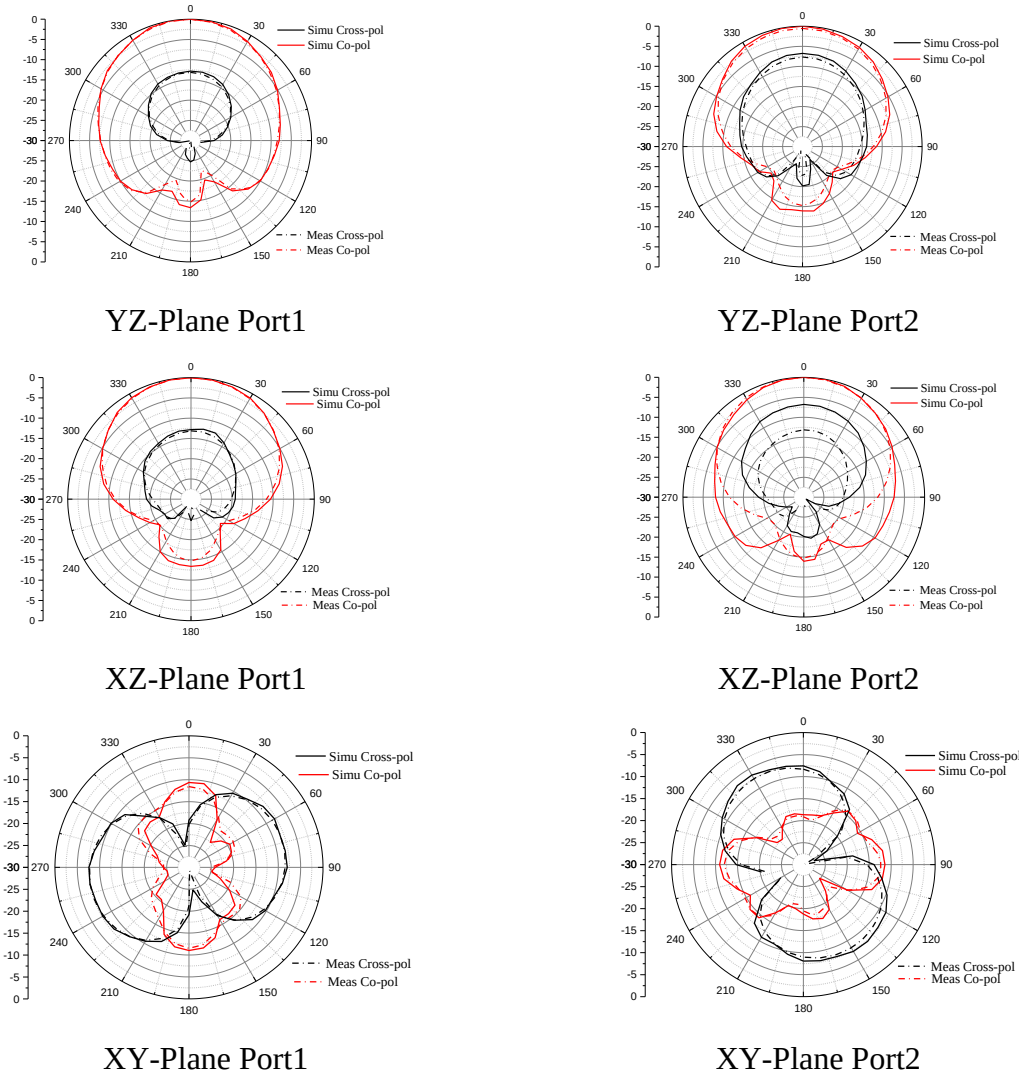

Figure II-12. Simulated and measured radiation patterns at 5.8 GHz in different planes.

The applied two-port excitation technique results in dual-hybrid modes $HE^{x}_{11\delta}$ and $HE^{y}_{11\delta}$. The port angular positions and radial distances are varied to control the E-field distribution within the CDR. This adjustment results in an axial ratio (AR) value well above 26.5 dB in the whole frequency band 5.5–6.1GHz as illustrated in Figure II-13. This guarantees that the proposed antenna is linearly polarized as AR is above 3 dB. The orthogonally of the electric field vectors is preserved with the help of approximately orthogonal ports as already shown in Figure II-7.Therefore; the proposed antenna is

orthogonal and linearly polarized.

The CDR-MIMO antenna front-to-back ratio (FBR) over the full-frequency span of interest is illustrated in Figure II-14. It is noticed that at resonance frequency 5.8 GHz the value of FBR is 9.72 dB. The lowest value of FBR is 9.66 dB.

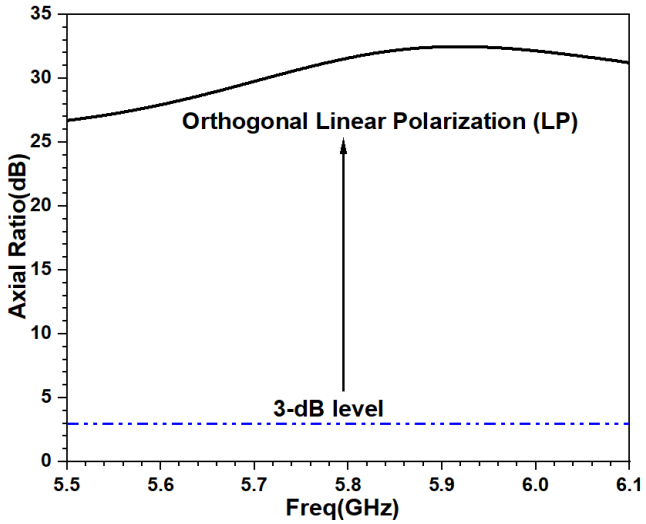

Figure II-13. Axial ratio plot of the proposed antenna.

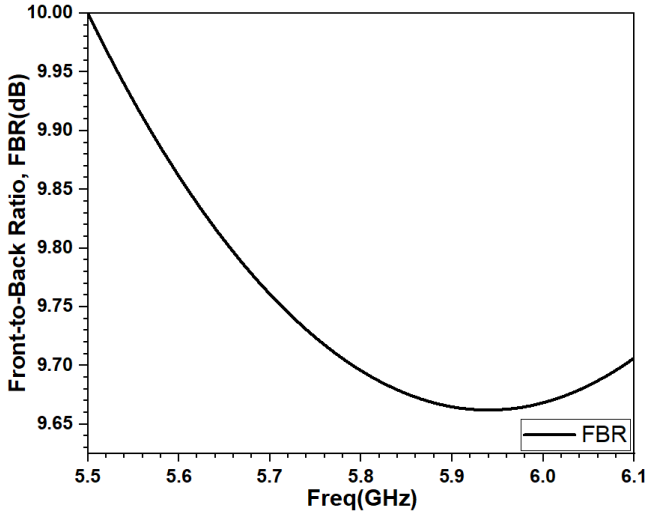

Figure II-14. CDR-MIMO antenna FBR.

II.5.MIMO Performance

In this section, we will introduce the various metrics to estimate the performance of the MIMO antenna, including envelope correlation coefficient (ECC), mean effective gain (MEG), diversity gain (DG), Total active reflection coefficient (TARC), and channel capacity loss (CCL).

II.5.1. Envelope Correlation Coefficient (ECC) and Diversity Gain (DG)

The correlation coefficient describes how much the communicating branches are correlated or isolated from each other [22]. ECC-measured values were obtained by using the following Equation [23].

$$ECC = \frac{\left|S_{11}^{*}S_{12} + S_{21}^{*}S_{22}\right|^{2}}{\left(1-\left(|S_{11}|^{2}+|S_{21}|^{2}\right)\right)\left(1-\left(|S_{22}|^{2}+|S_{12}|^{2}\right)\right)} \qquad \text{(II-1)}$$

In the MIMO antenna, system the amount of improvement obtained from a multiple antenna system relative to a single system gives the Diversity Gain (DG) [22, 23]. The DG can be represented by the following equation.

$$DG = 10\sqrt{\left(1-ECC^{2}\right)} \qquad \text{(II-2)}$$

Figure II-13 presents Simulated Diversity Gain and ECC versus frequency of the proposed MIMO CDRA. The calculated ECC using the S-Parameters is less than 0.002 in the desired band, which is good for wireless applications. The acceptable value of Diversity gain (DG) for MIMO applications must be almost 10 dB. From this figure, it can be observed a good diversity gain for the proposed MIMO antenna.

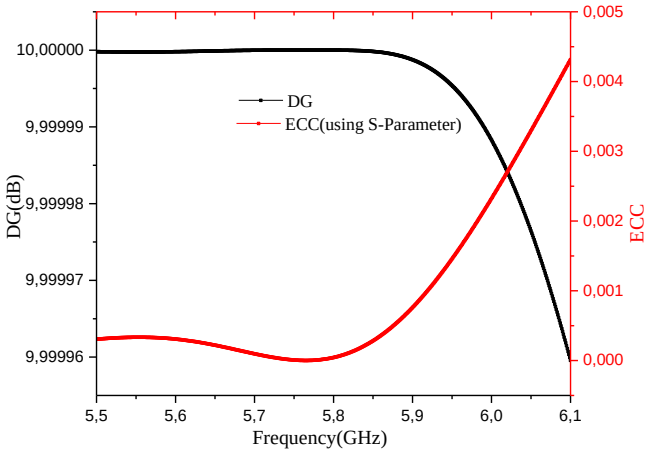

Figure II-15. Simulated Diversity Gain and ECC versus frequency of the proposed MIMO CDRA.

II.5.2. Channel capacity loss (CCL)

Channel Capacity Loss (CCL) is another crucial performance measure for MIMO systems, as it gives an idea of the maximum achievable message transmission rate limit within which the signal can be delivered reliably through the communication system. The tolerable limit for capacity loss is set at 0.4 bits per second per Hertz (b/s-Hz). The CCL can be calculated using the following formula [22].

$$C_{\text{loss}} = -\log_2 \det\left(\alpha^R\right) \qquad \text{(II-3)}$$

Where α^R is a correlation matrix for the MIMO antenna with two-ports.

$$\alpha^R = \begin{bmatrix} \alpha_{11} & \alpha_{12} \\ \alpha_{21} & \alpha_{22} \end{bmatrix} \qquad \text{(II-4)}$$

Figure II-14 gives the simulated CCL of the proposed CDRA MIMO antenna. From this figure, it can be seen that covers the acceptable value at the desired band.

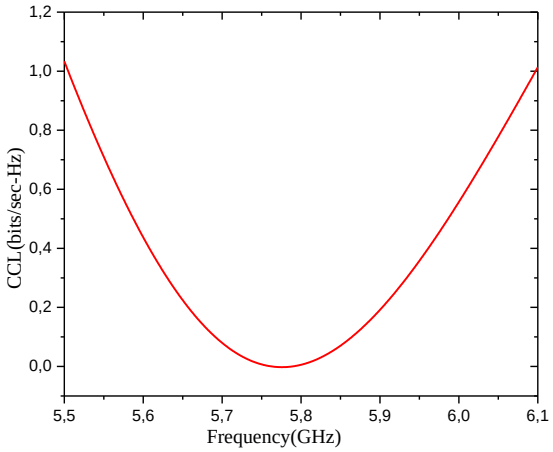

Figure II-16. Simulated channel capacity loss versus frequency of the proposed MIMO CDRA.

II.5.3. Total Active Reflection Coefficient (TARC)

The total active reflection coefficient (TARC) is an important performance parameter for MIMO systems, which defines the characteristics of the MIMO antenna system. It is quantified as the ratio of reflected incident power for the MIMO antenna system [22]. TARC can be determined using the following equation:

$$TARC = \frac{\sqrt{\left(\left(\left|S_{11} + S_{12}e^{j\theta}\right|^2\right) + \left(\left|S_{21} + S_{22}e^{j\theta}\right|^2\right)\right)}}{\sqrt{2}} \qquad \text{(II-5)}$$

Where θ is the difference in phase between the excitation of the MIMO antenna.

Figure II-15 shows the calculated TARC for the proposed MIMO antenna with different angles of θ from 0° to 180° with steps of 30°. It is obvious from this figure that around 5.8 GHz the TARC value is less than -22 dB.

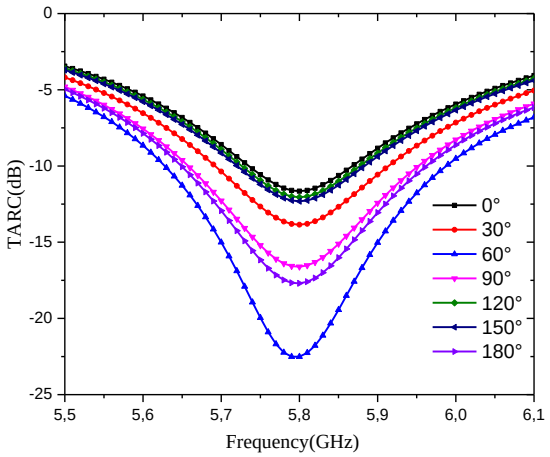

Figure II-17. Total active reflection coefficient (TARC) of the proposed antenna when changed from 0 to 180 degrees.

II.5.4. Mean Effective Gain (MEG)

The MEG (Mean Effective Gain) is one of the five crucial diversity parameters used to assess MIMO antennas. It quantifies the gain performance of an antenna while accounting for environmental effects. By taking into account the radiation efficiency of the two antenna ports, the MEG for both Port 1 and Port 2 can be calculated using the following equations [22, 24].

$$MEG_1 = 0.5\eta_{1,\text{rad}} = 0.5\left[1-\left|S_{11}\right|^2-\left|S_{12}\right|^2\right] \quad \text{(II-6)}$$

$$MEG_2 = 0.5\eta_{2,\text{rad}} = 0.5\left[1-\left|S_{12}\right|^2-\left|S_{22}\right|^2\right] \quad \text{(II-7)}$$

$$MEG_i = \int_0^{2\pi}\left[\frac{\Gamma}{1+\Gamma}E_\theta\left(\frac{\pi}{2},\varphi\right)+\frac{1}{1+\Gamma}E_\varphi\left(\frac{\pi}{2},\varphi\right)\right] \quad \text{(II-8)}$$

In practical applications, it is desirable for the MEG (Mean Effective Gain) to be less than -3dB. The variation plot of the MEG as a function of frequency for the proposed MIMO antenna is presented in Figure II-16. From this figure, it is evident that the MEG performance remains below -3dB across the desired frequency band of 5.8GHz.

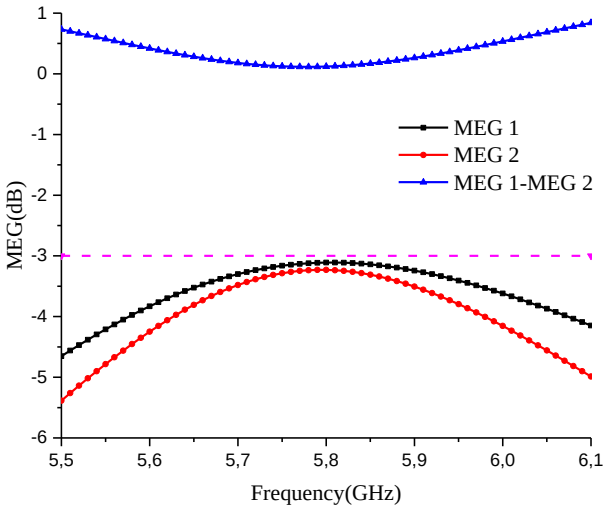

Figure II-18. Mean effective gain (MEG) of the proposed antenna.

Table II.2 compares the size, gain, DR shape, frequency range, bandwith, and isolation of the proposed MIMO antenna with some recently published works. It can be concluded that the proposed CDR MIMO antenna has a smaller size, high gain, and easy fabrication compared to the designs reported in the pieces of literature.

Table II.2. State-of-the-art Comparison with the Proposed Design.

Ref.	**f_0 (GHz)**	**DRA Type & Size (mm^3)**	**DR ε_r**	**Overall Antenna Size(mm^3)**	**Used Feed Type**	**Offset Angle (ɵ)**	**FBW (GHz)**	**Gain (dBi)**	**DRA Mode**	**S_{12}/ S_{21} (dB)**	**Polar.**	**Base Material**
[12] 2021	3.70	-----	------	66.3× 40× 10.8	Dual CPW-feed ports	NO	3.3–4.2	2.5	$HE^{x}_{11\delta}$ and $HE^{y}_{11\delta}$	<–15	CP	FR-4 ε_r=4.4 h=0.8 mm
[21] 2017	9.0–10.0	Rect. a × b× c = 31.5×17.8 ×13.3	10.2 Roger RT 6010	**56**.6× 56.6× 14.09	Three ports (two MSL-feed ports to feed DRA and one coax-feed port)	NO	9.12–10.0(P1), 8.97–9.84(P2), 8.90–11.5(P3)	10.25 (P1) 9.65 (P2) 9.55 (P3)	$TE^{x}_{\delta 21}$ $TE^{x}_{3\delta 2}$ and $TE^{y}_{2\delta 1}$	<–20	NG	RT5880 ε_r=2.2 h=0.79mm
[25] 2023	2.9	Cyl. $2\pi R^2 \times H = 2\pi \times 15^2 \times 13$	9.8 Alumina (Al_2O_3)	126× 78× 13.8	Dual MSL-feed	NO	2.8–3.05	5.50	$HE^{x}_{11\delta}$ and $HE^{y}_{11\delta}$	<–30	CP	FR-4 ε_r=4.4 h=0.8 mm

[26] 2018	2.50	Cyl. $2\pi R^2 \times H = 2\pi \times 15^2 \times 15$	9.8 Alumina (Al_2O_3)	50× 50× 16.6	Port1 : MS-feed Port2 : conformal CPW-stripline feed	NO	3.17–3.60	5.50	$HE^{x}_{11\delta}$ and $HE^{y}_{11\delta}$	<–25	CP	FR-4 ε_r=4.4 h=1.6mm
[27] 2016	2.60	Rect. a × b× d = 20×49×6	NG	80× 80× 7.6	------	NO	2.56–2.64	NG	TE^{x}_{111} and TE^{y}_{113}	<–20	NG	FR-4 ε_r=4.6 h=1.6 mm
[28] 2016	5.20	Cyl. $2\pi R^2 \times H = 2\pi \times 7 \times 8.5$	9.8 Alumina (Al_2O_3)	50× 50× 10.1	Dual MSL-feed	NO	4.9–5.5	4.50 (P1) 5.0 (P2)	$HE^{x}_{11\delta}$ and $HE^{y}_{11\delta}$	<–30	NG	FR-4 ε_r=4.6 h=1.6mm
[29] 2020	5.60	Cyl.	9.8 Alumina (Al_2O_3)	50× 50× 10.6	coplanar waveguide (CPW) and aperture-coupled feeding	NO	5.39–5.85 (P1) And 5.46–5.85(P2)	6.6 (P1) 3.9(P2)	$HE^{x}_{11\delta}$ and $HE^{y}_{11\delta}$	<–33	NG	FR-4 ε_r=4.6 h=1.6mm
[30] 2009	3.20	Rect. L ×B×H = 18×18×29	10 Alumina	205× 205× 32	Dual Coax feed	NO	2.7–3.8	2.1(3.0GHz) 6.1(3.7GHz)	TE^{x}_{111} and TE^{y}_{113}	<–15	CP	PEC h=3.0mm
[31] 2017	3.20	Cyl. $2\pi R^2 \times H = 2\pi \times 11^2 \times 23$	9.8 Alumina	55× 55× 24.6	Single MS-feed	NO	2.82–3.83, 2.75–3.52	5.50	$HE^{x}_{11\delta}$ and $HE^{y}_{11\delta}$	-----	CP	FR-4 ε_r=4.6 h=1.6 mm
[32] 2019	2.45	Rect. L ×B×H = 18×18×29	9.8 Alumina	50× 50× 19.6	Single right angled conformal MS-feed	NO	2.13–2.77	5.0	TE^{x}_{111} and TE^{y}_{113}	-----	LHCP	FR-4 ε_r=4.6 h=1.6mm
[33] 2022		Cyl. $2\pi R^2 \times H = 2\pi \times 6.5^2 \times 4$	9.8 Alumina (Al_2O_3)	50× 60× 5.6	MSL-feed 1×3 element	No	1.5, 2.4, 5.8	2.8(P1) 3.4(P2) 5.8(P3)	$HE^{x}_{11\delta}$ and $HE^{y}_{11\delta}$	-----	------	FR-4 ε_r=4.3 h=1.6mm

					array							
This Work	5.80	Cyl. $2\pi R^2 \times H = 2\pi \times 5^2 \times 7.3$	15	50× 50× 10.3	Dual Coax Probe	±10°	5.65–5.97	9.03(P1) 9.07(P2)	$HE^{x}_{11\delta}$ and $HE^{y}_{11\delta}$	<–21	Ortho. LP	PEC h=3.0mm

II.6. Conclusion

A dual port cylindrical DRA for MIMO applications has been proposed and carried out using HFSS software. One feeding technique is used: coaxial cable for Port 1 and Port 2. The two ports are fixed very near to enhance the isolation in the proposed structure which generates the hybrid modes HEM_{11} in the CDRA. The proposed antenna achieves a good ECC, DG, MEG, CCL, and TARC. The antenna has a simple configuration and miniaturized size making it a promising candidate for small handheld and portable communication devices. In the future, the above CDR antenna can be used as MIMO operation support by validating its diversity performance parameters. The multiple duplicate units of the same antenna can convert the same antenna to achieve higher antenna gain with array operations. Using RF switching this antenna could be converted to a reconfigurable antenna.

References

[1] Gollamudi, N.K., Narayana, Y.V. and Prasad, A.M., 2023. COMPACT MODIFIED CIRCULAR-SHAPED MULTIPLE-INPUT MULTIPLE OUTPUT ANTENNA FOR 5G SUB-6 GHZ (N77, N78, AND N79) AND WLAN BAND APPLICATIONS. *Telecommunications and Radio Engineering*, *82*.

[2] Das, G., Sharma, A. and Gangwar, R.K., 2018. Wideband self-complementary hybrid ring dielectric resonator antenna for MIMO applications. *IET Microwaves, Antennas & Propagation*, *12*(1), pp.108-114.

[3] Amroun, A., Zebiri, C., Sayad, D., Elfergani, I.T., Desai, A., Bouknia, M.L., Zegadi, R. and Rodriguez, J., 2023. Miniaturized six-ring elliptical monopole-based MIMO antenna for ultrawideband applications. *International Journal of Communication Systems*, *36*(14), p.e5557.

[4] Varshney, G., Singh, R., Pandey, V.S. and Yaduvanshi, R.S., 2020. Circularly polarized two-port MIMO dielectric resonator antenna. *Progress In Electromagnetics Research M*, *91*, pp.19-28.

[5] Malekar, R.R., Raut, H., Shevada, L. and Kumar, S., 2021. A review on MIMO dielectric resonator antenna for 5G application. *Micro-Electronics and Telecommunication Engineering: Proceedings of 4th ICMETE 2020*, pp.1-8.

[6] Varshney, G., Singh, R., Pandey, V.S. and Yaduvanshi, R.S., 2020. Circularly polarized two-port MIMO dielectric resonator antenna. *Progress In Electromagnetics Research M*, *91*, pp.19-28.

[7] Kiyani, A., Nasimuddin, N., Hashmi, R.M., Baba, A.A., Abbas, S.M., Esselle, K.P. and Mahmoud, A., 2022. A Single-Feed Wideband Circularly Polarized Dielectric Resonator Antenna Using Hybrid Technique With a Thin Metasurface. *IEEE Access*, *10*, pp.90244-90253.

[8] Zebiri, C.E., Lashab, M., Sayad, D., Elfergani, I.T.E., Sayidmarie, K.H., Benabdelaziz, F., Abd-Alhameed, R.A., Rodriguez, J. and Noras, J.M., 2017. Offset aperture-coupled double-cylinder dielectric resonator antenna with extended wideband. *IEEE Transactions on Antennas and Propagation*, *65*(10), pp.5617-5622.

[9] Al Salameh, M.S., Antar, Y.M. and Seguin, G., 2002. Coplanar-waveguide-fed slot-coupled rectangular dielectric resonator antenna. *IEEE Transactions on Antennas and Propagation*, *50*(10), pp.1415-1419.

[10] Fang, X.S., Luo, L., Xu, Y.J. and Sun, Y.X., 2023. Slots-fed polarization-and pattern-diversity cylindrical dielectric resonator antenna with high-gain characteristic. *IEEE Antennas and Wireless Propagation Letters*.

[11] Hu, Y., Pan, Y.M. and Di Yang, M., 2021. Circularly polarized MIMO dielectric resonator antenna with reduced mutual coupling. *IEEE Transactions on Antennas and Propagation*, *69*(7), pp.3811-3820.

[12] Dwivedi, A.K., Sharma, A., Pandey, A.K. and Singh, V., 2021. Two port circularly polarized MIMO antenna design and investigation for 5G communication systems. *Wireless personal communications*, *120*(3), pp.2085-2099.

[13] Singhwal, S.S., Matekovits, L., Peter, I. and Kanaujia, B.K., 2022. A study on application of dielectric resonator antenna in implantable medical devices. *IEEE Access*, *10*, pp.11846-11857.

[14] Boyuan, M., Pan, J., Wang, E. and Yang, D., 2020. Wristwatch-style wearable dielectric resonator antennas for applications on limps. *IEEE Access*, *8*, pp.59837-59844.

[15] Soren, D., Ghatak, R., Mishra, R.K. and Poddar, D., 2014. Dielectric resonator antennas: designs and advances. *Progress In Electromagnetics Research B*, *60*, pp.195-213.

[16] Sheriff, N., Kamal Abdul Rahim, S., Tariq Chattha, H. and Kim Geok, T., 2023. Multiport single element Mimo antenna systems: A review. *Sensors*, *23*(2), p.747.

[17] Patre, S.R. and Singh, S.P., 2018. Shared radiator MIMO antenna for broadband applications. *IET Microwaves, Antennas & Propagation*, *12*(7), pp.1153-1159.

[18] Chouhan, S. and Malviya, L., 2020. Four-port shared rectangular radiator with defected ground for wireless application. *International Journal of Communication Systems*, *33*(9), p.e4356.

[19] Roslan, S.F., Kamarudin, M.R., Khalily, M. and Jamaluddin, M.H., 2014. An MIMO rectangular dielectric resonator antenna for 4G applications. *IEEE antennas and wireless propagation letters*, *13*, pp.321-324.

[20] Varshney, G., Gotra, S., Chaturvedi, S., Pandey, V.S. and Yaduvanshi, R.S., 2019. Compact four-port MIMO dielectric resonator antenna with pattern diversity. *IET Microwaves, Antennas & Propagation*, *13*(12), pp.2193-2198.

[21]Abdalrazik, A., Abd El-Hameed, A.S. and Abdel-Rahman, A.B., 2017. A three-port MIMO dielectric resonator antenna using decoupled modes. *IEEE Antennas and Wireless Propagation Letters*, *16*, pp.3104-3107.

[22] Sharawi, M.S., 2014. *Printed MIMO antenna engineering*. Artech House.

[23] Ullah, H., Rahman, S.U., Cao, Q., Khan, I. and Ullah, H., 2020. Design of SWB MIMO antenna with extremely wideband isolation. *Electronics*, *9*(1), p.194.

[24] Chae, S.H., Oh, S.K. and Park, S.O., 2007. Analysis of mutual coupling, correlations, and TARC in WiBro MIMO array antenna. *IEEE Antennas and Wireless Propagation Letters*, *6*, pp.122-125.

[25] Pandey, A., Singh, A.P. and Kumar, V., 2023. Design and optimization of circularly polarized dielectric resonator-based MIMO antenna using machine learning for 5G Sub-6 GHz. *AEU-International Journal of Electronics and Communications*, *162*, p.154558.

[26] Das, G. and Gangwar, R.K., 2018, February. A high isolation MIMO cylindrical dielectric resonator antenna for 4G applications. In *2018 3rd International Conference on Microwave and Photonics (ICMAP)* (pp. 1-2). IEEE.

[27] Nasir, J., Jamaluddin, M.H., Khalily, M., Kamarudin, M.R. and Ullah, I., 2016. Design of an MIMO dielectric resonator antenna for 4G applications. *Wireless Personal Communications*, *88*, pp.525-536.

[28] Das, G., Sharma, A. and Gangwar, R.K., 2017. Dual feed MIMO cylindrical dielectric resonator antenna with high isolation. *Microwave and Optical Technology Letters*, *59*(7), pp.1686-1692.

[29] Biswas, B. and Gupta, A., 2021. A Single Element Dual Feed MIMO Cylindrical Dielectric Resonator Antenna with High Isolation for 5.6 GHz WLAN Application. In *Proceeding of Fifth International Conference on Microelectronics, Computing and Communication Systems: MCCS 2020* (pp. 69-75). Springer Singapore.

[30] Li, B., Hao, C.X. and Sheng, X.Q., 2009. A dual-mode quadrature-fed wideband circularly polarized dielectric resonator antenna. *IEEE Antennas and wireless propagation letters*, *8*, pp.1036-1038.

[31] Chowdhury, R., Mishra, N., Sani, M.M. and Chaudhary, R.K., 2017. Analysis of a wideband circularly polarized cylindrical dielectric resonator antenna with broadside radiation coupled with simple microstrip feeding. *IEEE Access*, *5*, pp.19478-19485.

[32] Reddy, R.V., Ameen, M., Chaudhary, R.K. and Gangwar, R.K., 2019, December. Compact wideband circularly polarized rectangular DRA with right angled conformal strip feed. In *2019 IEEE Indian Conference on Antennas and Propogation (InCAP)* (pp. 1-4). IEEE.

[33] Vahora, A. and Pandya, K., 2022. A miniaturized cylindrical dielectric resonator antenna array development for GPS/Wi-Fi/wireless LAN applications. *e-Prime-Advances in Electrical Engineering, Electronics and Energy*, *2*, p.100044.

Chapter III:

Equivalent Circuit of a Planar Microwave Liquid Sensor

III.1. Introduction

The measurement of electromagnetic properties makes it possible to determine the characteristics of various media: chemical, biological, or molecular [1]. In the microwave field, the use of microwave sensors facilitates this task. This is due to their low cost [2], their reliable and robust design [3], and their ease of integration and manufacture [4, 5]. These sensors have become indispensable, hence their use in various fields such as healthcare [6], biomedical [4], agriculture [7], environment and food, etc.

In the interests of reliable, accurate detection, research is focusing on a new generation of metamaterial-based sensors. The development of meta-materials has contributed significantly to the popularity of these sensors. The design of artificial materials (meta-materials: MTM) is known for its periodic structure. This periodicity enables precise measurements of the constituent parameters of the media: negative permittivity and permeability, using planar technology [8], [9]. Design shape and orientation influence the physical properties of meta-materials [10].

Chemical categorization and biomedical detection depend on sensors implemented using MTM technology [11], which is composed of a fused ring resonator (SRR) or a complementary fused ring resonator (CSRR) [11-14]. One of the two configuration features mentioned above is the establishment of an electric or magnetic field inducing an interaction with the sensitive structure in the presence of a nearby dielectric property [15]. This includes a direct relationship between the two sensor performances: resonance frequency f_{res} and quality factor Q with the measurements to be detected. Physical properties of metamaterials [10].

This work studies the optimization steps for designing a new planar sensor based on metamaterials. The designed sensor was simulated using the HFSS software. The proposed CSRR sensor, whose test tube is inserted in a horizontal position relative to the surface of the sensor plane, offers the possibility of easily changing the direction and diameter of the test tube. The presence of the sample filled into the tube placed above the sensor causes a strong electromagnetic interaction between the CSRR resonator and the liquid to be tested, resulting in a change in the resonant frequency and quality factor Q of the sensor. A model of the resonator CSRR was established using the ADS interface by schematizing a sequence of parallel RLC blocks.

III.2. Sensor geometry design

The proposed planar sensor structure is shown in Figure III-1. The sensor design is based on copper, which is implemented on Rogers RO3035 dielectric substrate with a thickness of 0.75 mm, a dielectric constant of $\varepsilon_r = 3.5$, and dielectric losses tan $\delta = 0.0015$. A microwave sensor is crucial for characterizing liquid media. The geometry is illustrated in Figures III-1 (a), (b), and (c), which show the proposed structure in perspective view, top view, and bottom view, respectively.

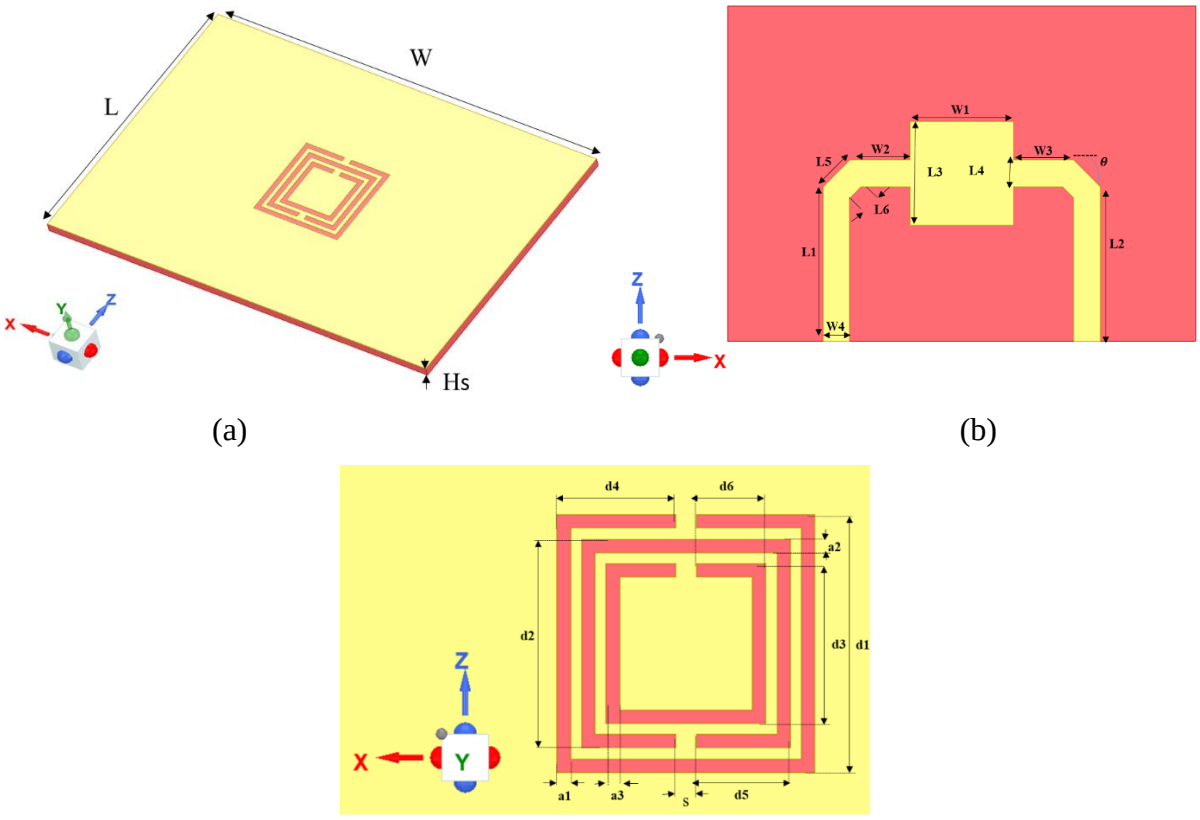

(a) (b)

(c)

Figure III-1.3D View of the proposed sensor, (a) perspective view, (b) top view, and (c) bottom view.

Table III.1. Geometrical parameters of the proposed sensor structure.

Parameters	**W**	**L**	**Hs**	**W1**	**W2**	**W3**	**W4**	**L1**	**L2**	**L3**	**L4**	**L5**
Value (mm)	28	20	0.75	6.2	3.6	2.94	1.6	9.2	8.54	6.2	1.6	2.26
Parameters	**L6**	**d1**	**d2**	**d3**	**d4**	**d5**	**d6**	**a1**	**a2**	**a3**	**s**	**θ**
Value (mm)	0.94	6.2	5.02	3.84	2.85	2.26	1.67	0.33	0.33	0.33	0.5	45°

III.3. Simulation and results discussion

III.3.1. Sensor Optimization

To design an optimized sensor, a change of direction was first achieved by varying the position of the capillary tube, and in the second stage a parametric study was carried out by varying the diameter r of the test tube

III.3.1.1. Effect of tube orientation

Microwave sensor performance was studied using two tube orientations (tube along z and x) (Figure III-2a and 2b). Figure III-3 illustrates a prototype of the proposed 2-ports microwave sensor, which has been manufactured using microstrip planar resonator technology. This sensor is employed for the characterization of water-ethanol mixtures. The ambient conditions were carefully observed and maintained at an average temperature of 25 °C (77 °F) and a relative humidity of 50%.

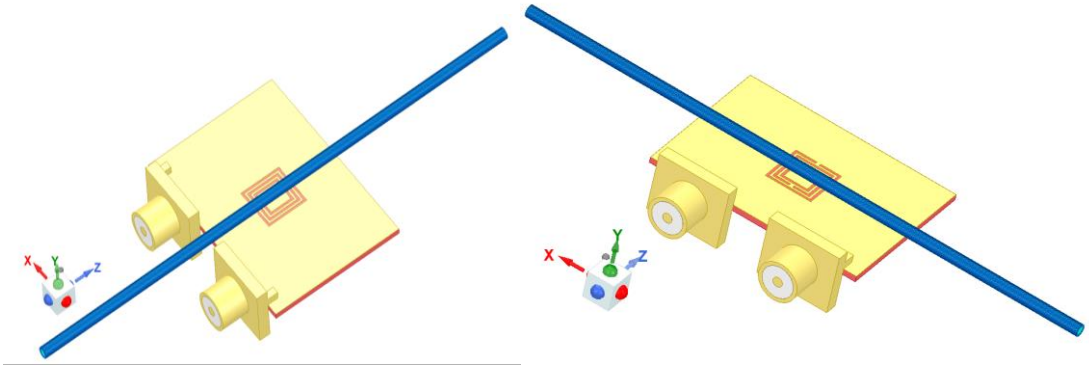

(a) (b)

Figure III-2. 3D view of the proposed sensor: (a) z-oriented and (b) x- oriented tube

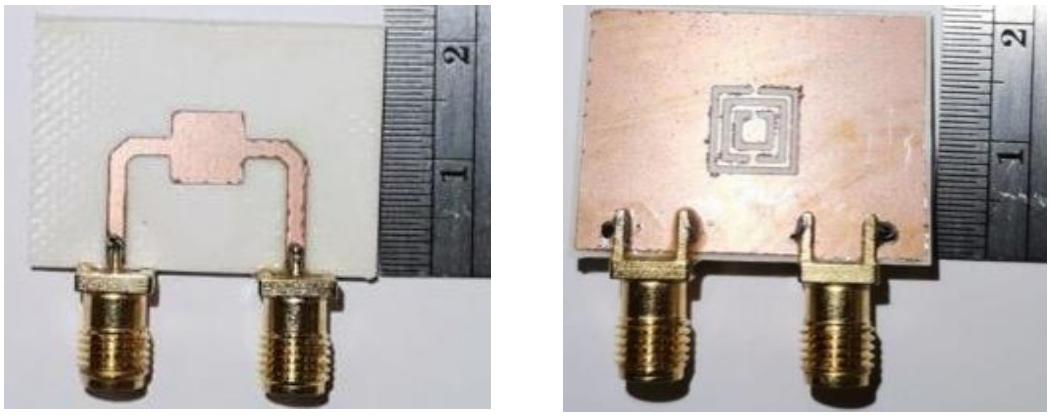

(a) (b)

Figure III-3. Fabricated prototype of the proposed sensor: (a) 2-port patch top view (b) bottom view.

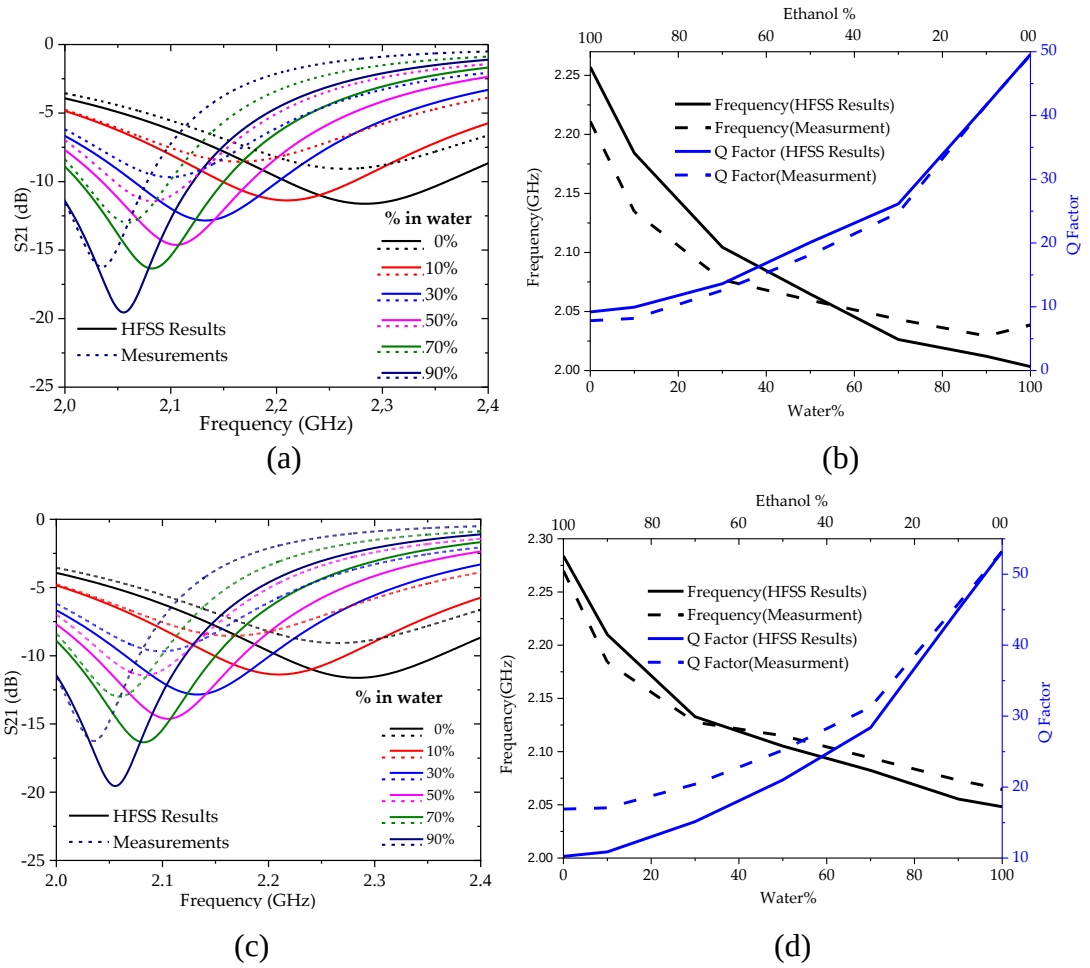

Figure III-4. Simulated and measured S_{21} versus frequency, Q-Factor, and resonant frequency versus water.

Figure III-4 displays the results simulated and measured by the proposed microwave sensor for various concentrations of the water-ethanol mixture for a radius r=5mm tube.

In the water-ethanol mixture: (a) and (b) x-oriented tube, (c) and (d) z-oriented tub. The S_{21} parameter simulated by HFSS compared with experimental measurements for two test tube orientations: along ox (Figure III-4. (a, b)) In addition, oz (Figure III-4. (c, d)) Shows good agreement. However, the case of the x orientation gives better results, so this configuration is adopted for future simulation and measurement procedures.

The calculation of the sensitivity S is given by: $S = \Delta F_r/\Delta\varepsilon_r$[16], where ΔF_r and $\Delta\varepsilon_r$ represent the resonant frequency shift and relative dielectric shift, respectively, for different water-ethanol concentrations between upper and lower mixture values ($\Delta fr = fr_{\_0\%} - fr_{\_100\%}$) and ($\Delta\varepsilon_r = \varepsilon_{r\_100\%} - \varepsilon_{r\_0\%}$)[16]. The quality factor is defined as the resonant frequency ratio to the frequency bandwidth for 3dB, $Q = \frac{F_{Res}}{\Delta F_{3dB}}$ [17].

Table III.2. Effect of the tube orientation on Sensitivity and Q-Factor.

Tube radius	Tube orientation	$\Delta F_{r0\%-100\%}$	Sensitivity S	Max Q-Factor
r=5 mm	oz	236 MHz	3.44	53
r=5 mm	ox	253.7 MHz	3.7	50

According to Table III.2, for the case of tube diameter r=5mm, we note that a very significant performance improvement is achieved, especially for the case of the tube in a position parallel to the ox. The performance obtained is optimal: a remarkable increase in sensitivity, and the frequency offset reaches the maximum value of 253.7 MHz As a result, the sensitivity value S expands to 3.7, and an acceptable quality factor value of 50 is obtained. The mean resonant frequency remains unchanged at 2.1 GHz.

III.3.1.2 Effect of tube radius

After first optimizing our structure by varying the orientation of the tube, the simulation results corresponding to this structure are shown in Figure III-2 (ox position), where the change is attributed mainly to the position of the test tube.

A second optimization test was carried out by varying the tube radius for different values 3, 5, and 7.5 mm. progressively until we obtained optimum performance results for our structure.

- **Design steps**

The simulation results for the proposed design are shown in Figure III-5 for an outside diameter of r=3 mm.

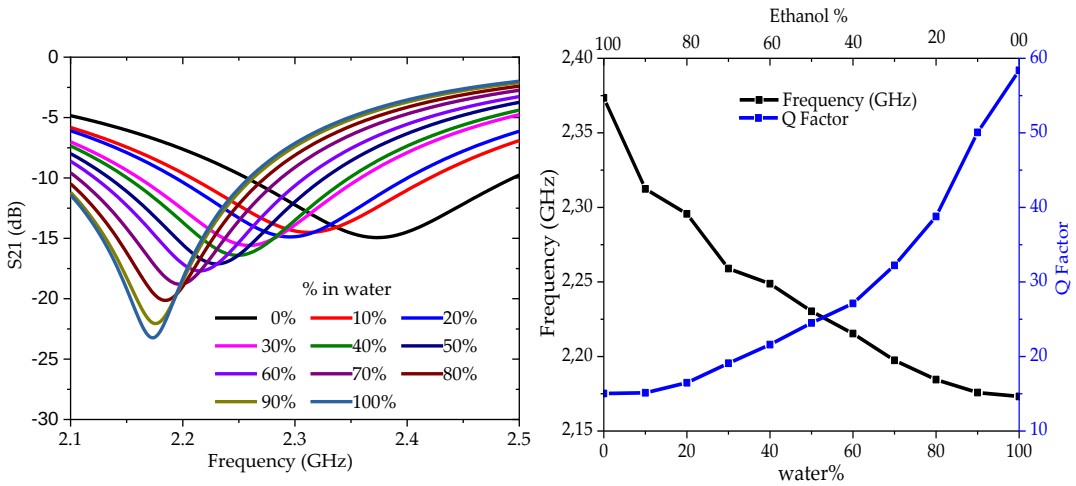

Figure III-5. Simulation results for r = 3 mm, orientation according to ox (a): transmission coefficient S_{21}, (b): quality factor and resonance frequencies.

According to Figure III-5 for an ox orientation with r=3mm, a performance improvement is observed compared. The frequency band decreases and reaches an average value of 2.2 GHz at resonance, with an increase in the frequency offset of 200 MHz, leading to an increase in sensitivity to 2.89, with a slight decrease in the quality factor (Q=58). In addition, the values of the S_{21} coefficient curves increase progressively with increasing concentrations of the water-ethanol mixture, i.e. dielectric losses decrease proportionally towards higher water concentrations.

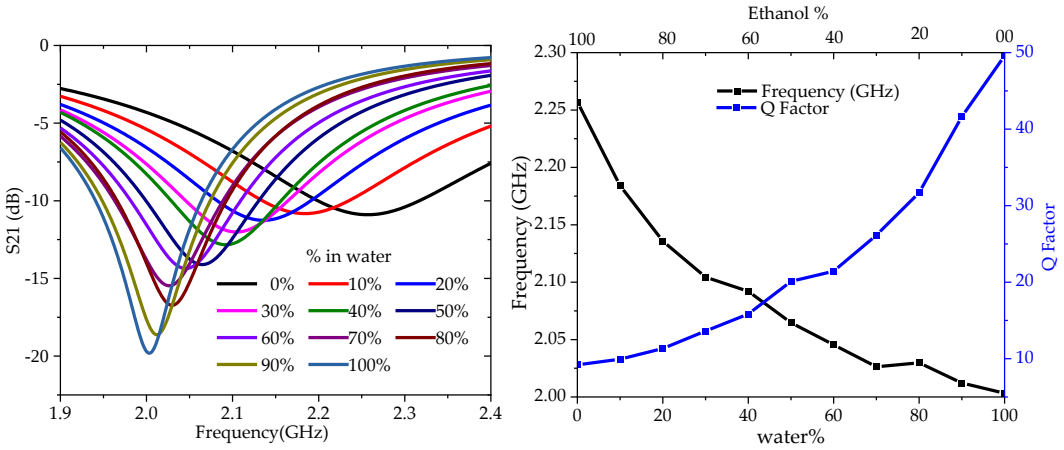

Figure III-6. Simulation results for r = 5 mm and orientation along ox, (a): transmission coefficient S_{21} and (b): quality factor and resonance frequency for different volume fractions of the water-ethanol mixture. .higher water concentrations.

Figure III-6 illustrates the simulation results for the case of r=5mm, where an increase in performance is deduced with a maximum realized sensitivity of 3.7 for a frequency band of 253.7 MHz against a slight decrease in the quality factor (Q= 50). The sensor operates at a center frequency of 2.1 GHz.

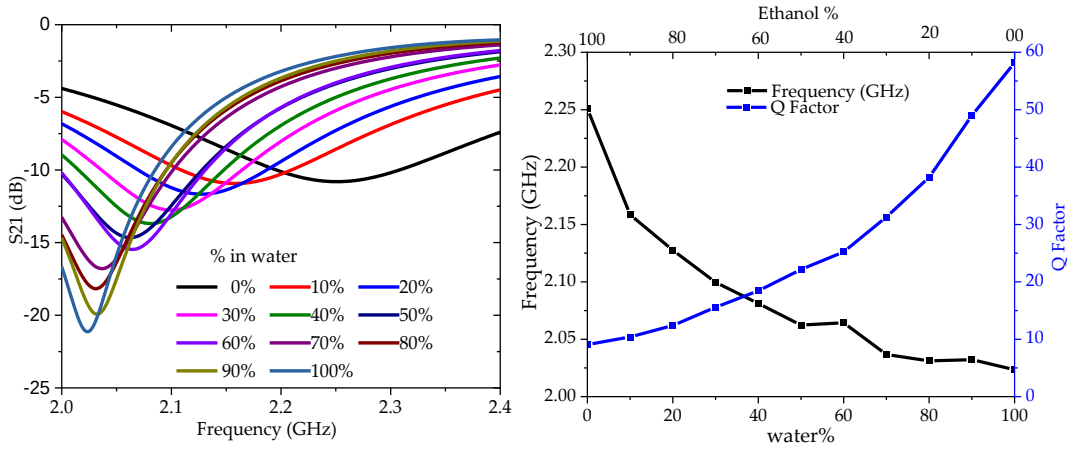

Figure III-7. Simulation results for r = 7.5 mm and orientation along ox, (a): transmission coefficient S_21 and (b): quality factor and resonance frequency for different volume fractions of the water-ethanol mixture.

Figure III-7 presents the simulation results for the r=7.5 mm case. The results demonstrate a decrease in sensitivity to a value of 3.32, corresponding to a bandwidth of over 228 MHz, and a quality factor increasing to 58.

Table III.3. Comparison of f_{res} and Q Factor simulation results for different tube diameters and orientations.

Diameter	**Max resonant frequency (MHz) 0%**	**Min resonant frequency (MHz) 100%**	**$\Delta f = f_{0\%} - f_{100\%}$ (MHz)**	**Max Q-Factor**
r= 3mm	2373.5	2173,2	200.3	58.3
r= 5mm	2257	2003,3	253.7	49.5
r= 7.5mm	2251	2023.5	227.5	58.1

III.4. Equivalent Circuit

An equivalent circuit serves as a simplified representation of a complex circuit, facilitating the analysis of the original circuit. It provides a concise model with specific parameters tailored to factors such as signal frequency, component temperature, and transducer inputs. Original circuits may have a voltage source with an internal resistor and several external resistors, while equivalent circuits in constant current analysis will have a voltage source and a single internal resistor, or this resistor is the resultant of the internal and external resistors. Equivalent circuits exist for any type of circuit with any type of component

The equivalent circuit is designed using the ADS (Advanced Design System) interface for microwave planar resonator operation (Figure III-8). This circuit model is designed to characterize and ensure impedance matching [18], where these impedances are translated into an equivalent circuit. The resulting equivalent circuit contains ten parallel RLC (resistor-inductance-capacitor) circuits connected with three inductors in series.

Using the results of the HFSS simulation of our sensor parameters, we show the different gaits of the parameters Z_{11}, Z_{21}, Figure. III-9 and Figure III-10.

The values associated with the components of the equivalent circuit of the proposed sensor (Figure III-8) are simulated and identified using ADS software and are grouped in Table III.4.

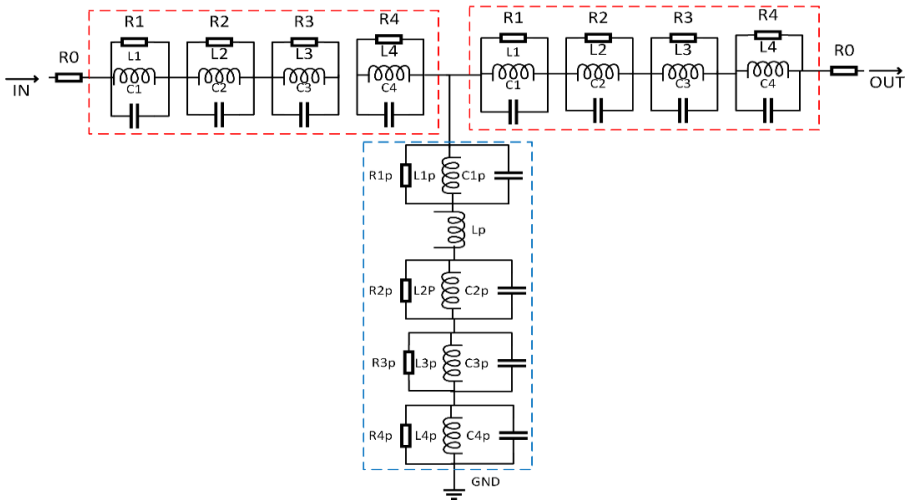

Figure III-8. Equivalent circuit for the proposed microwave sensor.

Table III.4. Values of different parameters of the equivalent circuit.

Resistance (Ohm)	*Inductance (pH)*	*Capacity (pF)*
R0=0.1	L1=94	C1=60
R1=4.4	L2=49	C2=39
R2=5	L3=4243.7	C3=0.9039
R3=52307.55	L4=6060	C4=167.2
R4=1645.73	L1p=2420	C1p=1.54
R1p=2400	L2p=361.5	C2p=14.5
R2p=74.22	L3p=72.07	C3p=6.66
R3p=114.3	L4p=40.48	C4p=54.68
R4p=55.8	Lp=198	

III.4.1. ADS and HFSS simulation results

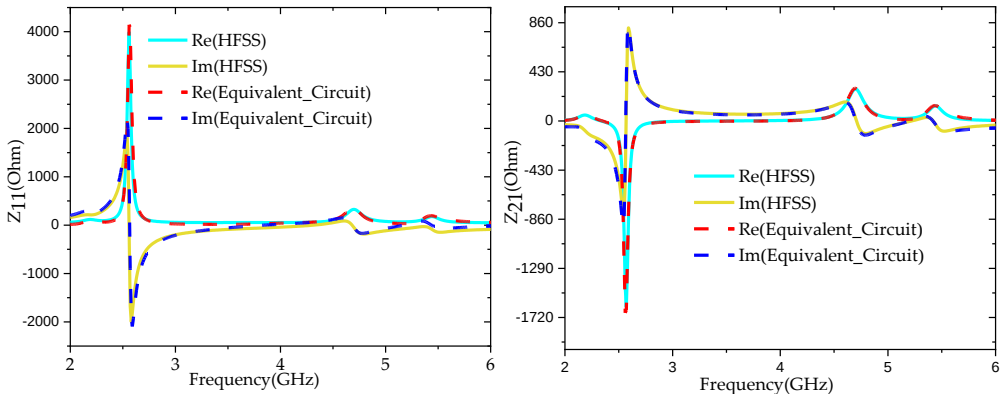

(a) (b)

Figure III-9. Input-output input impedance real and imaginary part of both ADS and HFSS simulators: (a) Z_{11} and (b) Z_{21}

Figure III-9 Shows the comparison of HFSS simulation results (Z_{11} and Z_{21}) for the proposed sensor with the results obtained using ADS. It can be seen that the electrical model designed expresses and interprets the operation of the proposed device. This is justified by the good agreement between the two simulated results**.**

The frequency range is extended in Figure III-10 to 6 GHz to enable the placement of the various parts, the deduction of component values, the various blocks, and essentially their number.

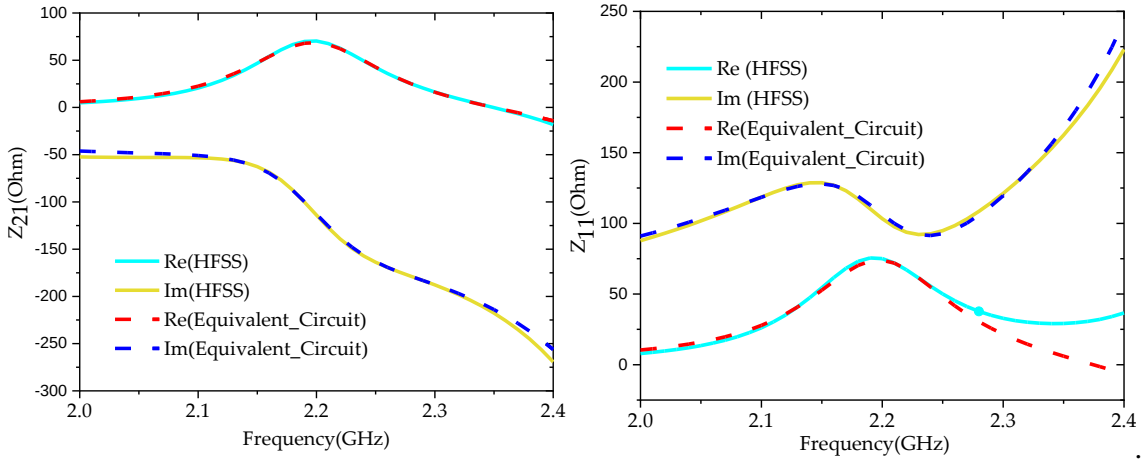

(a) **(b)**

Figure III-10. Comparison of input impedance parameters of both ADS and HFSS simulators: (a) Z_{11} and (b) Z_{21}.

Figure III-10 Shows the dominant capacitive part in Z_{21}, the working range of our circuit, which explains the coupling, as well as the high value of the quality factor. It can be seen that the equivalent circuit model resonates at the same frequency as the EM model, indicating very good concordance.

III.5. Conclusion

This work presents and discusses the design of a metamaterial-based Complementary Split Ring Resonator (CSRR) microwave planar sensor operating around 2.1 GHz, specifically for the characterization of binary water-ethanol mixtures. The resonance frequency and quality factor of the various mixture fractions were obtained using HFSS software. Additionally, a T-shaped equivalent circuit model was derived and optimized using ADS software. This model was developed by analyzing the impedance parameters of the proposed microwave sensor.

A good agreement was achieved between the circuit model and the electromagnetic (EM) model, demonstrating the validity and accuracy of the proposed design.

References

[1] La Spada, L. and Vegni, L., 2018. Electromagnetic nanoparticles for sensing and medical diagnostic applications. *Materials*, *11*(4), p.603.

[2] Omer, A.E., Shaker, G., Safavi-Naeini, S., Kokabi, H., Alquié, G., Deshours, F. and Shubair, R.M., 2020. Low-cost portable microwave sensor for non-invasive monitoring of blood glucose level: Novel design utilizing a four-cell CSRR hexagonal configuration. *Scientific Reports*, *10*(1), p.15200.

[3] Yu, H., Wang, C., Meng, F.Y., Liang, J.G., Kashan, H.S., Adhikari, K.K., Wang, L., Kim, E.S. and Kim, N.Y., 2020. Design and analysis of ultrafast and high-sensitivity microwave transduction humidity sensor based on belt-shaped MoO3 nanomaterial. *Sensors and Actuators B: Chemical*, *304*, p.127138.

[4] Chudpooti, N., Duangrit, N., Sangpet, P., Akkaraekthalin, P., Imberg, B.U., Robertson, I.D. and Somjit, N., 2020. In-situ self-aligned NaCl-solution fluidic-integrated microwave sensors for industrial and biomedical applications. *IEEE Access*, *8*, pp.188897-188907.

[5] Jasińska, L. and Malecha, K., 2021. Microfluidic modules integrated with microwave components—Overview of applications from the perspective of different manufacturing technologies. *Sensors*, *21*(5), p.1710.

[6] Marinković, Z., Gugliandolo, G., Latino, M., Campobello, G., Crupi, G. and Donato, N., 2020. Characterization and neural modeling of a microwave gas sensor for oxygen detection aimed at healthcare applications. *Sensors*, *20*(24), p.7150.

[7] Kim, H., Wigneron, J.P., Kumar, S., Dong, J., Wagner, W., Cosh, M.H., Bosch, D.D., Collins, C.H., Starks, P.J., Seyfried, M. and Lakshmi, V., 2020. Global scale error assessments of soil moisture estimates from microwave-based active and passive satellites and land surface models over forest and mixed irrigated/dryland agriculture regions. *Remote Sensing of Environment*, *251*, p.112052.

[8] Cao, C., Chen, L., Zhu, Z., Yang, Y., Huangfu, J., Qiao, S. and Ye, D., 2020. Homogenization of artificial media with a transmission line approach. *Applied Physics A*, *126*, pp.1-9.

[9] Askari, M., Hutchins, D.A., Thomas, P.J., Astolfi, L., Watson, R.L., Abdi, M., Ricci, M., Laureti, S., Nie, L., Freear, S. and Wildman, R., 2020. Additive manufacturing of metamaterials: A review. *Additive Manufacturing*, *36*, p.101562.

[10] Abdulkarim, Y.I., Deng, L., Luo, H., Huang, S., Karaaslan, M., Altıntaş, O., Bakır, M., Muhammadsharif, F.F., Awl, H.N., Sabah, C. and Al-badri, K.S.L., 2020. Design and study of

a metamaterial-based sensor for the application of liquid chemicals detection. *Journal of Materials Research and Technology*, *9*(5), pp.10291-10304.

[11] Khanna, Y. and Awasthi, Y.K., 2020. Dual-band microwave sensor for investigation of liquid impurity concentration using a metamaterial complementary split-ring resonator. *Journal of Electronic Materials*, *49*(1), pp.385-394.

[12] Mosbah, S., Zebiri, C., Sayad, D., Elfergani, I., Bouknia, M.L., Mekki, S., Zegadi, R., Palandoken, M., Rodriguez, J. and Abd-Alhameed, R.A., 2022. Compact and highly sensitive bended microwave liquid sensor based on a metamaterial complementary split-ring resonator. *Applied Sciences*, *12*(4), p.2144.

[13] Salim, A. and Lim, S., 2016. Complementary split-ring resonator-loaded microfluidic ethanol chemical sensor. *Sensors*, *16*(11), p.1802.

[14] Yeo, J. and Lee, J.I., 2019. High-sensitivity microwave sensor based on an interdigital-capacitor-shaped defected ground structure for permittivity characterization. *Sensors*, *19*(3), p.498.

[15] Ebrahimi, A., Withayachumnankul, W., Al-Sarawi, S. and Abbott, D., 2013. High-sensitivity metamaterial-inspired sensor for microfluidic dielectric characterization. *IEEE Sensors Journal*, *14*(5), pp.1345-1351.

[16] Mosbah, S., Zebiri, C., Sayad, D., Elfergani, I., Bouknia, M.L., Mekki, S., Zegadi, R., Palandoken, M., Rodriguez, J. and Abd-Alhameed, R.A., 2022. Compact and highly sensitive bended microwave liquid sensor based on a metamaterial complementary split-ring resonator. *Applied Sciences*, *12*(4), p.2144.

[17] Salim, A. and Lim, S., 2016. Complementary split-ring resonator-loaded microfluidic ethanol chemical sensor. *Sensors*, *16*(11), p.1802.

Chapter IV:

Equivalent Circuit Modeling of a Cylindrical Dielectric Resonator MIMO Antenna For WLAN Applications

IV.1. Introduction

With the growing need for mobile communication systems in many different areas, several problems have been emerging, such as congested channel capacity, slow transmission rates, and poor signal quality. To resolve these problems more effectively, MIMO antennas have gained the focus of attention. Dielectric resonator antennas (DRA) are emerging as an efficient and favored choice among various antennas. This is primarily due to their several characteristics, including low profile, high Q factor, high radiation efficiency, wide bandwidth, ease of fabrication, flexible shapes, and excitation methods [1, 2]. These benefits of dielectric resonator antenna over conventional antenna make them popular to be utilized for different wireless applications like MIMO operations.

The idea of using equivalent circuit models has recently gained importance as a research topic in antenna design. There are numerous ways of replacing an antenna with its dummy equivalent load for measurement to understand how the antenna works, and to specify the antenna's matching circuit [3, 4]. The analysis of antennas in communication systems generally requires simple, accurate modeling of antenna parameters [5]. The electrical equivalent circuit of traditional antennas with a point of resonance can be derived from the transmission line model [6, 7]. The use of electrical circuit models to represent antennas has continued to evolve over the years [8-10]. In [8], an equivalent circuit modeling for a helical antenna is introduced to generate the input impedance. The suggested model is composed of a shunt capacitance, an effective capacitance, an inductor, and a resistance to radiation in a series connection. Another model, proposed in [9], addresses dipole antennas of arbitrary length. It utilizes an equivalent circuit consisting of Z_0 (L_0 in series with C_0) in conjunction with parallel RLC networks. Furthermore, in [10], a circuit model is introduced for electrically small antennas based on their frequency-dependent polarization, which can be used to analyze various smaller antenna layouts. In recent years, there has been a trend towards developing more accurate circuit models that can represent the behavior of antennas over a wide range of frequencies [11-15]. However, in all these papers, the model accuracy has never been examined and it may not precisely derive the impedance parameters and the circuit RLC element values, hence, the excited modes for a variety of studied antennas, especially for MIMO designs.

This chapter presents an efficient equivalent circuit model for a CDRA MIMO antenna. In our approach, we employed the ADS software to analyze the proposed antenna. This analysis was based on the derivation of the equivalent circuit's complex-valued Zij

parameters, in contrast to the widely used approaches that primarily focus on the amplitudes of Sij parameters. The CDRA-based MIMO antenna was modeled with the help of a parallel RLC resonant circuitry. The proposed equivalent circuit model for the MIMO antenna takes the form of a T-shaped parallel RLC circuit with appropriately chosen values for resistors, capacitors, and inductors. We then compared the obtained antenna equivalent circuit parameters (Z_{11}, Z_{22}, Z_{21}, S_{11}, S_{22}, and S_{21}) with their HFSS simulated counterparts.

IV.2. Antenna construction

The proposed MIMO antenna includes a single CDR radiator of dimensions: height (H) = 7.3mm, radius (R) = 5mm, and dielectric constant (ε_r) = 15. It is positioned on a metal ground plane measuring 50×50×3mm³, as depicted in Figure IV-1. Two orthogonal 50Ω-coaxial probe feeds are employed to excite the CDRA and enable MIMO functionalities. Port 1, featuring an inner conductor of radius (r_f), is situated on the x-axis at the edge of the DR with a height (h_{f1}). Port 2, positioned at a height (h_{f2}), is located on the y-axis near the edge of the resonator at an off-center distance (R2) and an angular shift (θ), resulting in the excitation of HE_{x11} and HE_{y11} radiating modes, respectively. The dimensions of the required MIMO antenna are listed in Table IV .1.

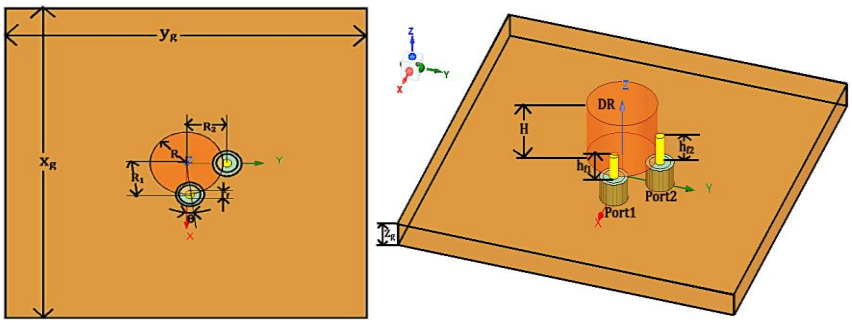

(a) (b)

Figure IV-1. Dimensional of the proposed MIMO antenna (a): top view, (b): 3D view.

Table IV.1. Geometrical Parameters

Parameter	***Value***	***Parameter***	***Value***
X_g	*50mm*	h_{f2}	*3mm*
Y_g	*50mm*	R_1	*5.6mm*
Z_g	*3mm*	R_2	*5.1mm*
R	*5mm*	θ	*5°*
H	*7.3mm*	r_f	*0.6mm*
h_{f1}	*3.8mm*		

To compute the HE_{11} mode resonant frequency in a cylindrical DRA, we apply the following expression [16].

$$f_0 = \frac{6.324}{\sqrt{\varepsilon_r + 2}} \frac{c}{2\pi a}\left[0.27 + 0.36\left(\frac{a}{2H}\right) + 0.02\left(\frac{a}{2H}\right)^2\right] \quad \text{(IV-1)}$$

Where ε_r is the effective dielectric constant, a is the radius, H is the DR height and c is the light speed in free space. This yields a resonant frequency of 5.8GHz.

IV.3. Validation results and discussion

The fabricated prototype of the recommended single-element MIMO antenna is depicted in Figure IV-2.

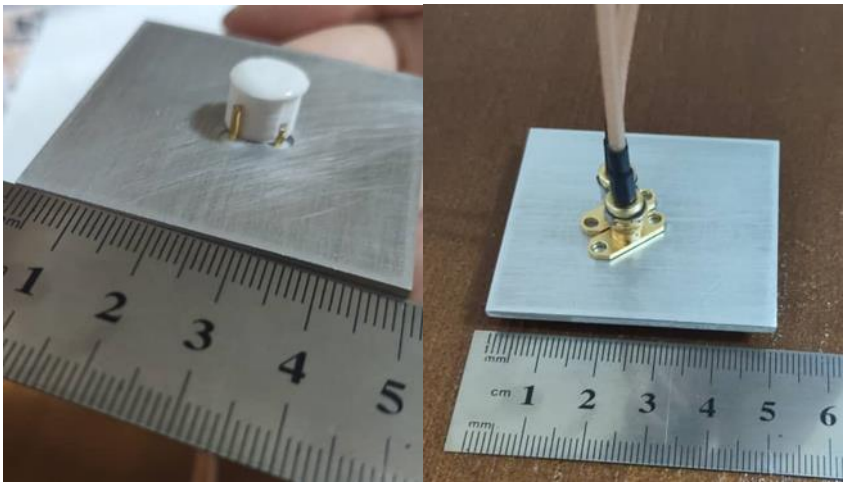

Figure IV-2. Prototype of the realized antenna: (a) top view (b) bottom view.

The simulated and measured S-parameters are displayed in Figure IV-3. The frequency of resonance of the simulated and measured HFSS results is in close accordance, with only a small difference. However, the bandwidth of the prototype is still within the targeted ISM band.

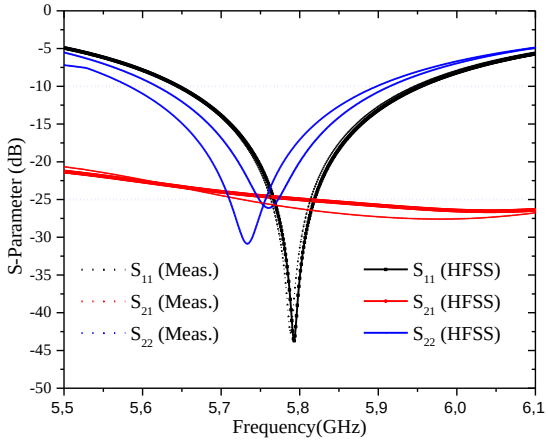

Figure IV-3. Simulated and measured S-parameters of the realized MIMO antenna.

The inter-port isolation at the desired bandwidth exceeds -20 dB, which is achieved by exciting the two orthogonal modes HE_{x11} to HE_{y11} within the DR, as shown in Figure IV-4.

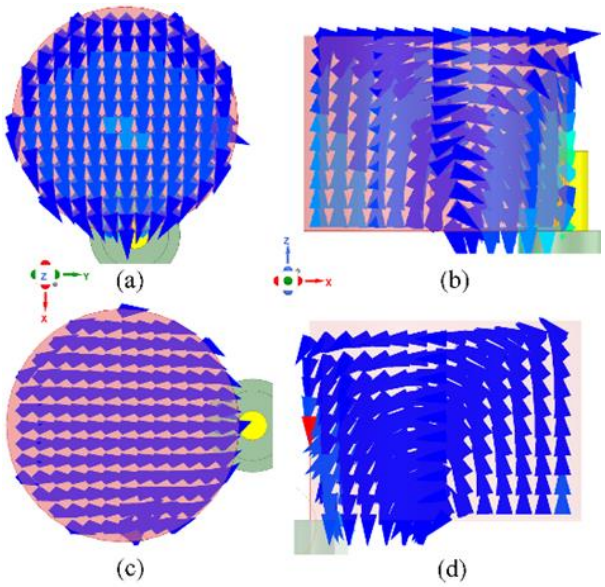

Figure IV-4. Simulated E-field distributions at 5. 8GHz, (a): top view, (b): side view Port 1, and (c): top view, (d): side view Port 2.

The simulated and measured gain graphs of the offered antenna are given in Figure IV-5. The simulated gain value of the double-port CDRA MIMO antenna is approximately 9 dB for both Port 1 and Port 2, in each case, operating at 5.8 GHz. The radiation efficiency of the MIMO antenna is presented in Figure IV-6. It is clear from the illustration that, for the two ports, the proposed MIMO antenna has a radiation efficiency of around 90% in the resonant frequency band.

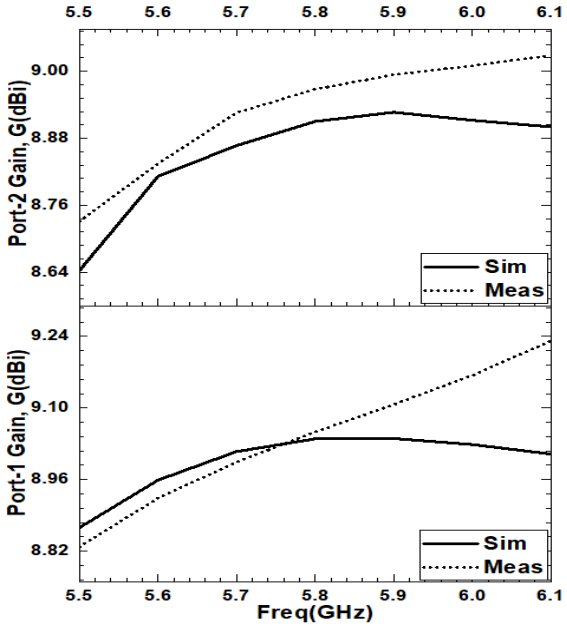

Figure IV-5. The simulated and measured gain of the CDRA MIMO antenna.

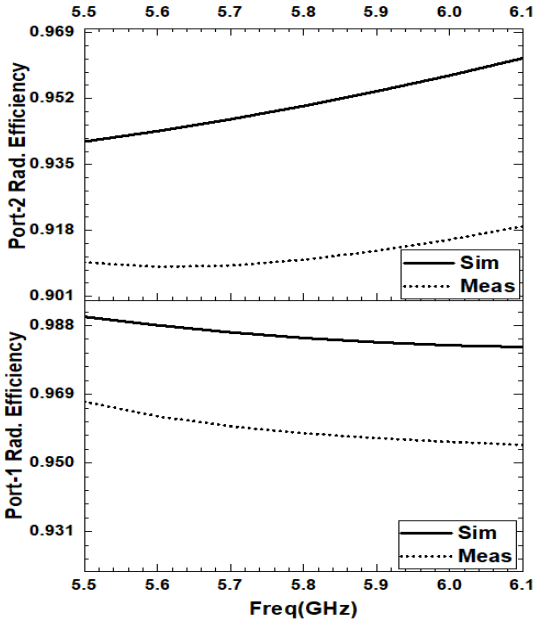

Figure IV-6. Radiation efficiency graphs for the suggested antenna.

Figure IV-7. Gives the radiation pattern normalized at the resonant frequency (5.8 GHz) for both Port 1 and Port 2. The proposed antenna mainly radiates in the beam direction because of the excitation of the $HE_{11\delta}$ mode in the DR. The proposed antenna reaches a degree of cross-polarization lower than the degree of co-polarization.

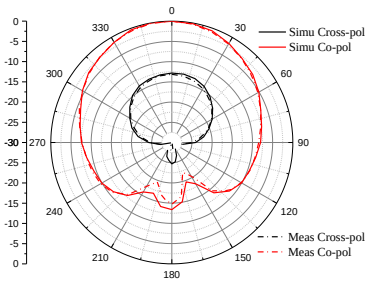

YZ-Plane Port1

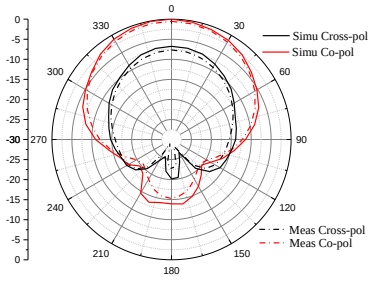

YZ-Plane Port2

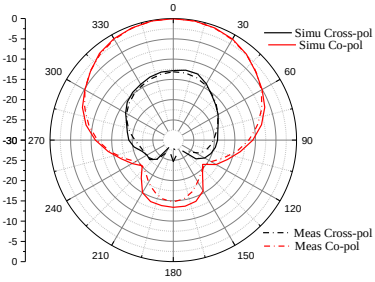

XZ-Plane Port1

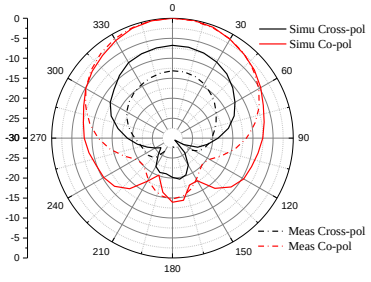

XZ-Plane Port2

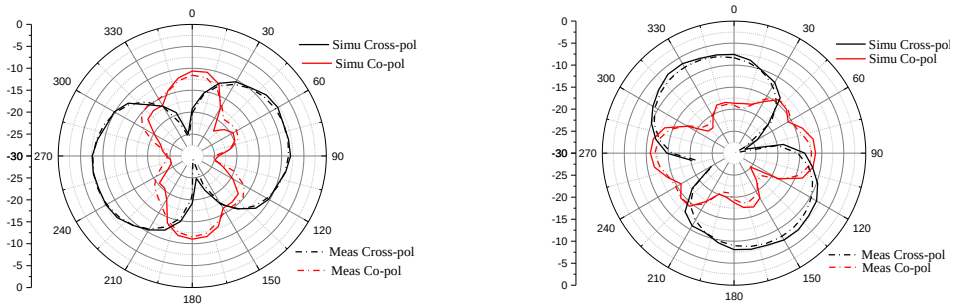

Figure IV-7. Measured and simulated radiation patterns in different planes of the suggested antenna at 5.8 GHz.

IV.4. MIMO Performance

To confirm a good MIMO performance, the recommended MIMO CDRA antenna is analyzed concerning its envelope correlation coefficient (ECC) and its diversity gain (DG), using equations (1 and 2). For good MIMO performance, the ECC must be below 0.5 [17] and the DG should be near to 10 dB.

$$ECC = \frac{\left|S_{11}^{*}S_{12} + S_{21}^{*}S_{22}\right|^{2}}{\left(1-\left(\left|S_{11}\right|^{2}+\left|S_{21}\right|^{2}\right)\right)\left(1-\left(\left|S_{22}\right|^{2}+\left|S_{12}\right|^{2}\right)\right)} \qquad \text{(IV-2)}$$

$$DG = 10\sqrt{\left(1-ECC^{2}\right)} \qquad \text{(IV-3)}$$

Figure IV-8 illustrates the simulated ECC and DG as a function of frequency for the proposed antenna. A weak inter-port correlation of 0.002 and a good DG, around 10 dB, are obtained in the desired band of 5.8 GHz.

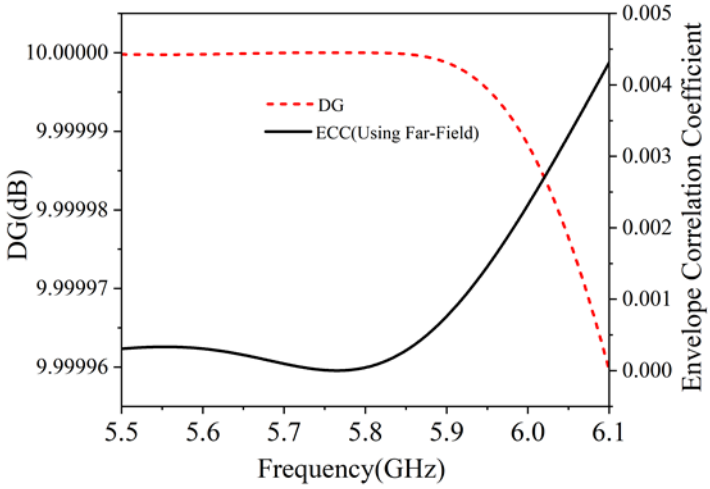

Figure IV-8. Simulated ECC and DG versus frequency of the proposed MIMO CDRA.

IV.4. Equivalent Circuit

In antenna design, a resonant structure may be modeled as an RLC parallel circuit [18, 19]. This model of equivalent circuit is used to replace the original antenna on either terminal, which is connected to a transmitter [20]. It is recommended to get the equivalent circuit model to investigate the performance of the antenna. To better understand the antenna's electrical response and resonance, the circuit elements (R_i, C_i, and L_i) need to be derived using optimized impedance parameters obtained through ADS. In lieu of considering the S-parameters, the value of the input impedance could be used to figure out the resonant mode. The frequencies at which certain elements of the input impedance, such as peaks or nulls in the magnitude or notable phase changes, indicate resonance conditions are known as resonant modes. Researchers can precisely as certain the resonance frequencies and differentiate between the resonant-radiating and non-radiating modes by examining the input impedance[21, 22]. Since the input impedance comparable to the impedance of the input signal, it provides a more direct estimation of the resonant modes compared to the S-parameters. On the other hand, the S-parameters are a measurement of the antenna's transmission and reflection coefficients, which can be affected by a number of variables including the radiation pattern of the antenna and the surrounding environment.

Once an agreement is reached between Z-ADS and Z-HFSS results, the S-parameters will also be in agreement. This allows us to distinguish between different resonant radiating, resonant non-radiating, and adaptation modes. Many studies [14, 15, 23-27] propose lumped equivalent circuit models based exclusively on the amplitude of S-parameters. However, these models do not provide accurate values for RLC elements, resulting in a lack of accurate description of the antenna behavior within the working spectrum.

In this research, the resonant modes of the CDRA are identified by measuring the input impedance. Using the equivalent circuit model of the CDRA, which includes the series and parallel resonant circuits, we estimate the input impedance. Two isolate probe feed lines, with each one at different heights and location, are incorporated in the proposed setup. Every component is represented by an RLC parallel circuit. Similar elements can unite into a single RLC parallel circuit due to their connection. Because each elements are different, each one also has a unique coupling impedance, which is shown by an RLC circuit. As a result, this work contains two distinct RLC coupling circuits.

In the design of antennas, a radiating structure can be represented using an RLC electrical equivalent circuit model (ECM). To understand the electrical behavior and

resonance characteristics of the radiator, the values of circuit elements (R, L, and C) must be accurately derived.

The objective of this study is twofold: firstly, to establish an equivalent circuit by utilizing findings derived from complex-valued Z and S-parameters, and secondly, to critically evaluate the widely used methodology that relies solely on the extraction of S-parameter amplitudes. The equivalent circuit model for the proposed antenna is obtained by the use of a parallel T-shaped RLC circuit, as seen in Figures IV-9 and IV-10. The T-shaped impedance model is determined using equations (4), (5) and (6) [28].

$$Z_i = Z_{11} - Z_{21} \quad \text{(IV-4)}$$

$$Z_o = Z_{22} - Z_{21} \quad \text{(IV-5)}$$

$$Z_c = Z_{21} \quad \text{(IV-6)}$$

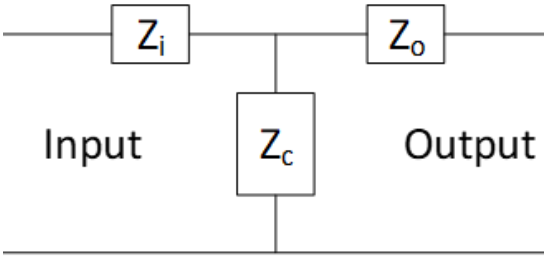

Figure IV-9. T-shaped Z-equivalent circuit for the proposed MIMO antenna.

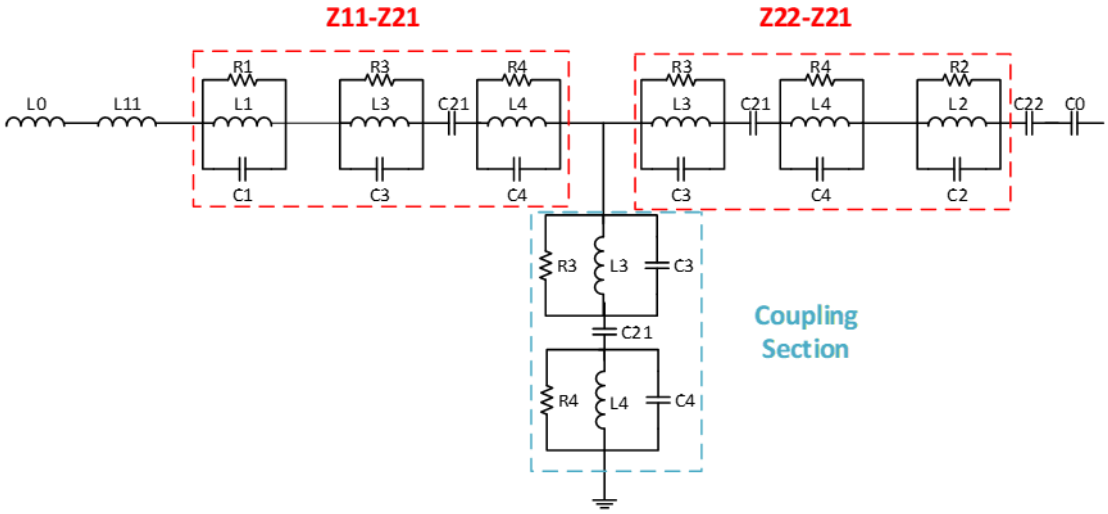

Figure IV-10. RLC equivalent circuit configuration of the CDRA MIMO antenna.

The equivalent circuit model is carried out and optimized using ADS. The optimum values for both ports are given in Table IV.2.The equivalent circuit model Z and S-parameters results are shown in Figure IV-11 and IV-12, respectively, compared with electromagnetic model (HFSS) simulations. The results exhibit remarkable concordance, a level of agreement unattainable through S-parameters amplitude-based approaches. C_0 and L_0 serve to fine-tune

the impedance for the 50 Ω feed line, compensating for the reactive impedance to optimize impedance matching of the parallel-resonant circuit. They allow the reactive impedance of the parallel-resonant circuit to be compensated for, maximizing impedance matching [29]. In theoretical terms, a resonant frequency F_{res} for a circuit comprising L_n and C_n may be given from equation (7) [29].

$$f_{res} = \frac{1}{2*\pi\sqrt{L_n c_n}} \qquad \text{(IV-7)}$$

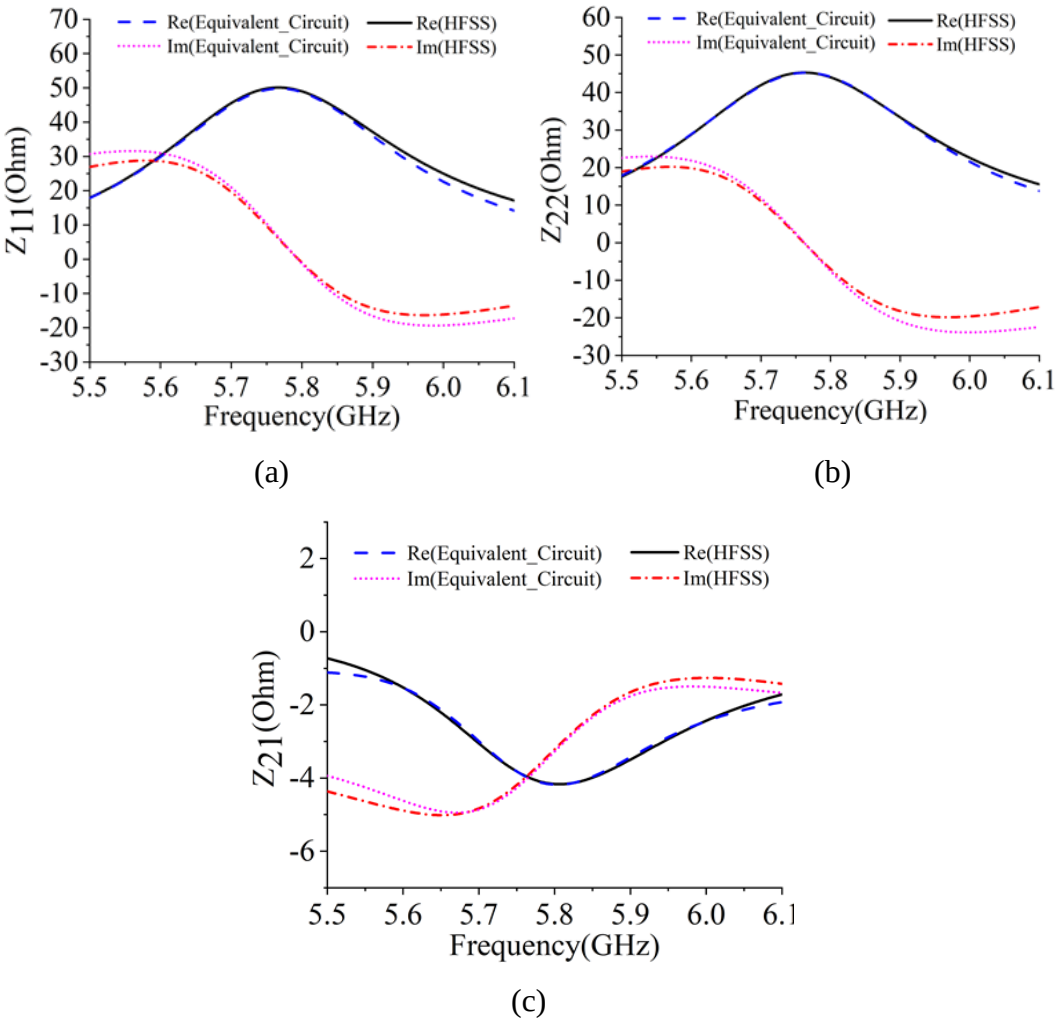

Figure IV-11. Electromagnetic HFSS model and equivalent circuit model input impedance at 5. 8GHz. (a): Z_{11}, (b): Z_{22}, and (c): Z_{21}

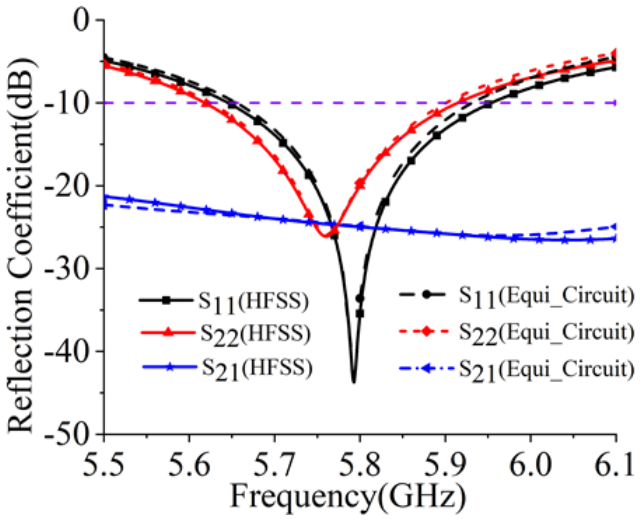

Figure IV-12. Electromagnetic HFSS model and equivalent circuit model S-parameters.

Table IV.2. Equivalent circuit model elements values

R_1	*51.4* Ω	C_3	*11. 144 pF*
L_1	*105. 44 pH*	R_4	*29. 1* Ω
C_1	*7. 22 pF*	L_4	*67. 3 pH*
R_2	*46. 85* Ω	C_4	*11. 36 pF*
L_2	*102.32 pH*	L_{11}	*168. 02 pH*
C_2	*7. 45 pF*	C_{22}	*60 pF*
R_3	*31. 49* Ω	C_{21}	*9. 84 pF*
L_3	*68. 42 pF*	C_0	------
L_0			

Table IV.3. Comparison with other similar work

Ref.	(GHz)	DRA Type & Size (mm^3)	DR	Size (mm^3)	Used Feed Type	ɵ	FBW (GHz)	Gain (dBi)	DRA Mode	/ (dB)	Polar. Mode
[30]	3.2	Rect. L ×B×H = 18×18×29	10	205×205×32	Dual Coax feed	Not did	2.7–3.8	2.1(3.0GHz) 6.1(3.7GHz)	and	<–15	CP
[31]	3.2	Cyl. 2π×H=2π××23	9.8 Ceramic	55×55×24.6	Single MS-feed	Not did	2.82–3.83, 2.75–3.52	5.50	and	-----	CP
[32]	2.45	Rect. L ×B×H = 18×18×29	9.8 Alumina	50×50×19.6	Single MS-feed	Not did	2.13–2.77	5.0	and	<–15	LHCP
This work	5.8	Cyl. 2π×H=2π××7.3	15 Ceramic	50×50×10.3	Dual Coax Probe	±10˚	5.65–5.97	9.03(P1) 9.07(P2)	and	<–21	Ort. LP

* =Design frequency; ɵ=Orthogonal ports Offset angle; =Dielectric constant of DR; FBW=-10dB fractional Bandwidth; S_{12}/S_{21}=Isolation; CP=circularly polarized; LHCP=left hand circularly polarized; Ort. LP= Orthogonal Linearly Polarized; NG=Not Given

Table IV. 3 demonstrates that the proposed study has exhibited decent performance to other related research where several parameters like type of DRA, size of the structure, feed type, modes, isolation, and polarization are taken into account.

IV.5. Conclusion

In the present chapter, a CDRA-based two-port single-element MIMO antenna is offered for GHz WLAN requirements at 5.8 GHz. The antenna is designed using electromagnetic HFSS and analyzed through both the electromagnetic model and the electrical equivalent circuit model. An equivalent circuit model of T-shaped is generated and tuned using ADS software. This model employs a novel approach, investigating the complex-valued impedance parameters (Z_{ij}) of the proposed MIMO antenna, and utilizes this data to deduce the Sij parameters. Results are compared with experimental measurements, showing excellent agreement. The findings demonstrate that the Z-based equivalent circuit model accurately represents the Z- and S-parameters of MIMO antennas. The RLC equivalent circuit model's efficacy in characterizing antennas can be significantly improved by accurately

determining the values of circuit elements through complex Z-parameters, which faithfully mimic the antenna's behavior. A high level of consistency is achieved between the electrical equivalent circuit model and the electromagnetic model.

References

[1] Malekar, R.R., Raut, H., Shevada, L. and Kumar, S., 2021. A review on MIMO dielectric resonator antenna for 5G application. *Micro-Electronics and Telecommunication Engineering: Proceedings of 4th ICMETE 2020*, pp.1-8.

[2] Alanazi, M.D., 2023. A review of dielectric resonator antenna at mm-wave band. *Eng*, *4*(1), pp.843-856.

[3] Badawy, M.M., Malhat, H.A.E.A., Zainud-Deen, S.H. and Awadalla, K.H., 2015. A simple equivalent circuit model for plasma dipole antenna. *IEEE Transactions on Plasma Science*, *43*(12), pp.4092-4098.

[4] Yousaf, J., Jung, H., Kim, K. and Nah, W., 2016. Design, analysis, and equivalent circuit modeling of dual band PIFA using a stub for performance enhancement. *Journal of electromagnetic engineering and science*, *16*(3), pp.169-181.

[5] Huang, Y., Alieldin, A. and Song, C., 2021. Equivalent circuits and analysis of a generalized antenna system [antenna applications corner]. *IEEE Antennas and Propagation Magazine*, *63*(2), pp.53-62.

[6] Hamid, M. and Hamid, R., 1997. Equivalent circuit of dipole antenna of arbitrary length. *IEEE transactions on Antennas and Propagation*, *45*(11), pp.1695-1696.

[7] Kim, J.P., 2011. Network Modeling and Circuit Characteristics of Aperture-Coupled Vertically Mounted Strip Antenna. *Journal of electromagnetic engineering and science*, *11*(2), pp.122-127.

[8] Liao, Y., Hubing, T.H. and Su, D., 2012. Equivalent circuit for dipole antennas in a lossy medium. *IEEE Transactions on Antennas and Propagation*, *60*(8), pp.3950-3953.

[9] Shin, D.R., Lee, G. and Park, W.S., 2013. Simplified vector potential and circuit equivalent model for a normal-mode helical antenna. *IEEE Antennas and Wireless Propagation Letters*, *12*, pp.1037-1040.

[10] Pfeiffer, C. and Grbic, A., 2012. A circuit model for electrically small antennas. *IEEE transactions on antennas and propagation*, *60*(4), pp.1671-1683.

[11] Singh, R. and Varshney, G., 2023. Isolation enhancement technique in a dual-band THz MIMO antenna with single radiator. *Optical and Quantum Electronics*, *55*(6), p.539.

[12] Lodhi, D., Bhaskar, S. and Singhal, S., 2023. Quad port wheel shaped superwideband MIMO antenna. *Journal of Ambient Intelligence and Humanized Computing*, *14*(3), pp.2691-2707.

[13] Aminu Gambo, A., Kolawale, S.F., Saminu, S., Danladi, A. and Jabire, A.H., 2023. Circuit Modeling of Dual Band MIMO Diversity Antenna for LTE and X-Band Applications. *Jurnal Ilmiah Teknik Elektro Komputer dan Informatika (JITEKI)*, *9*(3), pp.511-521.

[14] Iqbal, A., Alazemi, A.J. and Mallat, N.K., 2019. Slot-DRA-based independent dual-band hybrid antenna for wearable biomedical devices. *IEEE access*, *7*, pp.184029-184037.

[15] Hasan, M.N., Chu, S. and Bashir, S., 2019. A DGS monopole antenna loaded with U-shape stub for UWB MIMO applications. *Microwave and optical technology letters*, *61*(9), pp.2141-2149.

[16] Mukherjee, B. and Chauhan, M., 2021. *Dielectric resonator antennas*. Artech House.

[17] Mahto, S.K., Singh, A.K., Sinha, R., Ali bakhshikenari, M., Khan, S. and Pau, G., 2023. High isolated four-element MIMO antenna for ISM/LTE/5G (Sub-6GHz) Applications. *IEEE Access*.

[18] Elfergani, I., Iqbal, A., Zebiri, C., Basir, A., Rodriguez, J., Sajedin, M., Pereira, A.D.O., Mshwat, W., Abd-Alhameed, R. and Ullah, S., 2020. Low-profile and closely spaced four-element MIMO antenna for wireless body area networks. *Electronics*, *9*(2), p.258.

[19] Iqbal, A., Selmi, M.A., Abdulrazak, L.F., Saraereh, O.A., Mallat, N.K. and Smida, A., 2020. A compact substrate integrated waveguide cavity-backed self-triplexing antenna. *IEEE Transactions on Circuits and Systems II: Express Briefs*, *67*(11), pp.2362-2366.

[20] Badawy, M.M., Malhat, H.A.E.A., Zainud-Deen, S.H. and Awadalla, K.H., 2015. A simple equivalent circuit model for plasma dipole antenna. *IEEE Transactions on Plasma Science*, *43*(12), pp.4092-4098.

[21] Obeidat, K.A., Raines, B.D. and Rojas, R.G., 2010. Discussion of series and parallel resonance phenomena in the input impedance of antennas. *Radio Science*, *45*(06), pp.1-9.

[22] Lopez-Rivera, N.D. and Rodriguez-Solis, R.A., 2003, June. Input impedance and resonant frequency characterization for folded slot antennas through DOE techniques. In *IEEE Antennas and Propagation Society International Symposium. Digest. Held in conjunction with: USNC/CNC/URSI North American Radio Sci. Meeting (Cat. No. 03CH37450)* (Vol. 2, pp. 545-548). IEEE.

[23] Alazemi, A.J. and Iqbal, A., 2021. A high data rate implantable MIMO antenna for deep implanted biomedical devices. *IEEE Transactions on Antennas and Propagation*, *70*(2), pp.998-1007.

[24] Altaf, A., Iqbal, A., Smida, A., Smida, J., Althuwayb, A.A.,Hassan Kiani, S., Alibakhshikenari, M., Falcone, F. and Limiti, E., 2020. Isolation improvement in UWB-MIMO antenna system using slotted stub. *Electronics*, *9*(10), p.1582.

[25] Elkorany, A.S., Mousa, A.N., Ahmad, S., Saleeb, D.A., Ghaffar, A., Soruri, M., Dalarsson, M., Alibakhshikenari, M. and Limiti, E., 2022. Implementation of a miniaturized planar tri-band microstrip patch antenna for wireless sensors in mobile applications. *Sensors*, *22*(2), p.667.

[26] Gangwar, A.K. and Alam, M.S., 2019. A miniaturized quad-band antenna with slotted patch for WiMAX/WLAN/GSM applications. *AEU-International Journal of Electronics and Communications*, *112*, p.152911.

[27] Meher, P.R. and Mishra, S.K., 2023. Design and development of mathematical equivalent circuit model of broadband circularly polarized semi-annular ring-shaped monopole antenna. *Progress In Electromagnetics Research C*, *129*, pp.73-87.

[28] Eldosoky, M.A., 2008. The equivalent circuit of the tumor-skin model using ultra-wide band. *XXIX General Assembly, International Union of Radio Science*, pp.7-16.

[29] Tuovinen, T. and Berg, M., 2014. Impedance dependency on planar broadband dipole dimensions: An examination with antenna equivalent circuits. *Progress In Electromagnetics Research*, *144*, pp.249-260.

[30] Li, B., Hao, C.X. and Sheng, X.Q., 2009. A dual-mode quadrature-fed wideband circularly polarized dielectric resonator antenna. *IEEE Antennas and wireless propagation letters*, *8*, pp.1036-1038.

[31] Chowdhury, R., Mishra, N., Sani, M.M. and Chaudhary, R.K., 2017. Analysis of a wideband circularly polarized cylindrical dielectric resonator antenna with broadside radiation coupled with simple microstrip feeding. *IEEE Access*, *5*, pp.19478-19485.

[32] Reddy, R.V., Ameen, M., Chaudhary, R.K. and Gangwar, R.K., 2019, December. Compact wideband circularly polarized rectangular DRA with right-angled conformal strip feed. In *2019 IEEE Indian Conference on Antennas and Propogation (InCAP)* (pp. 1-4). IEEE.

General Conclusion and some future works

General Conclusion

In conclusion, this thesis has provided valuable insights into dielectric resonator antenna DRAs, we have focused on the presentation of different methods related to the study, design, and characterization of novel antenna design based on dielectric resonators (DRs) for new wireless communication standards. The purpose is to provide solutions to a variety of practical problems such as congestion, electromagnetic interference, and transmission rates, by examining the possibilities offered by the development of original and promising solutions.

The research work presented in this thesis is concerned with the study of dielectric resonator antennas. In our study, we have simulated cylindrical dielectric resonator antenna-based MIMO antennas suitable for WLAN applications, using version 2021 of the HFSS electromagnetic simulator.

As a first step, a literature review has enabled us not only to identify dielectric resonator antennas, but also to present some basic concepts that will help us to understand their theory, and to focus on the possibilities offered by this type of antenna. Next, we set out to understand their advantages over other types of antenna, such as printed antennas. A comprehensive review of techniques for bandwidth enhancement, and miniaturization in the first part of this chapter. Finally, we focus on the fundamental characteristics of cylindrical DR antennas, the most common form used.

The compactness of the antenna as well as the reduction of electromagnetic interference was therefore the objective to be achieved in the second chapter. We proposed the optimization steps for designing a cylindrical DR antenna-based MIMO antenna with dual ports to operate at 5.8GHz for WLAN applications. The suggested antenna contains only a single radiator with two coaxial cables feed, compared to Traditional MIMO systems typically include multiple radiators. Therefore, with this new design the size of the antenna is significantly reduced.

A planar CSRR resonator with three-square rings, placed with a capillary tube suspended vertically in the center of the structure for characterization and identification of the liquid in the tube, was treated in the third chapter. The liquid to sample is a mixture of water and ethanol. The first modification is based on changing the position of the test tube from vertical to horizontal according to ox or oz, while the second is based on changing the diameter of the tube. The planar sensor with CSRR resonator in horizontal tube position was

modeled in the form of a series of parallel RLC blocks, using the ADS simulator to find its equivalent circuit.

Finally, the most important part of this work is the equivalent circuit models which have recently gained importance as a research topic in antenna design, an efficient equivalent circuit model for a CDRA MIMO antenna using ADS software to analyze the proposed antenna was traited in the last chapter. This analysis was based on the derivation of the equivalent circuit's complex-valued Z_{ij} parameters, in contrast to the widely used approaches that primarily focus on the amplitudes of S_{ij} parameters. The CDRA-based MIMO antenna was modeled with the help of a parallel RLC resonant circuit. The proposed equivalent circuit model for the MIMO antenna takes the form of a T-shaped parallel RLC circuit with appropriately chosen values for resistors, capacitors, and inductors. We then compared the obtained antenna equivalent circuit parameters (Z_{11}, Z_{22}, Z_{21}, S_{11}, S_{22}, and S_{21}) with their HFSS simulated counter parts.

As future work, and considering the great promise of dielectric resonators, we can look forward to a wide range of applications and studies on a variety of different topics:

- We plan to continue our research on the use of a dielectric resonator as a sensor. We have already started this study and will carry out in-depth experiments to validate the theoretical results and evaluate the performance of the sensor. This will include prototype design and manufacturing, as well as rigorous testing to measure the sensor's sensitivity, linearity, and accuracy.
- Proposed a DRA for multi-permittivity structures, which have shown promising results in terms of bandwidth and radiation Properties.
- Design of new multi-band dielectric resonator antenna architectures for the 5G standard, and design of radiation patterns.

Abstract

This thesis aims to model and optimize planar resonator structures, including antennas and filters, utilizing advanced simulation tools such as HFSS, and ADS. The primary focus is on dielectric resonator antennas (DRAs), particularly the design of a simple, compact cylindrical dielectric resonator antenna (CDRA) based on MIMO technology for WLAN applications. Additionally, a highly sensitive and compact microwave sensor is presented, based on meta-materials complementary split-ring resonator (CSRR), designed to characterize liquid media in the microwave frequency range. A key aspect of this work is the development of equivalent circuit models, a topic that has recently gained significant interest in antenna design. Using ADS software, two effective equivalent circuit models were created: one for a sensor and another for a CDRA MIMO antenna. These models provide a deeper understanding of the behavior of this type of resonator, thereby enhancing the overall quality and performance of the designs.

Keywords: MIMO, DRA, CDRA, WLAN, Sensor, Equivalent circuit, ADS.

Résumé

Cette thèse vise à modéliser et optimiser les structures de résonatrices planaires, y compris les antennes et les filtres, en utilisant des outils de simulation avancés tels que HFSS et ADS. L'accent principal est mis sur les antennes à résonateur diélectrique (DRA), en particulier la conception d'une antenne à résonateur diélectrique cylindrique (CDRA) simple et compacte basée sur la technologie MIMO pour les applications WLAN. De plus, un capteur micro-ondes très sensible et compact est présenté, basé sur des métamatériaux à résonateur à anneau divisé complémentaire (CSRR), conçu pour caractériser les milieux liquides dans la gamme de fréquences micro-ondes. Un aspect clé de ce travail est le développement de modèles de circuits équivalents, un sujet qui a récemment suscité un intérêt considérable dans la conception d'antennes. À l'aide du logiciel ADS, deux modèles de circuits équivalents efficaces ont été créés : un pour un capteur et un autre pour une antenne CDRA MIMO. Ces modèles permettent de mieux comprendre le comportement de ce type de résonateur, améliorant ainsi la qualité et les performances globales des conceptions.

Mots clés : DRA, MIMO, CDRA, WLAN, Circuit équivalent, ADS.

ملخص

تهدف هذه الأطروحة إلى نمذجة وتحسين هياكل الرنان المستوية، بما في ذلك الهوائيات والمرشحات، باستخدام أدوات المحاكاة المتقدمة مثل HFSSو ADSينصب التركيز الأساسي على هوائيات الرنان العازلة(DRAs) ، وخاصة تصميم هوائي مرنان عازل أسطواني بسيط ومدمج (CDRA) يعتمد على تقنية MIMO لتطبيقات WLAN بالإضافة إلى ذلك، يتم تقديم مستشعر ميكروويف حساس للغاية ومدمج، استنادًا إلى مواد تكميلية للرنان ذي الحلقة المنقسمة(CSRR) ، مصممة لتوصيف الوسائط السائلة في نطاق تردد الميكروويف .أحد الجوانب الرئيسية لهذا العمل هو تطوير نماذج الدوائر المكافئة، وهو موضوع اكتسب مؤخرًا اهتمامًا كبيرًا بتصميم الهوائي .باستخدام برنامجADS ، تم إنشاء نموذجين فعالين للدائرة المكافئة: أحدهما لجهاز الاستشعار والآخر لهوائي .CDRA MIMO توفر هذه النماذج فهمًا أعمق لسلوك هذا النوع من الرنان، وبالتالي تعزيز الجودة الشاملة وأداء التصميمات.

الكلمات المفتاحية: DRA، MIMO، CDRA ، WLAN، الدارة المكافئة، ADS.